C.P. No. 1386

C.P. No. 1386

PROCUREMENT EXECUTIVE, MINISTRY OF DEFENCE

AERONAUTICAL RESEARCH COUNCIL

CURRENT PAPERS

The Design and Aerodynamic Characteristics of the RAE 5215 Aerofoil

by

P. G. Wilby

Aerodynamics Dept., R.A.E., Farnborough Hants

LONDON: HER MAJESTY'S STATIONERY OFFICE

1977

£3-00 NET

Editor's Note

The series of Current Papers (CP) of the Aeronautical Research Council will shortly be discontinued.

The series of Reports and Memoranda (R&M) will continue to be published. Some papers which would otherwise have appeared in the CP Series will be published as R&Ms.

UDC 533.692 : 533.6.013.12 : 533.6.011.35

*CP No.1386
December 1974

THE DESIGN AND AERODYNAMIC CHARACTERISTICS OF THE RAE 5215 AEROFOIL

by

P. G. Wilby

SUMMARY

The design and aerodynamic characteristics of a series of aerofoils leading to the RAE 5215 aerofoil are described. This 9.7% thick section was developed to achieve a drag-rise Mach number of about 0.8 with a C_L of 0.4, without suffering from a rear separation at low (3×10^6) Reynolds numbers. Section characteristics are compared with those of a thicker section (RAE 5212) designed for operation at lower Mach numbers.

---

* Replaces RAE Technical Report 74172 - ARC 36124

CONTENTS

1 INTRODUCTION

In recent years considerable interest has grown up in aerofoils on the upper surface of which large regions of supersonic flow can be generated before drag-rise occurs[1]. When the stage is reached at which drag-rise appears on these aerofoils there is usually a well defined shock-wave standing well back (60 to 80%) on the upper surface and a considerable proportion of the total lift is attributable to the supersonic region. If, furthermore, a large amount of rear loading is introduced, through a concavity on the lower surface, then the resulting aerofoil is capable of generating substantial additional lift at high subsonic Mach numbers without incurring appreciable wave drag[2]. The main problem in designing these aerofoils lies in the design of the upper surface, which typically has a large extent of very low curvature profile. There are now numerical methods available[3-6] for this purpose but this was not the case when the work reported here was begun. The object of the present work was to develop an aerofoil which would generate a C_L of 0.4 at a Mach number as close to 0.8 as possible without drag-rise occurring. The resulting section was then to be incorporated into a swept-wing design as part of a research programme to evaluate the methods, and problems, of designing a swept-wing to have a drag-rise Mach number greater than 0.90 with only a moderate amount of sweep back. As both aerofoil and swept-wing models could be tested at only a fairly low Reynolds number (about 3×10^6) the design targets for the aerofoil were not set as high as was known to be attainable. The rear pressure gradient was kept to acceptable levels from the point of view of rear separation and the shock-wave was intended to be only moderately far back on the upper surface at the design condition.

The final aerofoil design (RAE 5215) was arrived at, through an intermediate profile (RAE 5214), from an initial design (RAE (NPL) 5213) by two stages of modification to the upper surface. This Report gives the basis for the initial design and describes how the modifications were made in order to effect changes in the measured pressure distributions. The aerodynamic characteristics of the final aerofoil (which has a maximum thickness of 9.7% chord) are compared with those for a 12% thick aerofoil (RAE (NPL) 5212) that is typical of those used in recent transport aircraft designs.

Although numerical design methods are now available, the experimental results obtained are still of value in giving an indication of what it is possible to achieve, not only in terms of the design condition but also in terms of the separation margins that apply.

The work described in this Report was carried out between 1970 and 1972.

2 THE DESIGN OF RAE (NPL) 5213

At the time of the design of the RAE (NPL) 5213 aerofoil, no theoretical method was available for calculating pressure distributions on aerofoils in supercritical conditions. The only theoretical results available, for supercritical aerofoils, were for a series of symmetric NLR sections[7] with isentropic recompressions in inviscid flow. Modifications to a particular one of these NLR sections were thus planned with the object of producing a lifting aerofoil which had the same upper surface pressure distribution in viscous flow, in the supercritical region, as the NLR section had in inviscid flow. However, as a first step the modifications were aimed at reproducing the desired pressure distribution on a lifting aerofoil in inviscid flow. Even with this approach to design there was still the basic difficulty of being unable to calculate the supercritical pressure distribution on the new aerofoil in order to check that it was in fact of the desired form. The only possible procedure was to calculate the pressure distribution on the NLR section using an approximate method valid only for subcritical flow, and then design the new section to have the same pressure distribution, as calculated by the same method, over the supercritical part of the other surface. To give the best chance of success in modifying the NLR section it was decided to retain exactly the same profile in the supercritical region and to retain the same attitude to the free stream direction. It was realised that the lifting aerofoil would have to be much thinner than the basic NLR section as the combination of thickness and camber velocities on the upper surface had to be the same as the thickness velocities for the symmetric NLR section. Furthermore it became apparent that the required reduction in thickness would be so large that the chord line had to be displaced vertically in order that an acceptable nose shape could be produced. This latter consideration necessitated a rearward shift of the leading-edge in addition to the vertical shift and it was found necessary to move the trailing edge rearwards by the same amount so as to retain the same extent of supercritical flow as a proportion of the overall chord.

The new chord line was kept parallel with the basic chord line so that the incidence of the lifting aerofoil was still zero.

With these aspects of the necessary modifications in mind we can now list various points that were considered when selecting the basic NLR aerofoil.

(1) The design Mach number must be sufficiently high.

(2) The section must be sufficiently thick to leave adequate thickness in the derived lifting aerofoil.

(3) The peak local Mach number should not be too high and should be as far back from the leading-edge as possible. Such features help to minimise the suction peak height at off-design conditions.

(4) The chord-wise extent of supercritical flow should be as large as possible in order to generate as much lift as possible without, at the same time, causing a danger of rear separation.

(5) The forward sonic point should be well back from the leading-edge so as to make the design change possible.

The selected aerofoil was 14.65% thick with a design Mach number of 0.776 and its theoretical isentropic pressure distribution is given in Fig.1. Also shown is the pressure distribution given by approximate theory for this aerofoil, using the first-order inviscid method of Ref.8. This was to form the target pressure distribution in the design of a new lifting aerofoil.

The aerofoil shape that was arrived at, at the end of the first stage in the design, is shown in Fig.2, in comparison with the basic NLR aerofoil (Profile No.7 of Ref.7). The reduced thickness and raised chord line are clearly evident. It is also seen that the raised chord line results in a rearward movement of the leading-edge (the new chord line intersects the NLR profile aft of its leading-edge and a modification to the basic profile is required to give a surface slope of 90° at the new leading-edge), but the new profile blends into the basic one ahead of the forward sonic point. In order to keep the same chord length as the basic aerofoil, the new trailing-edge cannot be taken as the point of intersection of the new chord line and the basic profile, and a new rear profile must be designed. In this case, the modification to the profile starts behind the rear sonic point and has the advantage of reducing the surface curvature in this region, which should be of benefit to the development of the pressure distribution as Mach number increases beyond the design value.

So far, no allowance has been made for viscous effects, and although the new profile (shown in Fig.2) reproduces the theoretical target pressure distribution in inviscid flow (see Fig.3) this is not the case for viscous flow. As the final aim is to reproduce the target pressure distribution in the practical case of viscous flow, some further modifications to the profile shown in Fig.2 are necessary. These take the form of a slight downward displacement

of the trailing-edge with appropriate reshaping of the rear profile (all upper surface modifications being aft of the rear sonic point). Theoretical pressure distributions for the final shape are given in Fig.4 and now the target pressure distribution is achieved except for a slight reduction of suction peak in viscous flow. This aerofoil was designated RAE (NPL) 5213 and tested in the 20in × 8in wind tunnel at Teddington.

3 WIND-TUNNEL TESTS

All aerofoils in the series discussed in this Report were tested in the 20in × 8in (0.51m × 0.20m)* wind-tunnel at Teddington with the models spanning the smaller dimension. The models were supported by tongues set into slots in optical glass plates which were mounted in turntables. These turntables could be rotated to give the desired angle of incidence. The junction between the ends of the model and the windows were sealed by means of rubber strips to prevent leakage between lower and upper surfaces of the model. Schlieren and shadowgraph systems were used for flow visualisation.

The chord length of all the models was 125 mm and tests were carried out with roughness bands along the whole span of the models to give boundary layer transition ahead of the shock-waves at, and near, the design conditions. For the 5213, 5214 and 5215 aerofoils the roughness band was composed of grains of carborundum sparsely distributed between 12% and 15% chord. The RAE (NPL) 5212 model had a band of the same grain size and distribution, but situated between 5% and 10% chord. As the wind-tunnel operated only at atmospheric stagnation pressure the Reynolds number varied from 1.5×10^6 at M = 0.5 to 2.4×10^6 at M = 0.8.

Values of lift and pitching moments were obtained from integration of the measured pressure distributions (see Table 2 for pressure hole positions) and drag was derived from wake survey using a Pitot traverse tube.

No corrections were applied to the results for interference effects, but the slotted walls of the tunnel (with an open area ratio of 0.0143) were designed to minimize both blockage and incidence effects.

4 ANALYSIS OF EXPERIMENTAL RESULTS FOR RAE (NPL) 5213

Fig.5 compares the measured pressure distribution with the target pressure distribution at the design condition of M = 0.775, C_L = 0.39 and it is immediately

---

* The actual vertical dimension of the test section was 0.46 m rather than 0.51 m with the particular walls used.

seen that the target pressure distribution has not been achieved. Local velocities over the forward part of the upper surface are too low, and those between 30% and 50% chord are too high, with a shock wave appearing at about 50% chord. In an attempt to explain these differences the detailed pressure distribution over the first 10% chord is plotted in Fig.6. It is seen that although the desired position of the sonic point has been attained, the Mach number gradient through the sonic point is not the same as for the NLR section. This suggests the possibility of a change in the shape of the sonic line with a resulting change in the characteristics in the supersonic flow region. Thus, although the sonic point and the surface slope in the supersonic region are correctly reproduced, the way in which the expansion waves are reflected back to the surface as compression waves is altered. The net velocity at the surface is thus different.

One might at this point question the accuracy of the model, particularly as the basic NLR profile has a rather special feature in the region of the velocity peak. This feature involves a very rapid (almost discontinuous) change in surface slope, as shown in Fig.7, giving a local peak in surface curvature. However, a slope discontinuity is not difficult to produce and the model inspection showed that any error in this region was extremely small (see Fig.7). It is concluded that the change in the pressure distribution is due to the overall change in the flow field that results from the introduction of circulation.

In spite of the difference in pressure distribution, and the appearance of a shock wave, the design condition has in fact been met without any rise in C_D (see Fig.8). Apparently, the shock wave that has appeared at the design condition is not significant as far as drag is concerned. In Fig.9 we show plots of C_L against M for constant values of α, and a plot of the boundary at which shock-induced separation occurs is superimposed. This boundary usually passes roughly through the peaks in the C_L against M curves but is in fact defined by the points at which divergence of the trailing-edge pressure occurs. (An illustration of the way in which this type of boundary is defined is given in Fig.25 and 28 which present results for the RAE 5215 aerofoil). It is seen in Fig.9 that an increase in M of 0.02 above the design value (0.775) is possible, at the design C_L (0.4), before shock-induced separation is encountered. Also, an increase in C_L of 0.23 is possible at the design Mach number before separation occurs. Thus, in the sense of aerofoil performance, the RAE (NPL)

5213 section is quite satisfactory. However, the measured pressure distributions for the RAE (NPL) 5213 aerofoil, given in Fig.6, suggest that there would be advantages in modifying the aerofoil upper surface so as to bring the pressure distribution closer to the shock-free NLR form. The reduction in velocity in the region of 50% chord with a corresponding reduction in shock strength should lead to delayed drag-rise and separation onset and hence improved aerofoil performance.

5 DESIGN OF UPPER SURFACE MODIFICATIONS TO RAE (NPL) 5213

It was decided to modify the model of the RAE (NPL) 5213 aerofoil in an attempt to produce performance improvements, and the main object of such modifications was to reduce the magnitude of local velocities in the mid-chord region and so reduce the strength of the shock wave at, and above, the design Mach number. Such a change in local velocity can be achieved by reducing surface curvature in that region of the chord, thereby cutting down the expansion that occurs there when the flow is locally supersonic (see Fig.5). Now a decrease in curvature can be effected by a suitable decrease in surface ordinates with the new profile blending back into the original profile at either end of the modified region. However, over each of these two blending regions there must be an increase in surface curvature which would cause extra local expansions and increased local velocities; thus, the chord-wise location of the blending regions was an important factor in the design of the modifications.

The profile modifications had to be arranged so that at the design Mach number the rear blending region, with its locally increased curvature, would lie behind the shock wave. However, as M increases above the design value and the shock moves back along the aerofoil, the region of increased curvature would eventually become enveloped in the supersonic flow region and would generate an undesirable expansion ahead of the shock, thereby increasing the shock strength. In redesigning the upper surface it was therefore necessary to keep the rear blending region as far back along the aerofoil as possible so as not to detract from the off-design performance of the aerofoil. The rear blending point could of course have been eliminated (or at least the associated curvature problem minimised) through the incorporation of a thick trailing-edge, but in the present case this was not permitted as the modification was required quickly and was therefore limited to one that involved only the removal of material from the model. The introduction of a thick trailing-edge would of course have involved the addition of material.

A local increase of curvature at the forward blending region would of course generate an extra expansion and higher velocities which would tend to alter the pressure distribution in the direction of the NLR pressure distribution. At this stage it is useful to examine the chord-wise variation of surface slope θ given in Fig.11 along with the plots of $\theta + \omega$ and $\theta - \omega$ where ω is the Prandtl-Meyer function. A local curvature increase will produce a more rapid fall in θ and a steepening of the slope distribution, as given in Fig.11, with an associated increase in ω. Now if this curvature increase is confined to the region $0.05 < x/c < 0.15$ then a connected points analysis[9] (using Fig.10) shows that the extra expansion waves generated there would return to the surface as compression waves well ahead of the shock position. For such a case, the local curvature increase would be unlikely to lead to an increase of shock strength at the design Mach number. On the other hand, at lower values of M and higher values of α for which supercritical flow exists with a shock wave standing well forward on the upper surface, it is to be expected that the local increase of curvature would lead to an increase of velocity (or decrease of pressure) immediately ahead of the shock wave and hence an increase of shock strength.

With these various considerations in mind the upper surface of RAE (NPL) 5213 was modified to give a new surface slope distribution as shown in Fig.12. The modified aerofoil was designated RAE 5214 and its upper surface ordinates (see Table 1) are given in Fig.13 along with those for the original aerofoil. It is clearly seen in Figs.12 and 13 that a decrease in curvature (i.e. a decrease in slope of the curve in Fig.12) in the mid-chord region requires an increase in curvature at the two blending regions. The pressure distribution given by the approximate theory for viscous flow for the new aerofoil at the design condition is given in Fig.14, and this indicates that the changes in local velocity, relative to those for RAE (NPL) 5213, are qualitatively of the desired form.

6 WIND-TUNNEL TEST RESULTS FOR RAE 5214

The experimental pressure distribution for the RAE 5214 aerofoil at the design condition is shown in Fig.15, and comparison with Fig.5 shows that the aims of the redesign of the upper surface have been met, in that local velocities have been increase in the range $0.05 < x/c < 0.25$ and decreased over the central part of the chord. However, the previous single shock wave has been replaced by two shock waves. The pressure distributions over the range of conditions tested

(Fig.16) show that the two-shock system exists only for a very small part of the range, and elsewhere the usual single shock system is found. The drag measurements (Fig.17) show that there has been a slight increase in drag at the design condition as a result of the modifications and this may be due to a thickening of the boundary-layer resulting from the combined effects of two shock waves and a greater extent of adverse pressure gradient. However, at $\alpha = 0.35$ the drag-rise has been delayed slightly by the modification and so has separation onset. The latter is implied by the fact that C_L maintains its increase with M to a higher value of M (see Fig.18). A comparison of the pressure distributions shown in Figs.10a and 16a shows that the strength of the shock at $M = 0.8$ is less for the RAE 5214 aerofoil.

As incidence increases, it is seen that a drag-creep appears for the new aerofoil giving higher values of C_D over a certain range of Mach number. This usually seems to be associated with a stronger shock, or a less favourable pressure gradient ahead of the shock or a combination of the two. However, at the higher Mach numbers, for each value of incidence, the shock stands well back on the aerofoil and the reduced surface curvature in the mid-chord region begins to take effect in reducing shock strength. This allows a slightly delayed separation onset for the RAE 5214 aerofoil and higher values of C_L are attained.

The objective of the upper surface modification has been achieved in that a slight delay in drag-rise and separation onset has been effected at the design C_L. As was expected, these gains have been at the expense of losses, in the form of drag-creep, at off-design conditions.

7 THE DESIGN OF RAE 5215 AND ITS MEASURED CHARACTERISTICS

In an attempt to get a further improvement in drag-rise Mach number at design C_L, a third aerofoil (RAE 5215) was designed. As a completely new model was to be made, a thick trailing-edge was incorporated and this allowed a greater reduction in surface curvature over the mid-chord region than was possible with RAE 5214. This of course led to a further increase in curvature over the forward part of the upper surface, but the increase was minimised through a rearward shift of the crest position. The surface slope distribution for this new aerofoil is given in Fig.19, where it is compared with those for the previous two aerofoils, and the upper surface ordinates (see Table 1) are plotted in Fig.20. Fig.21 shows the pressure distribution given by the approximate theory for viscous flow and it is seen that the changes in upper

surface pressure distribution, relative to the pressure distribution for RAE (NPL) 5213, are qualitatively the same as those for RAE 5214 but of greater magnitude.

The experimental results show that the RAE 5215 aerofoil has an even greater degree of drag-creep than the RAE 5214 section (Fig.22), but there is an improvement at the design incidence ($\alpha = 0.35$) in that the final rapid drag-rise has been delayed slightly. It is at this particular value of α that a rather unusual variation of C_D with M is found, with C_D rising gradually until $M = 0.785$ where it begins to drop to a slightly lower value at $M = 0.8$ before the final rapid drag-rise begins. This characteristic was found, to a much greater degree, by Hall[2] in his work on high speed aerofoils. In the present case this feature of the drag variation seems to be because the changes in upper surface profile have led to a progressive decrease in shock strength at $M = 0.8$ (see Figs.10a, 16a and 24a) when the shock stands well back on the aerofoil, but a progressive increase in shock strength at slightly lower Mach numbers when the shock lies well forward on the aerofoil. The very rapid rearward movement of the shock wave for M between 0.775 and 0.8 is an important factor, as this takes the shock wave from a position just behind the region of curvature increase to a position just behind the region of curvature decrease in a very short interval of Mach number.

Fig.23 shows that there has been very little change, relative to the RAE 5214 aerofoil, in lifting characteristics. This means that an $\alpha = 0.35$ the margin between separation onset and drag-rise has been reduced for the RAE 5215 section and is now quite small. This is explained by the very rapid rise in shock strength as M increases beyond 0.8 and the shock wave moves across the region of increased curvature (see Figs.24 and 19). The margin could presumably be considerably improved if the region of curvature increase could be moved further aft, and this would be possible with either a still thicker trailing-edge or a much steeper adverse pressure gradient over the last 10% chord. It was desirable to avoid the latter because of the danger of invoking a rear separation at the low Reynolds number of the tests.

The RAE 5215 aerofoil was tested over a much wider range of incidence than were the previous aerofoils and the measured pressure distributions are given in Fig.24. Here, the essentially flat nature of the supercritical part of the pressure distributions will be noted. Figs.25 and 26 give the complete plots of the variation of C_L with M, and Fig.27 gives the measured values of C_D.

Superimposed on Fig.24 is the separation boundary which is derived from the divergence of trailing-edge pressure as presented in Fig.28. In the latter figure, the trailing-edge pressure ratio is plotted against M for constant values of α and the point of divergence of this ratio corresponds to the onset of trailing-edge separation. In Fig.29 the pitching-moment coefficient C_m (about the quarter-chord position) is plotted against M for various values of α. A particular feature of the plot is the rapid and large increase in nose-down pitching-moment as Mach number increases. This of course follows from the rapid rearward extension of the supercritical region on the upper surface. At the lower values of Mach number, pitching-moment varies only a small amount with incidence; thus the variation of C_m with M at the design value of M^2C_L is not very different from the variation of C_m with M at $\alpha = 0.35$. This variation of C_m corresponds to a centre of pressure that moves from 30% chord at $M = 0.5$ to 50% chord at $M = 0.8$, and is likely to create problems in maintaining trim with an aircraft using this aerofoil as a wing section. However, on the credit side it will be seen that an increase of C_L above the design value produces a stabilising nose-down pitching-moment.

All the measured force and moment coefficients for this aerofoil are listed in Table 3.

8 COMPARISON OF RAE 5215 WITH RAE (NPL) 5212

At this stage it is interesting to compare the RAE 5215 section with an earlier aerofoil, RAE (NPL) 5212, which was designed in a more conventional way. This aerofoil was designed using the calculation method of Ref.8 to have just slightly supercritical conditions over the forward part of the upper surface at $M = 0.7$ and $C_L = 0.5$. At such conditions the method is at the limits of its range of validity (essentially valid only for subcritical flow) but can still be relied upon to give a reasonably accurate prediction of the pressure distribution. The design principle was to achieve a slightly sloping sonic roof-top pressure distribution back to about 50% chord, which is typified by the pressure distribution shown in Fig.30. Here, the pressure distribution is contrasted with that for the RAE 5215 aerofoil at the same conditions, but the nearly identical form of rear loading should be noted. This commonality allows a true comparison of the different developments of supercritical conditions on the two aerofoils to be made, but it must be pointed out that there is an appreciable difference in the thickness of the two aerofoils (see Fig.31), the RAE (NPL) 5212 section being 12% thick. Obviously, thickness is an important factor in the difference

between the characteristics of these aerofoils and the charts of Ref.10 show that at a C_L of 0.4 the thinner section could be expected to have an increase of 0.02 in drag-rise Mach number relative to the RAE (NPL) 5212 aerofoil, assuming the same type of pressure distribution (i.e. sonic roof top back to 50% chord). However, it is seen in Figs.33 and 34 that the difference in drag-rise Mach number for the two sections at $C_L = 0.4$ is as high as 0.065 and the difference in separation Mach number is a little less at 0.055. Thus the difference in design philosophy is seen to produce an appreciable improvement in performance for the RAE 5215 aerofoil, even when the decrease in thickness is taken into account. Fig.30 is a clear illustration of how thickness (Fig.31) and upper-surface slope distribution (Fig.32), and hence curvature, have been chosen for the RAE 5215 aerofoil to give high local velocities over the forward part of the chord and low local velocities on the mid-chord region. At the higher Mach numbers, this allows the RAE 5215 aerofoil to attain a higher incidence, and hence a higher C_L for a given Mach number and given shock strength, as shown in Fig.35a. Also, a higher Mach number can be attained for a given shock strength at a given C_L, as demonstrated by Fig.35b. This results in a considerable displacement of the boundary for the onset of shock-induced separation (Fig.34) at the higher values of Mach number. However, a penalty is paid in the form of a decreased $C_{L_{max}}$ at Mach numbers below 0.65. This is to be expected at conditions where the shock wave forms well forward on the upper surface and is strengthened by the increased suction peak. (Compare, for instance, the pressure distributions for $M = 0.5$ in Figs.24h and 36j and 36k.)

With reference to the separation boundaries shown in Fig.34 it should be pointed out that over the lower end of the Mach number range, the boundaries are really plots of the maximum values of C_L taken from Figs.26 and 38. However, these values are not well defined as incidence was not taken sufficiently high in the tests to reach a true maximum value of C_L. Furthermore, it is seen in Figs.26 and 38 that for the lower Mach numbers the lift slopes begin to fall off well before the maximum values of C_L are attained. This seems to occur only when the shock wave on the upper surface is located in the first 10% or 15% of the chord. The latter feature corresponds to different ranges of M, depending upon the aerofoil geometry, being $M < 0.65$ for RAE 5215 and $M < 0.60$ for RAE (NPL) 5212 (for some aerofoils the range is $M < 0.55$). The most probable explanation for the gradual falling-off of the lift slope is that with a combination of low R and a shock that is well forward on the aerofoil,

considerable thickening of the boundary-layer occurs leading to a reduced rate of increase of circulation. It has been found with aerofoils tested both as a 125mm chord model in the 20in × 8in (0.51m × 0.20m) tunnel and also as a 250mm chord model in the 36in × 14in (0.90m × 0.36m) tunnel, that for the latter case, with double the Reynolds number, the gradual stall characteristic has disappeared and a higher value of maximum C_L attained. With this in mind, the separation boundaries as presented in Fig.34 could be at least 10% too low at the low end of the Mach number range.

As far as transport aircraft are concerned, the drag-rise Mach number is important as this sets the limit to cruising speed. However, it is equally important that there should be adequate margins between the cruise condition and separation onset. Thus, it is of interest to return to Fig.33 and compare the separation margin for the two aerofoils. It is found that at $C_L = 0.4$, when the RAE (NPL) 5212 is at $M = 0.735$ and the RAE 5215 aerofoil is at $M = 0.785$ then they both have the same Mach number margin (0.025) to separation and the same C_L margin (0.2 or 50% of the design value) to separation. Similarly, at $C_L = 0.5$, when the RAE (NPL) 5212 aerofoil is at $M = 0.725$ and the RAE 5215 aerofoil is at $M = 0.775$ then they both have the same Mach number margin (0.025) and the same C_L margin (0.02 or 40% of the design value). In each case the aerofoil concerned can be said to be either at or below the drag-rise Mach number, and in terms of potential cruise condition the RAE 5215 aerofoil has a 0.05 advantage in two-dimensional Mach number. Judged on this basis, the advantage is somewhat less than indicated by a straight comparison of drag-rise Mach numbers, because the RAE 5215 aerofoil has a smaller margin between drag-rise and separation onset than has the RAE (NPL) 5212 aerofoil. However, there is still an appreciable gain coming from the new approach to design, even allowing for the expected gain from reduced thickness.

On comparing the pitching-moments for the two aerofoils (Figs.29 and 41) it is seen that there is much less variation of C_m with M for the RAE (NPL) 5212 aerofoil, with a corresponding reduction in the movement of the centre of pressure at constant values of M^2C_L. On the other hand, the increase of nose-down pitching-moment with increase of incidence at the design Mach number is much less pronounced for the RAE (NPL) 5212 section, indicating a lower degree of stability.

9 CONCLUDING REMARKS

Although the original design approach employed did not produce an aerofoil with a shock-free pressure distribution at the design condition, a successful design was achieved in the sense that the target performance was achieved with a drag-rise Mach number of 0.78 at a lift coefficient of 0.4. Modifications to the upper surface produced some delay in drag-rise at the design incidence but produced increases in drag at off-design conditions. However, a feature of the final design was a peak value of maximum C_L (1.06) that occurred at a Mach number as high as 0.7. For lower values of Mach number the maximum C_L dropped to about 1.0.

The performance of the last of the three designs has been compared with that of a more conventional, although thicker design, which is more typical of present day aircraft. The importance of the type of pressure distribution, in association with the appropriate thickness to chord ratio, in achieving improved performance at the higher Mach numbers has been demonstrated.

An examination of the pressure distributions show that at the design condition the upper surface shock sits at about 60% chord, and a strong rear pressure gradient has been avoided. This was a deliberate design aim so as to avoid the possibility of a rear separation at the low Reynolds numbers of the tests. At a much higher Reynolds number, an aerofoil could be designed to have a shock wave that sits much further aft, thereby providing an appreciable increase in C_L . Thus the performance of the present aerofoil (RAE 5215) should not be taken to be the best that can be attained.

Table 1

AEROFOIL ORDINATES

X/c	5212		5213 Zu/c	5214 Zu/c	5215 Zu/c	5213 to 5215 ZL/c
	Zu/c	ZL/c				
0	0	0	0	0	0	0
0.00050	0.00424	-0.00347	0.00522	0.00522	0.00522	-0.00410
0.00100	0.00603	-0.00482	0.00732	0.00732	0.00732	-0.00545
0.00160	0.00765	-0.00599	0.00925	0.00925	0.00925	-0.00665
0.00241	0.00943	-0.00723	0.01128	0.01128	0.01128	-0.00785
0.00350	0.01142	-0.00855	0.01343	0.01343	0.01343	-0.00900
0.00500	0.01371	-0.01001	0.01580	0.01580	0.01580	-0.01030
0.00650	0.01567	-0.01121	0.01778	0.01778	0.01778	-0.01139
0.00800	0.01743	-0.01224	0.01940	0.01940	0.01940	-0.01228
0.00961	0.01914	-0.01322	0.02090	0.02090	0.02090	-0.01316
0.01500	0.02407	-0.01586	0.02480	0.02480	0.02480	-0.01533
0.02153	0.02877	-0.01831	0.02841	0.02841	0.02841	-0.01727
0.03000	0.03341	-0.02090	0.03216	0.03216	0.03216	-0.01947
0.03806	0.03689	-0.02295	0.03496	0.03496	0.03496	-0.02118
0.05904	0.04325	-0.02723	0.04029	0.04029	0.04033	-0.02459
0.08427	0.04904	-0.03132	0.04444	0.04434	0.04421	-0.02786
0.11349	0.05427	-0.03509	0.04828	0.04776	0.04719	-0.03074
0.14645	0.05900	-0.03840	0.05170	0.05045	0.04995	-0.03332
0.18280	0.06309	-0.04141	0.05476	0.05276	0.05231	-0.03556
0.22221	0.06647	-0.04385	0.05719	0.05480	0.05427	-0.03731
0.26430	0.06918	-0.04580	0.05904	0.05640	0.05581	-0.03856
0.30866	0.07114	-0.04696	0.06021	0.05744	0.05697	-0.03915
0.35486	0.07231	-0.04715	0.06061	0.05778	0.05763	-0.03889
0.40245	0.07261	-0.04619	0.06017	0.05742	0.05779	-0.03773
0.45099	0.07207	-0.04401	0.05892	0.05642	0.05735	-0.03560
0.50000	0.07051	-0.04051	0.05688	0.05478	0.05637	-0.03232
0.54901	0.06791	-0.03539	0.05394	0.05234	0.05462	-0.02788
0.59755	0.06424	-0.02954	0.05017	0.04917	0.05208	-0.02267
0.64514	0.05948	-0.02324	0.04574	0.04524	0.04876	-0.01716
0.69134	0.05402	-0.01736	0.04087	0.04071	0.04455	-0.01199
0.73570	0.04815	-0.01245	0.03586	0.03586	0.03976	-0.00768
0.77779	0.04202	-0.00844	0.03082	0.03082	0.03472	-0.00424
0.81720	0.03579	-0.00537	0.02581	0.02581	0.02971	-0.00175
0.85355	0.02976	-0.00310	0.02094	0.02094	0.02484	-0.00010
0.88651	0.02403	-0.00153	0.01641	0.01641	0.02031	0.00085
0.91573	0.01863	-0.00055	0.01236	0.01236	0.01626	0.00130
0.94096	0.01336	-0.00006	0.00870	0.00870	0.01260	0.00126
0.96194	0.00861	0.00011	0.00562	0.00562	0.00950	0.00098
0.97847	0.00465	0.00009	0.00302	0.00302	0.00706	0.00062
0.99039	0.00197	0.00005	0.00133	0.00133	0.00525	0.00029
0.99759	0.00047	0.00001	0.00034	0.00034	0.00416	0.00006
1.0	0	0	0	0	0.00380	0

Table 2

CHORDWISE POSITIONS OF MODEL PRESSURE HOLES

RAE (NPL) 5212	
Upper	Lower
0	
0.005	0.003
0.01	0.01
0.02	0.05
0.04	0.14
0.08	0.27
0.15	0.40
0.22	0.50
0.28	0.60
0.34	0.70
0.40	0.80
0.46	0.90
0.52	0.96
0.58	
0.64	
0.70	
0.80	
0.90	
0.96	
1.00	

RAE 5213-5	
Upper	Lower
0	
0.01	0.01
0.02	0.03
0.04	0.06
0.06	0.14
0.10	0.27
0.16	0.40
0.22	0.50
0.28	0.60
0.34	0.70
0.40	0.80
0.46	0.90
0.52	0.96
0.58	
0.64	
0.70	
0.80	
0.90	
0.96	
1.00	

Table 3

RAE 5215 - TABULATED DATA

α	M	C_L	C_D	$C_{m_{\frac{1}{4}c}}$	α	M	C_L	C_D	$C_{m_{\frac{1}{4}c}}$
-0.15	0.75	0.259	-	-0.0826	2.85	0.50	0.583	0.0110	-0.0642
	0.775	0.270	0.0099	-0.0861		0.60	0.642	0.0119	-0.0671
	0.8	0.280	0.0105	-0.0920		0.65	0.663	0.0142	-0.0663
	0.825	0.303	0.0146	-0.1138		0.70	0.788	0.0207	-0.0698
	0.85	0.179	-	-0.1035		0.725	0.884	-	-0.0870
						0.75	0.929	-	-0.1287
0.35	0.60	0.301	0.0099	-0.0671					
	0.70	0.330	0.0100	-0.0769	3.85	0.50	0.712	0.0121	-0.0666
	0.75	0.361	0.0103	-0.0810		0.60	0.781	0.0158	-0.0622
	0.775	0.385	0.0107	-0.0860		0.65	0.826	-	-0.0595
	0.788	0.395	0.0110	-0.0892		0.675	0.903	-	-0.0635
	0.80	0.432	0.0107	-0.0962		0.70	0.992	-	-0.0777
	0.815	0.427	0.0148	-0.1089		0.725	1.033	-	-0.1087
	0.825	0.411	-	-0.1216					
					4.85	0.50	0.857	-	-0.0614
0.85	0.60	0.363	0.0098	-0.0699		0.60	0.879	-	-0.0541
	0.70	0.405	0.0103	-0.0760		0.65	0.986	-	-0.0553
	0.75	0.450	0.0112	-0.0812		0.675	1.028	-	-0.0638
	0.775	0.503	0.0124	-0.0870		0.70	1.060	-	-0.0806
	0.785	0.534	-	-0.0936					
	0.80	0.541	-	-0.1128	5.35	0.65	1.034	-	-0.0556
	0.815	0.490	-	-0.1178					
					5.85	0.50	0.951	-	-0.0557
1.35	0.60	0.427	-	-0.0676		0.60	0.962	-	-0.0550
	0.70	0.473	0.0110	-0.0761		0.625	0.975	-	-0.0542
	0.725	0.506	0.0117	-0.0772		0.65	1.026	-	-0.0599
	0.75	0.557	0.0134	-0.0794					
	0.76	0.601	0.0143	-0.0848	6.35	0.60	0.987	-	-0.0535
	0.775	0.633	-	-0.0977					
	0.79	0.633	-	-0.1166	6.85	0.50	1.007	-	-0.0477
	0.80	0.607	-	-0.1230					
1.85	0.60	0.494	0.0104	-0.0675					
	0.70	0.578	0.0126	-0.0726					
	0.725	0.633	0.0142	-0.0755					
	0.75	0.719	-	-0.0890					
	0.775	0.738	-	-0.1200					

REFERENCES

No.	Author	Title, etc.
1	L.T. Goodmanson	Transonic transports. Astronautics and Aeronautics, AIAA, November 1971
2	D.J. Hall V.G. Quincey R.C. Lock	Some results of wind-tunnel tests on an aerofoil section (NPL 9510) combining a 'peaky' upper surface pressure distribution with rear loading. ARC CP No.1292 (1969)
3	E.M. Murman J.D. Cole	Calculation of plane steady transonic flows. AIAA Journal, Vol.9, No.1, pp.114-121, January 1971
4	J.A. Krupp E.M. Murman	The numerical calculation of steady transonic flows past thin lifting airfoils and slender bodies. AIAA Paper 71-566, Palo Alto, California (1971)
5	A.F. Jones M.C.P. Firmin	On the calculation of viscous effects on the super-critical flow over an aerofoil. RAE Technical Report 72233 (1972)
6	C. Albone D. Catherall M.G. Hall Gaynor Joyce	An improved numerical method for solving the transonic small perturbations equations for the flow past a lifting aerofoil. RAE Technical Report 74056 (1974)
7	H.J. Baurdoux J.W. Boerstoel	Symmetric transonic potential flows about quasi-elliptical aerofoil sections. NLR TR 69007-U
8	R.C. Lock P.G. Wilby B.J. Powell	The prediction of aerofoil pressure distributions for sub-critical viscous flows. The Aeronautical Quarterly, Vol.XXI, Part 3, August 1970
9	H.H. Pearcey	The aerodynamic design of section shapes for swept wings. Advances in Aeronautical Sciences, Vol.3, Pergamon Press Ltd. (1962)

REFERENCES (concluded)

No.	Author	Title, etc.
10	-	Drag-rise Mach number of aerofoils having a specified form of pressure distribution. Royal Aeronautical Society, TDM 71019

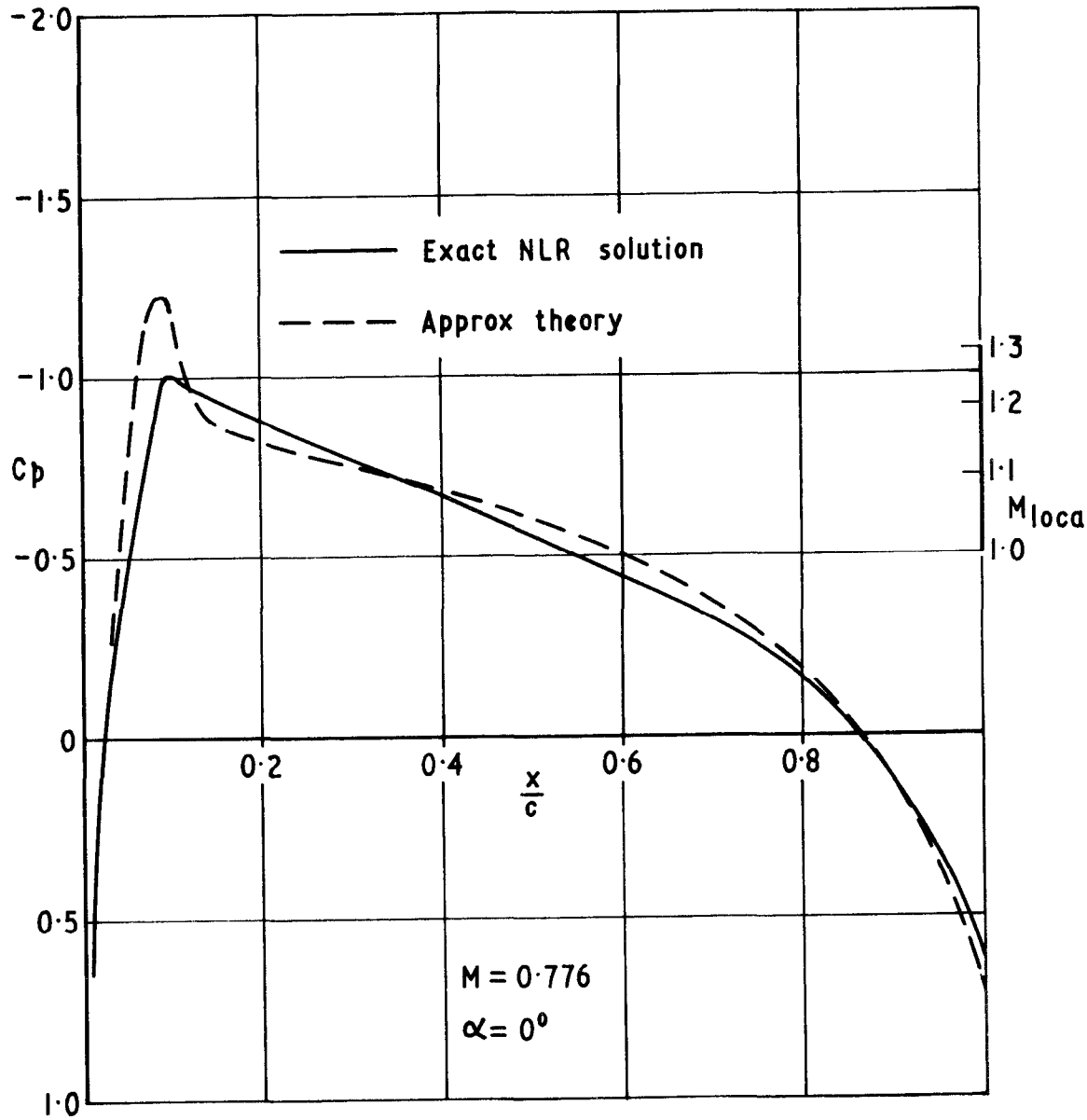

Fig. 1 Upper surface target pressure distribution

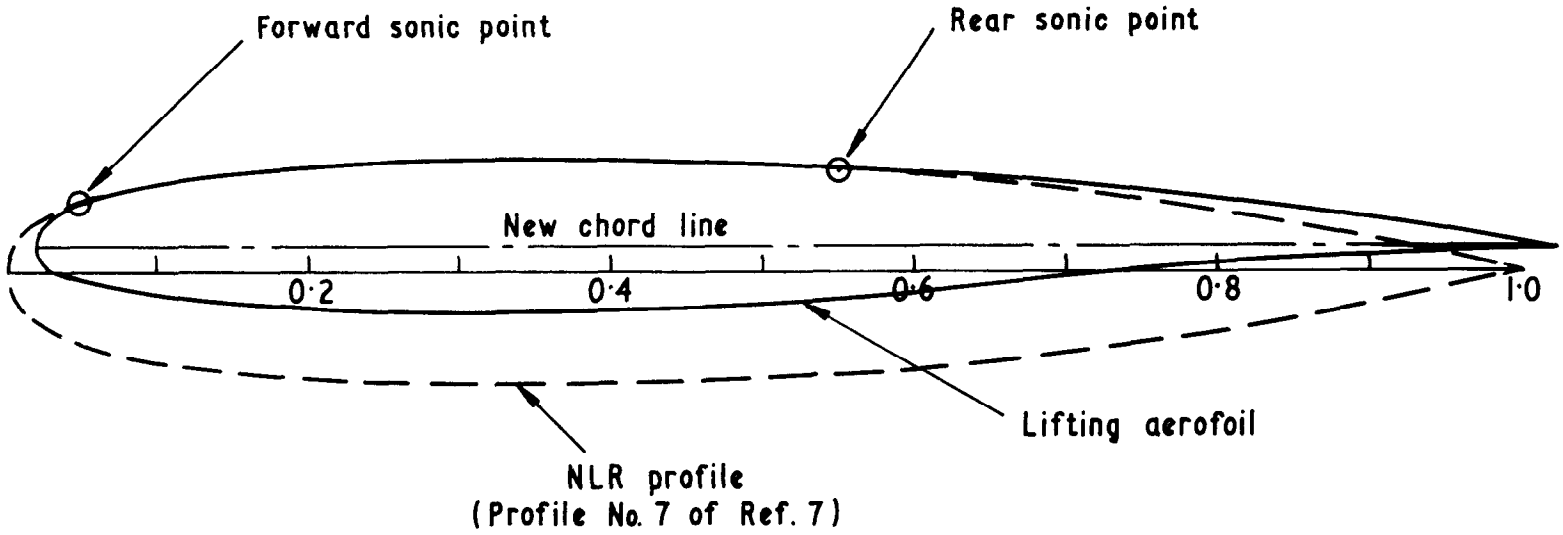

Fig. 2 Lifting profile as developed from basic symmetric aerofoil

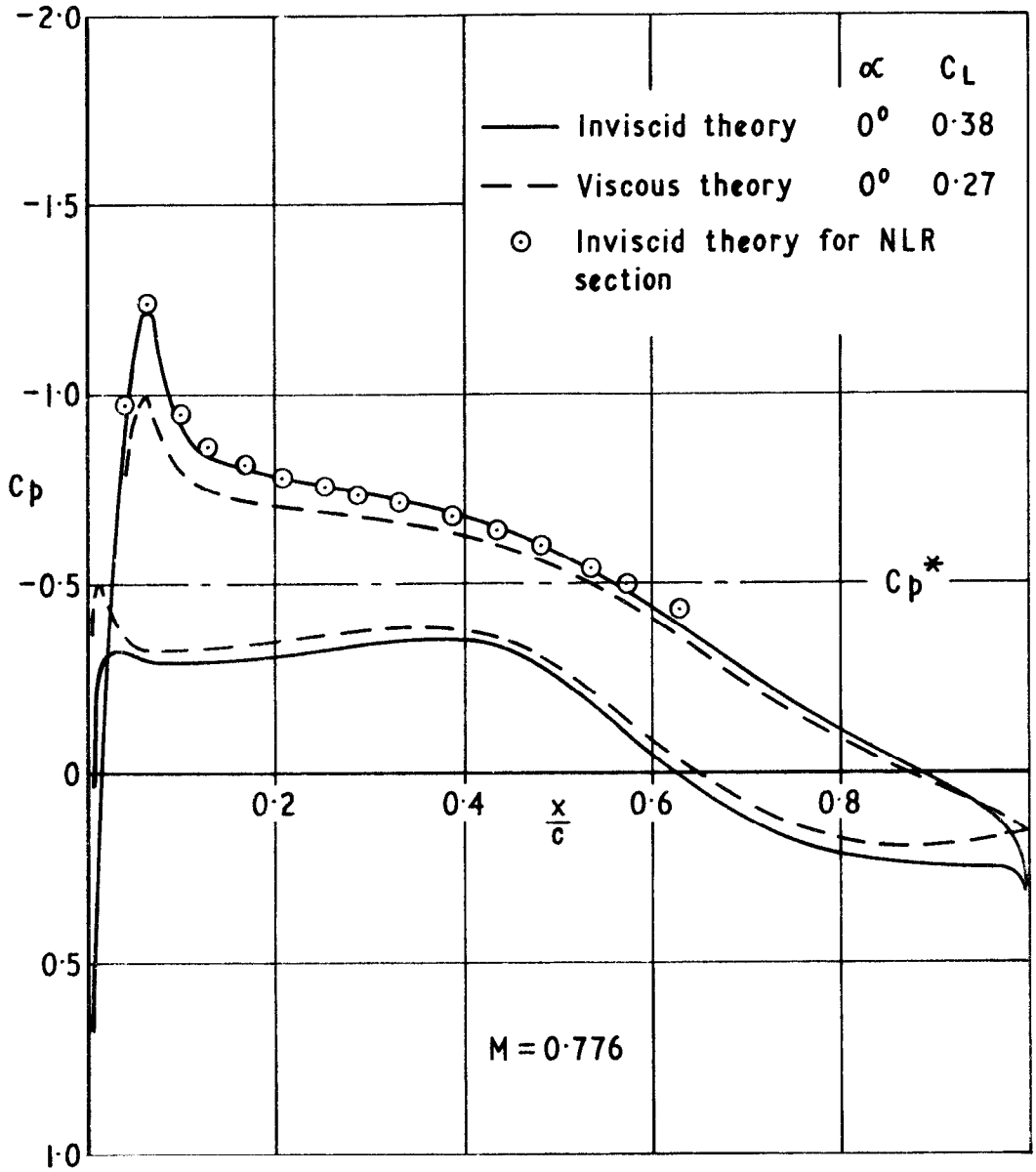

Fig. 3 Theoretical pressure distribution for inviscid design

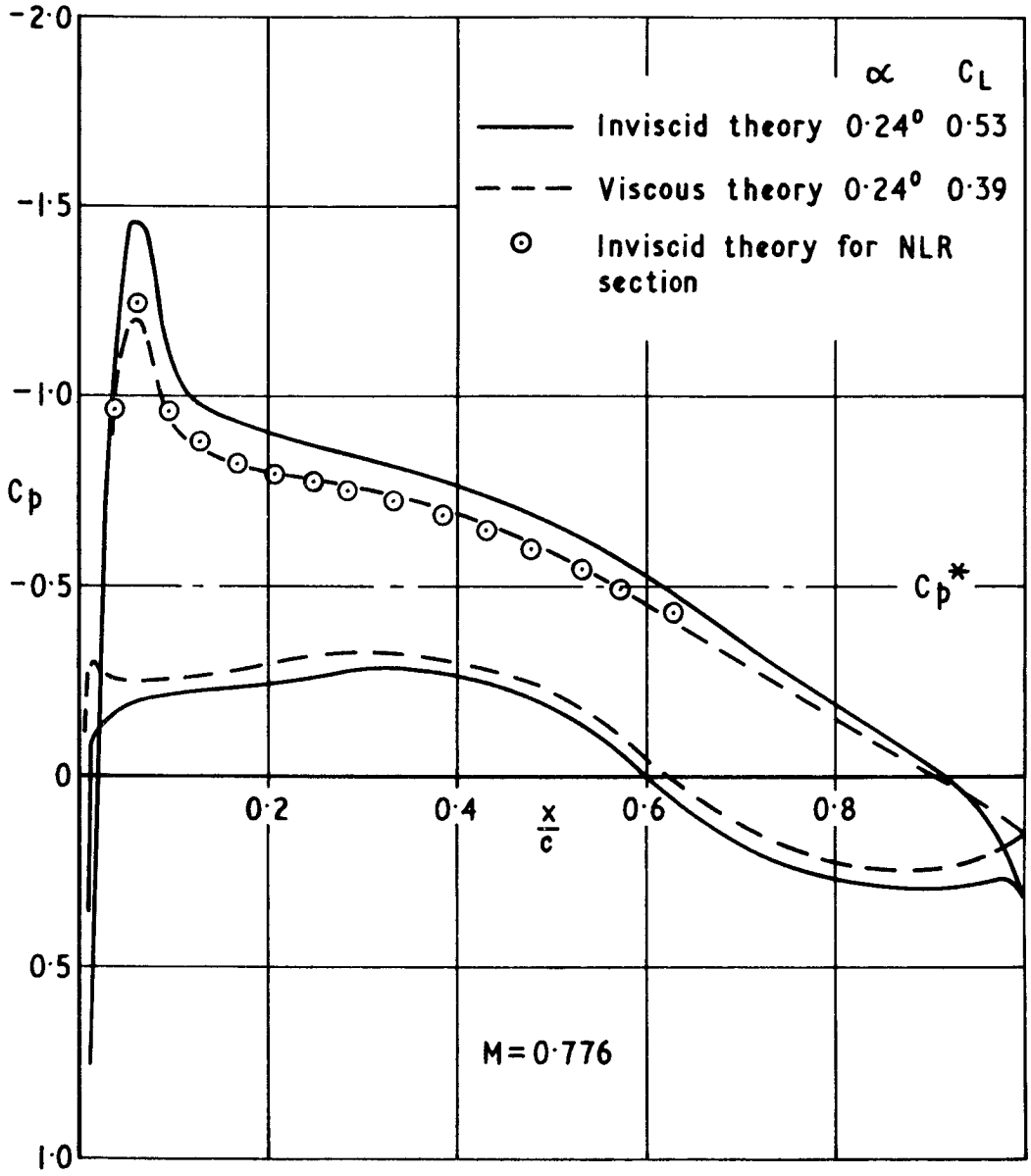

Fig. 4 Theoretical pressure distribution for profile when modified for viscous effects

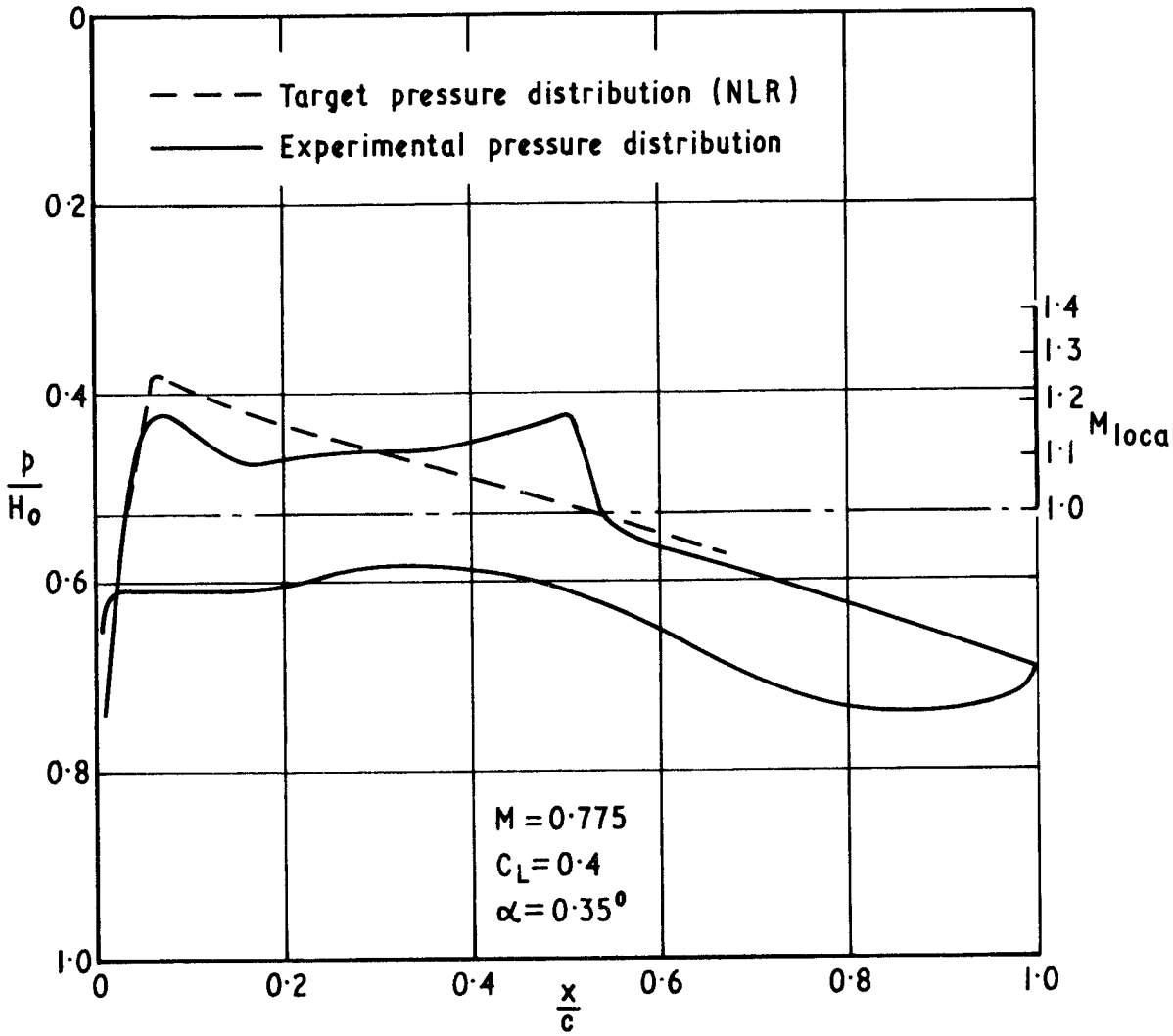

Fig. 5 Experimental pressure distribution for RAE (NPL) 5213 at design condition

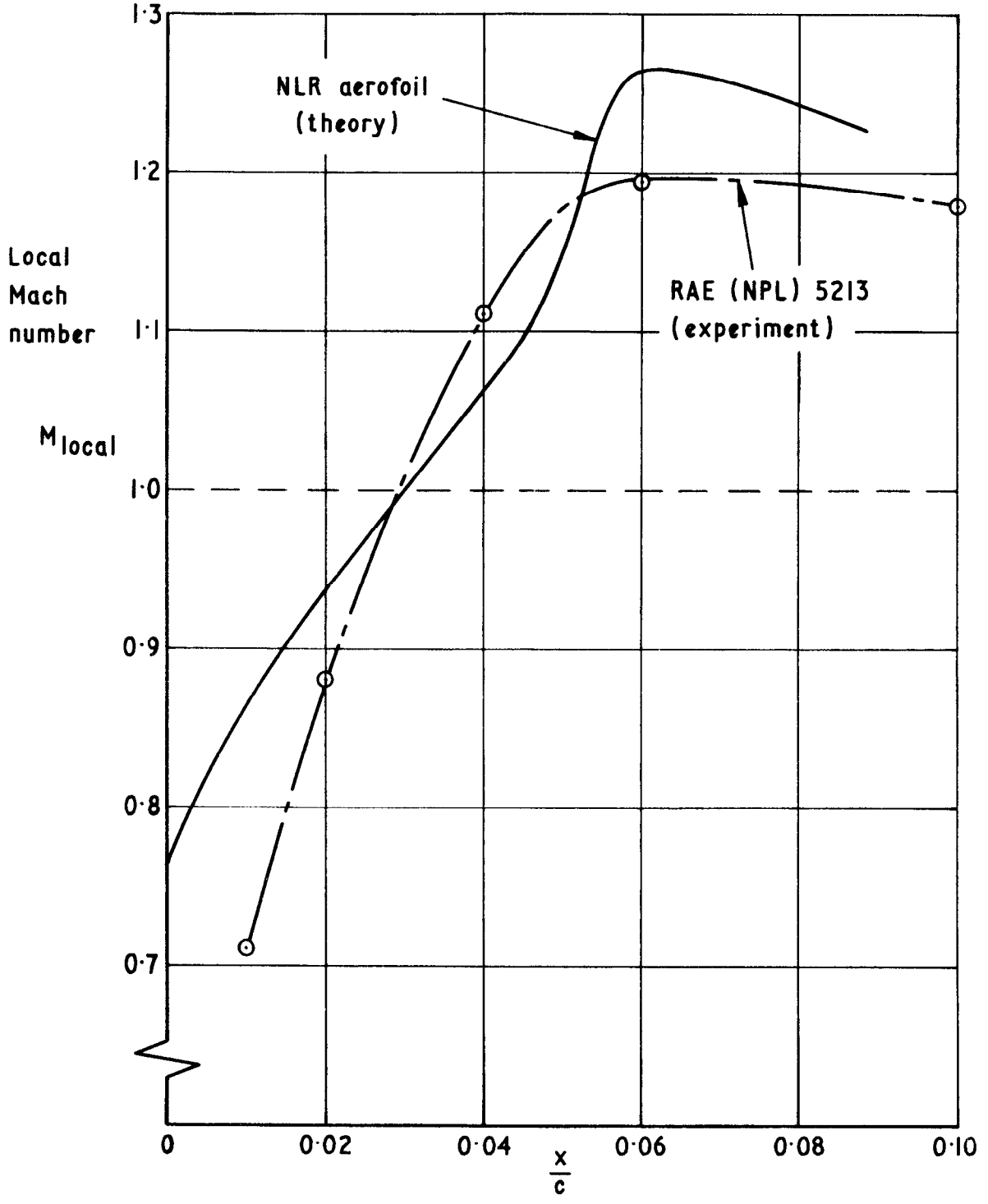

Fig. 6 Velocity distribution in region of the sonic point for RAE (NPL) 5213

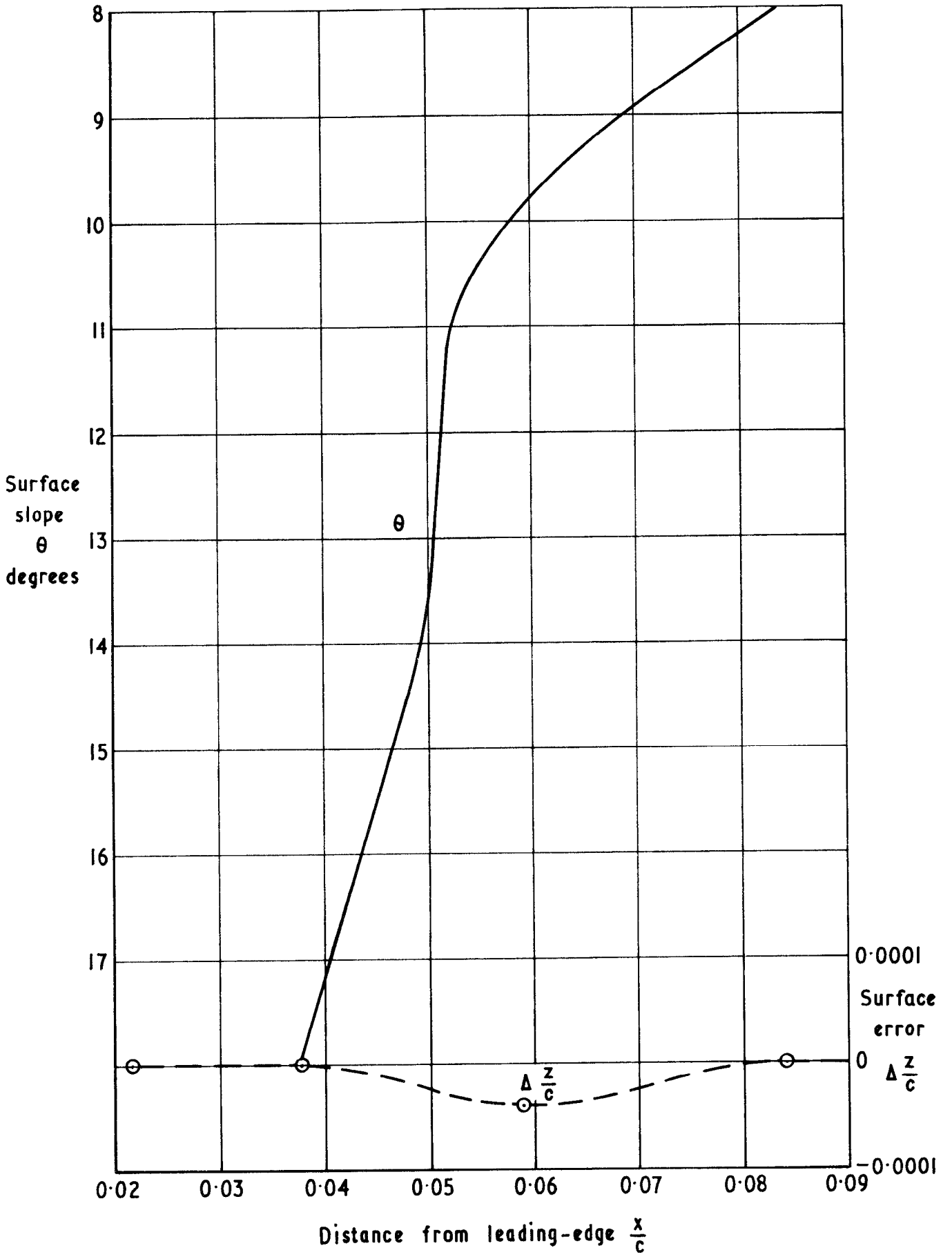

Fig. 7 Details of upper surface profile in leading-edge region

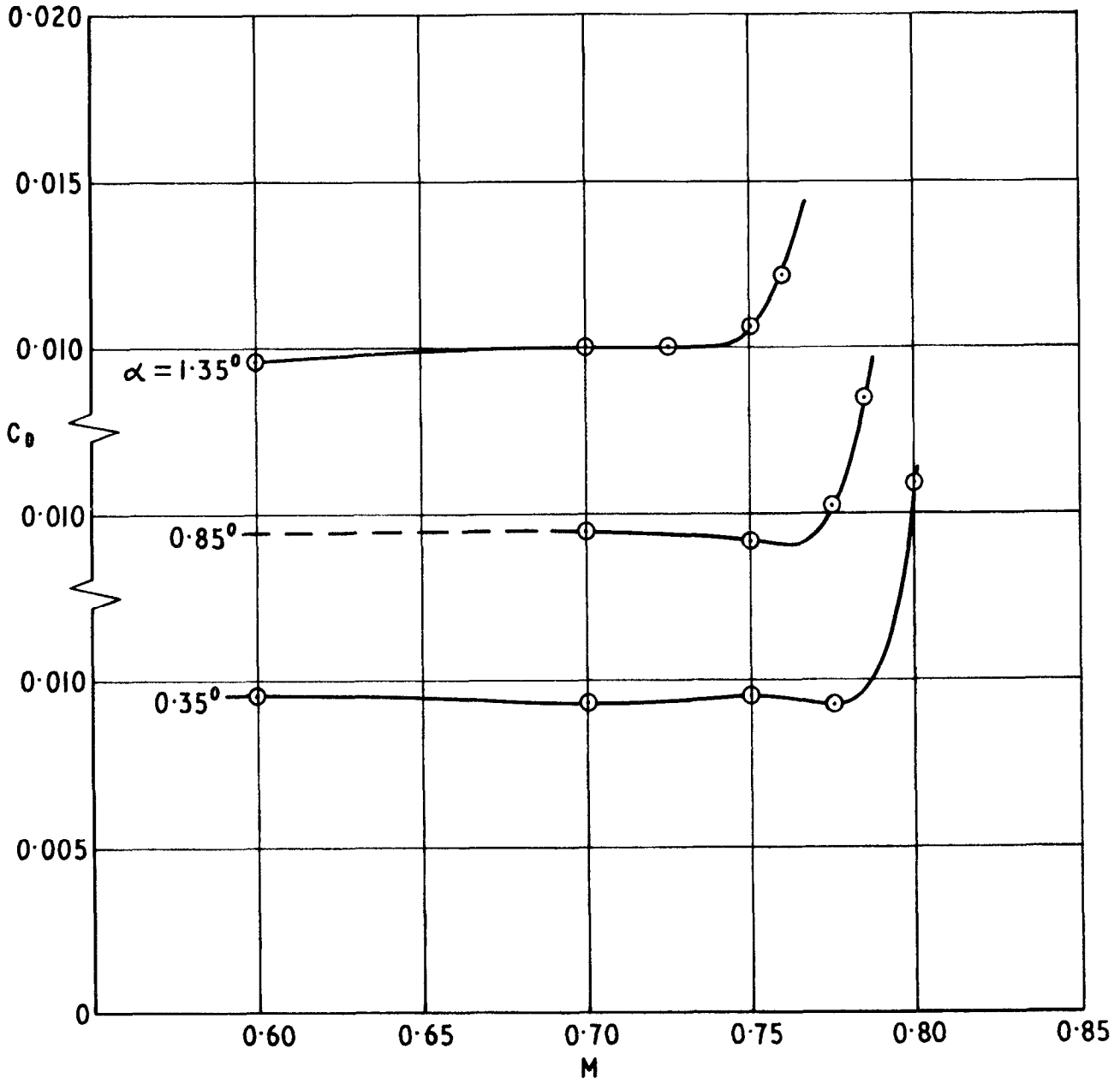

Fig. 8 Measured values of drag coefficient for RAE (NPL) 5213

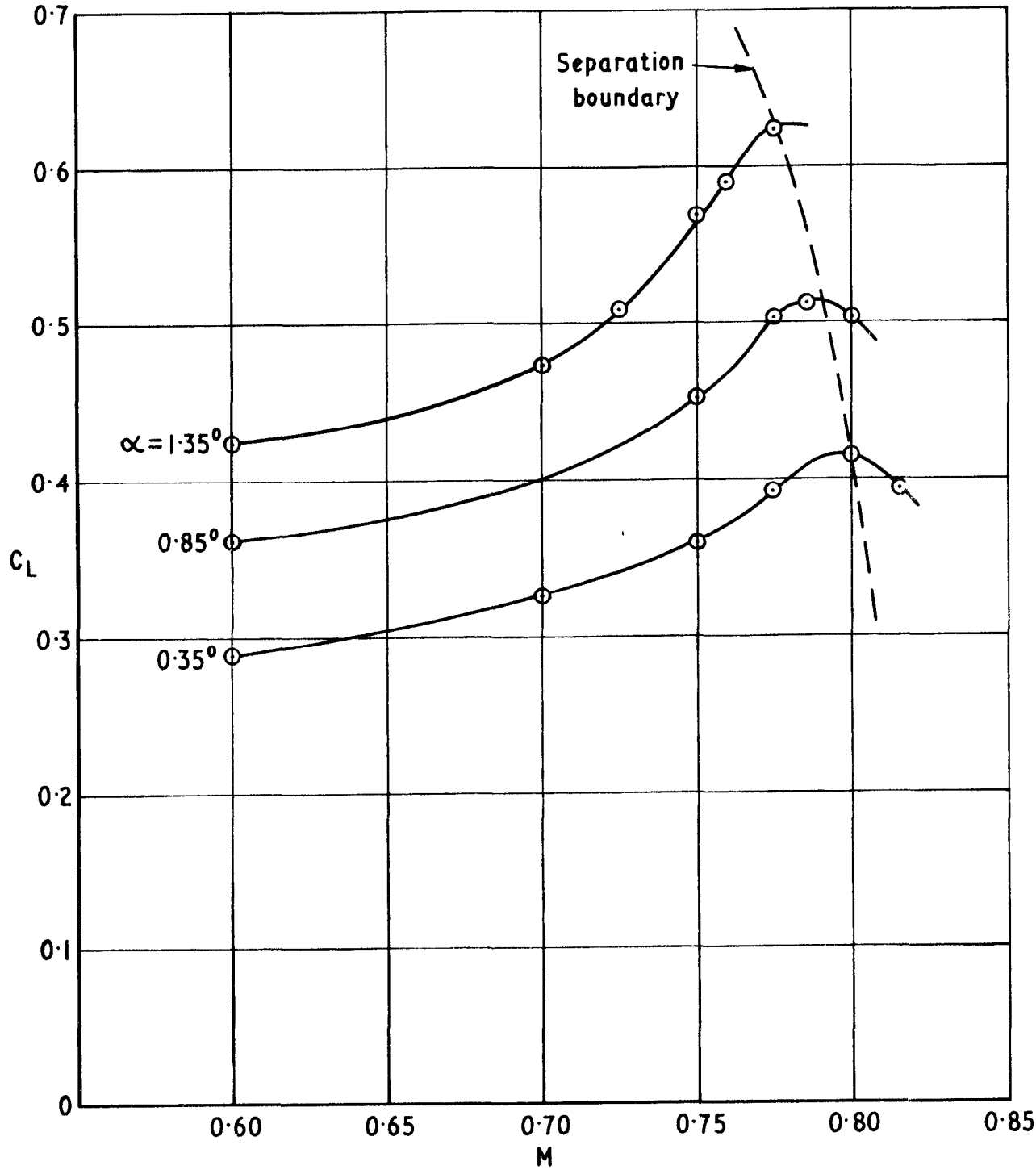

Fig. 9 Measured values of lift coefficient for RAE (NPL) 5213

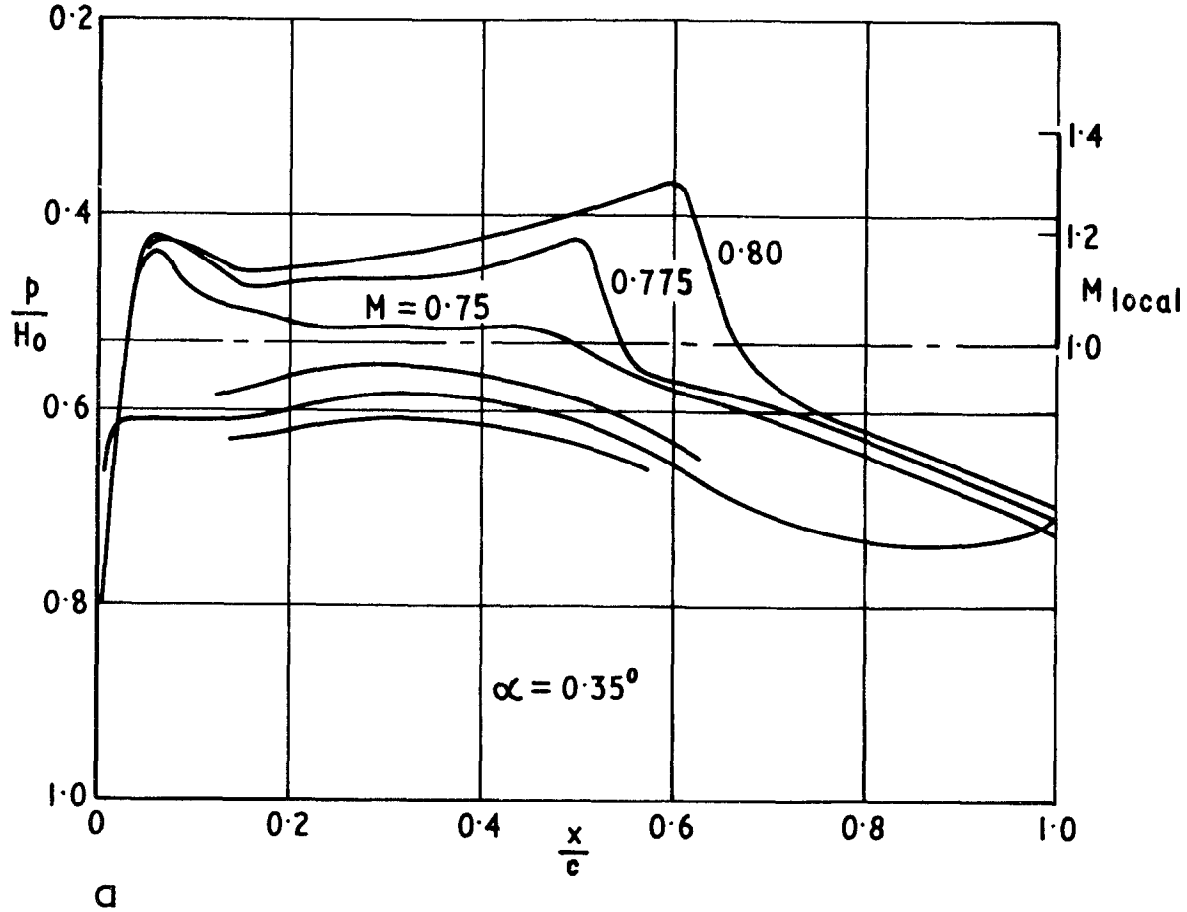

a

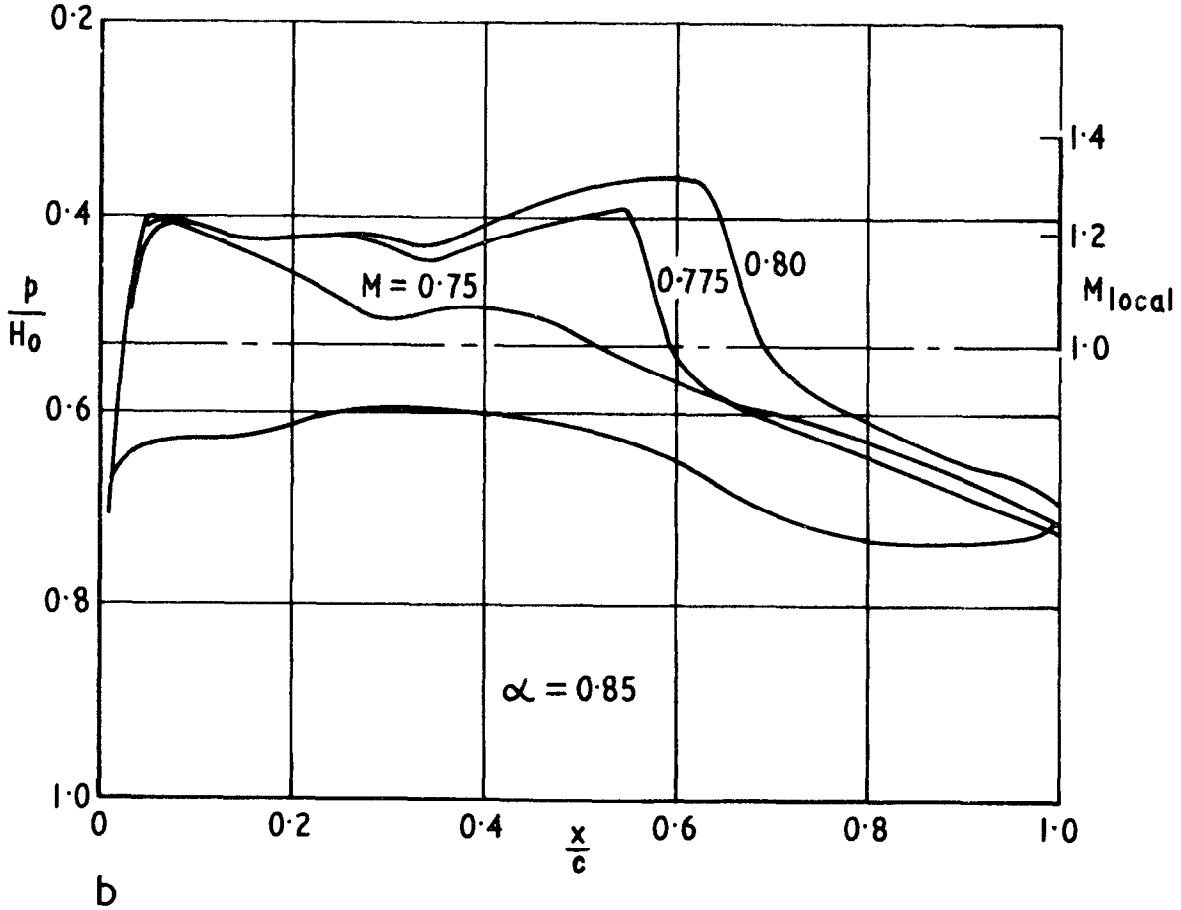

b

Fig. 10a & b Experimental pressure distributions for RAE (NPL) 5213

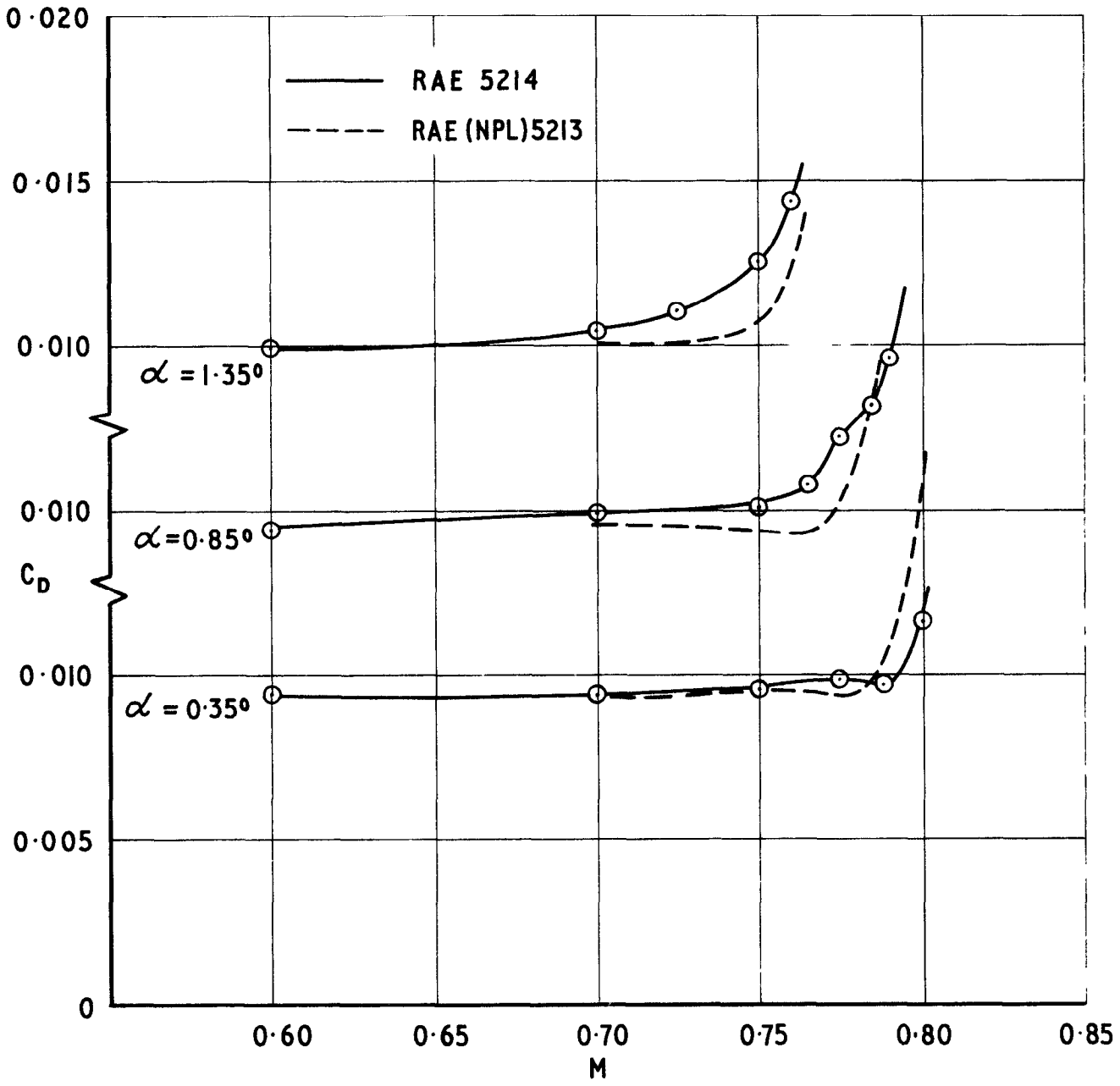

Fig.17 Measured values of drag coefficient

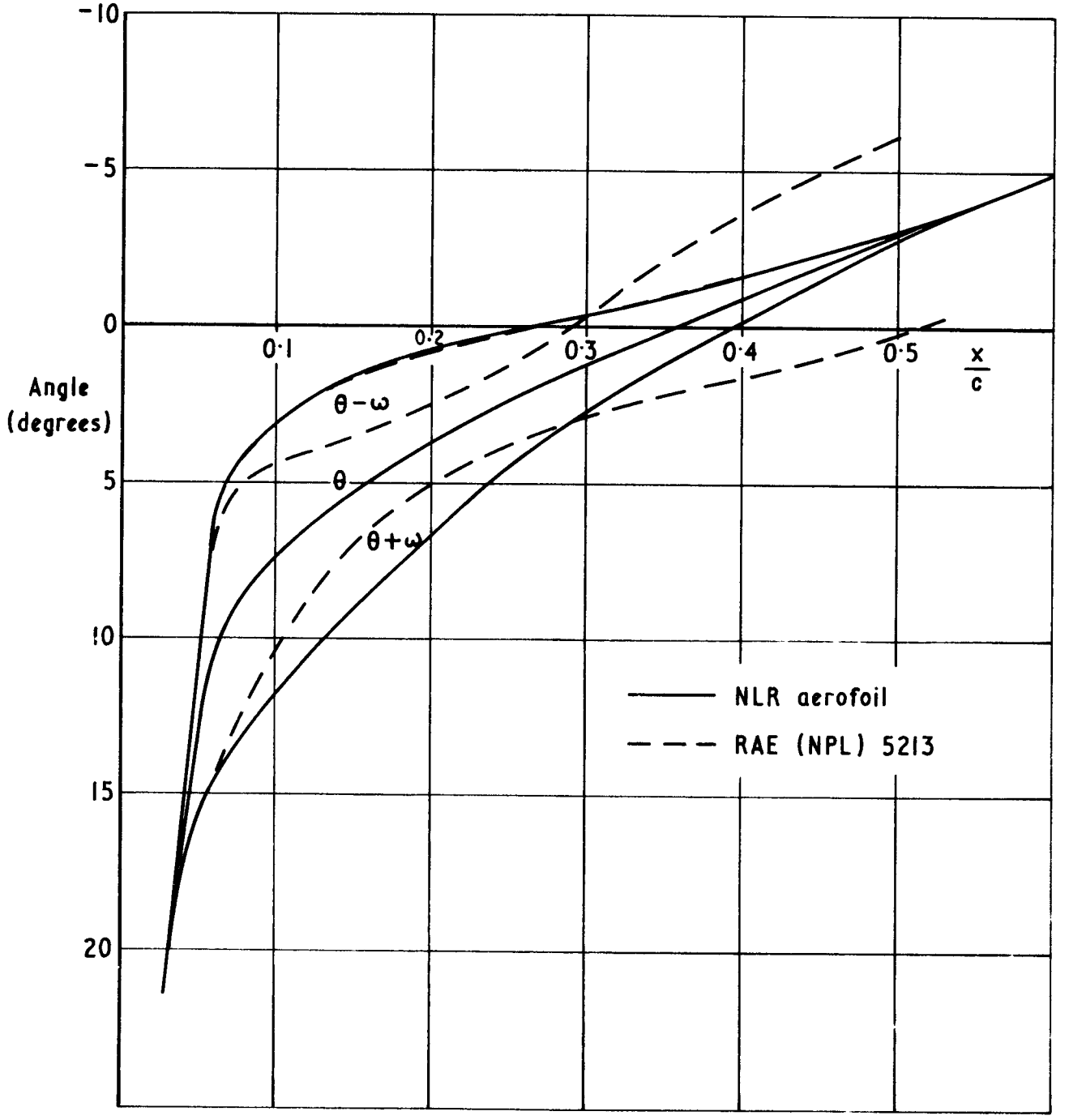

Fig. 11 Surface slope and characteristics plot for RAE (NPL) 5213 and basic NLR aerofoil

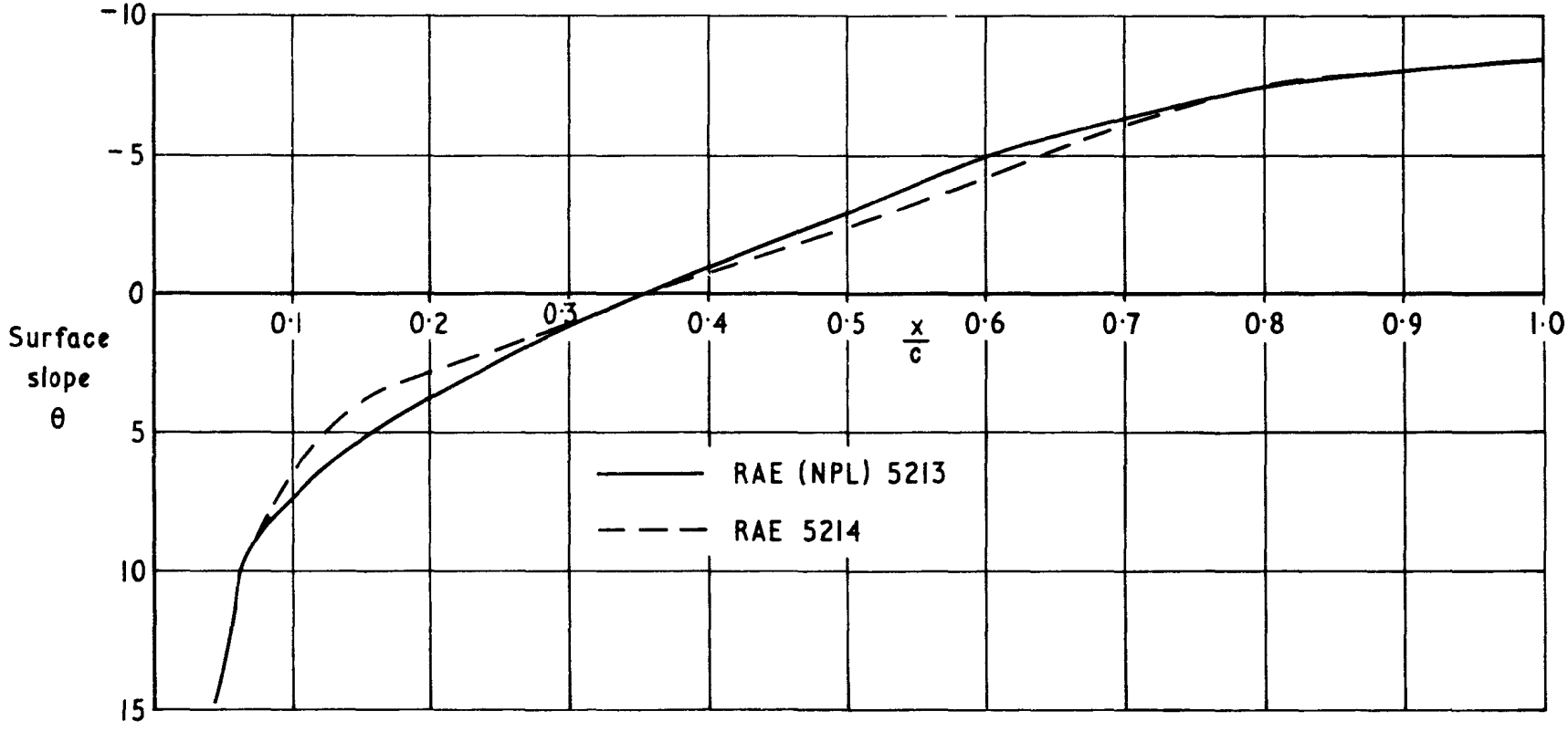

Fig. 12 Surface slope distributions for RAE (NPL) 5213 and RAE 5214

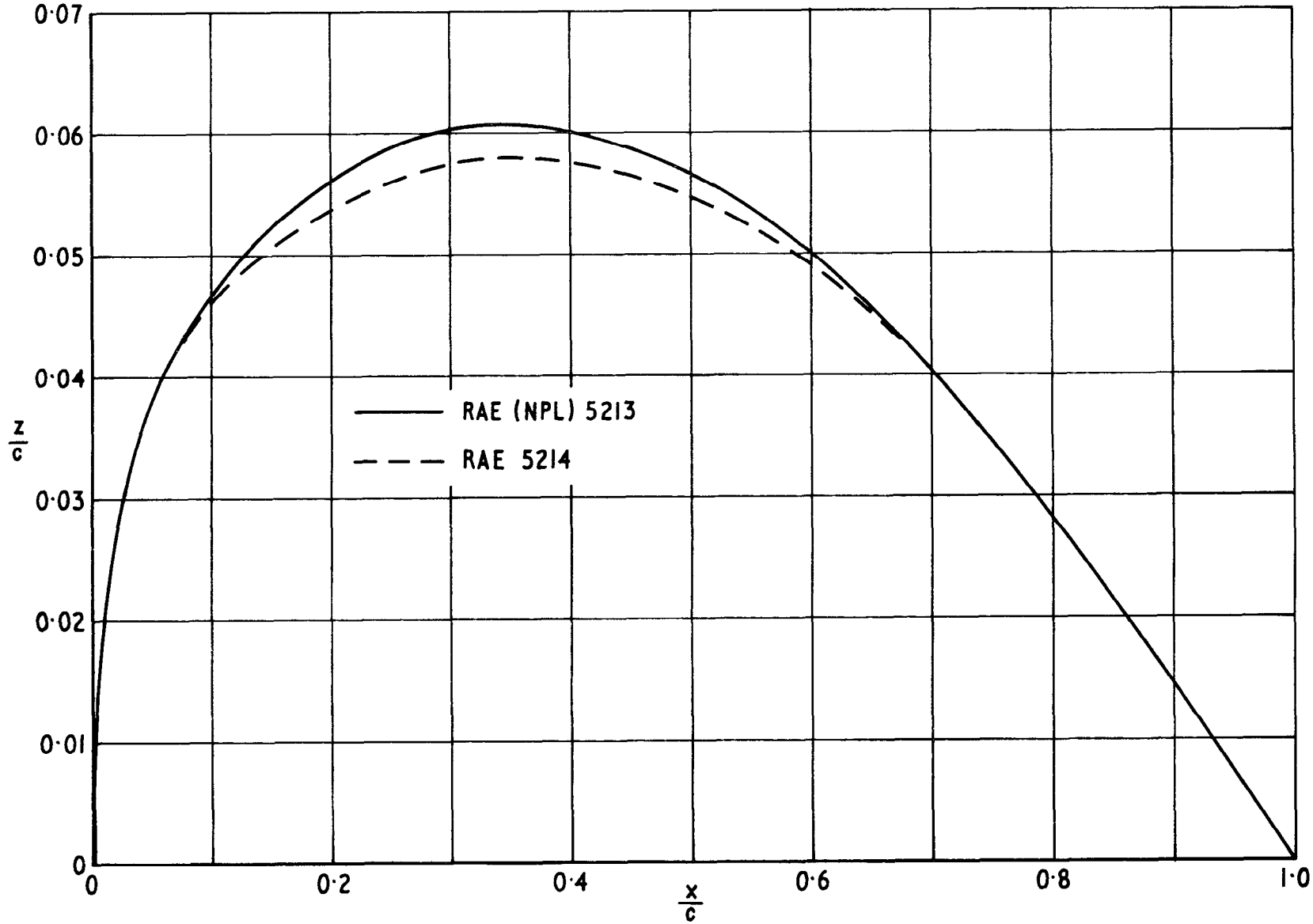

Fig. 13 Upper surface ordinates for RAE (NPL) 5213 and RAE 5214

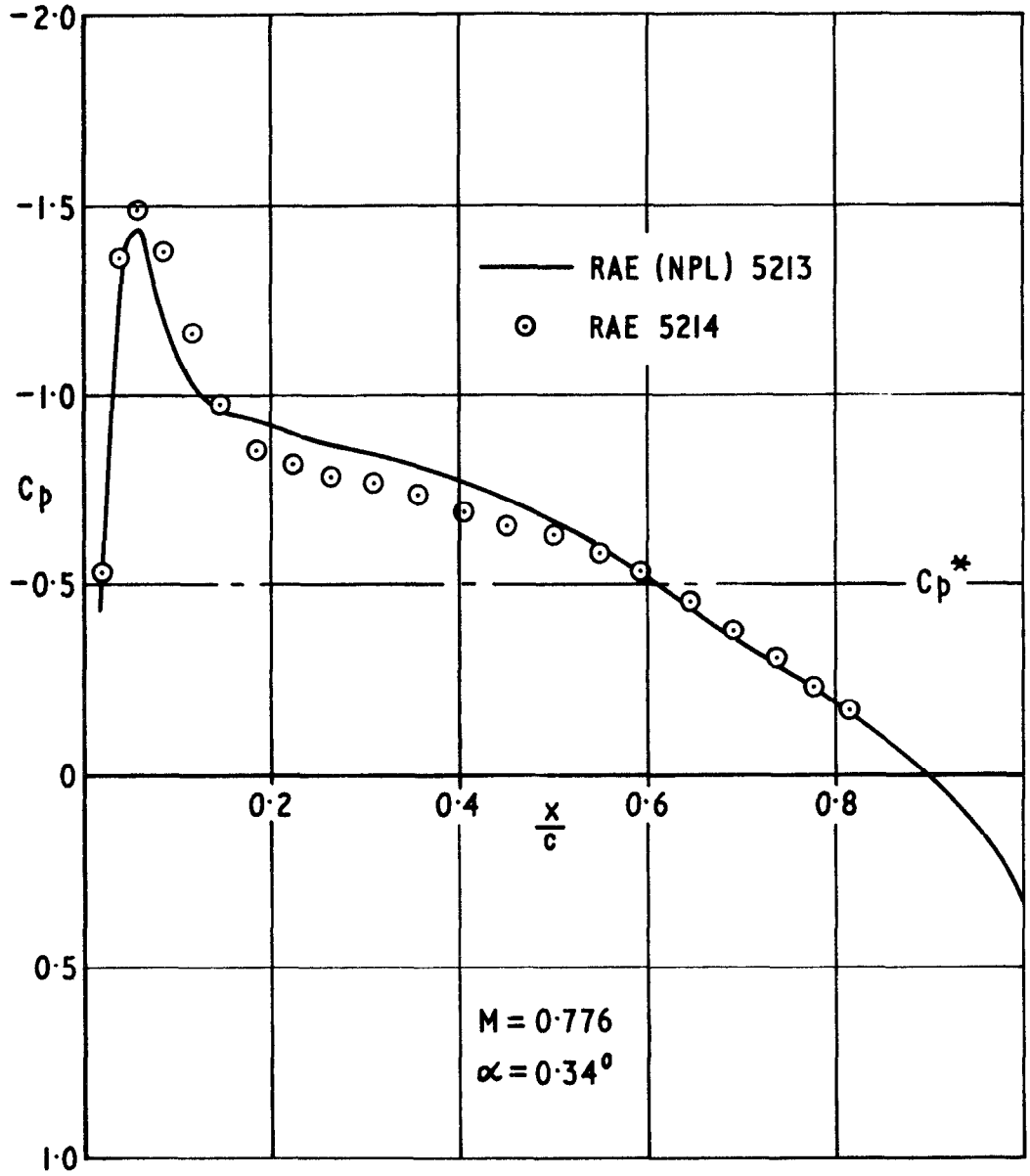

Fig. 14 Comparison of upper surface pressure distributions given by approximate theory

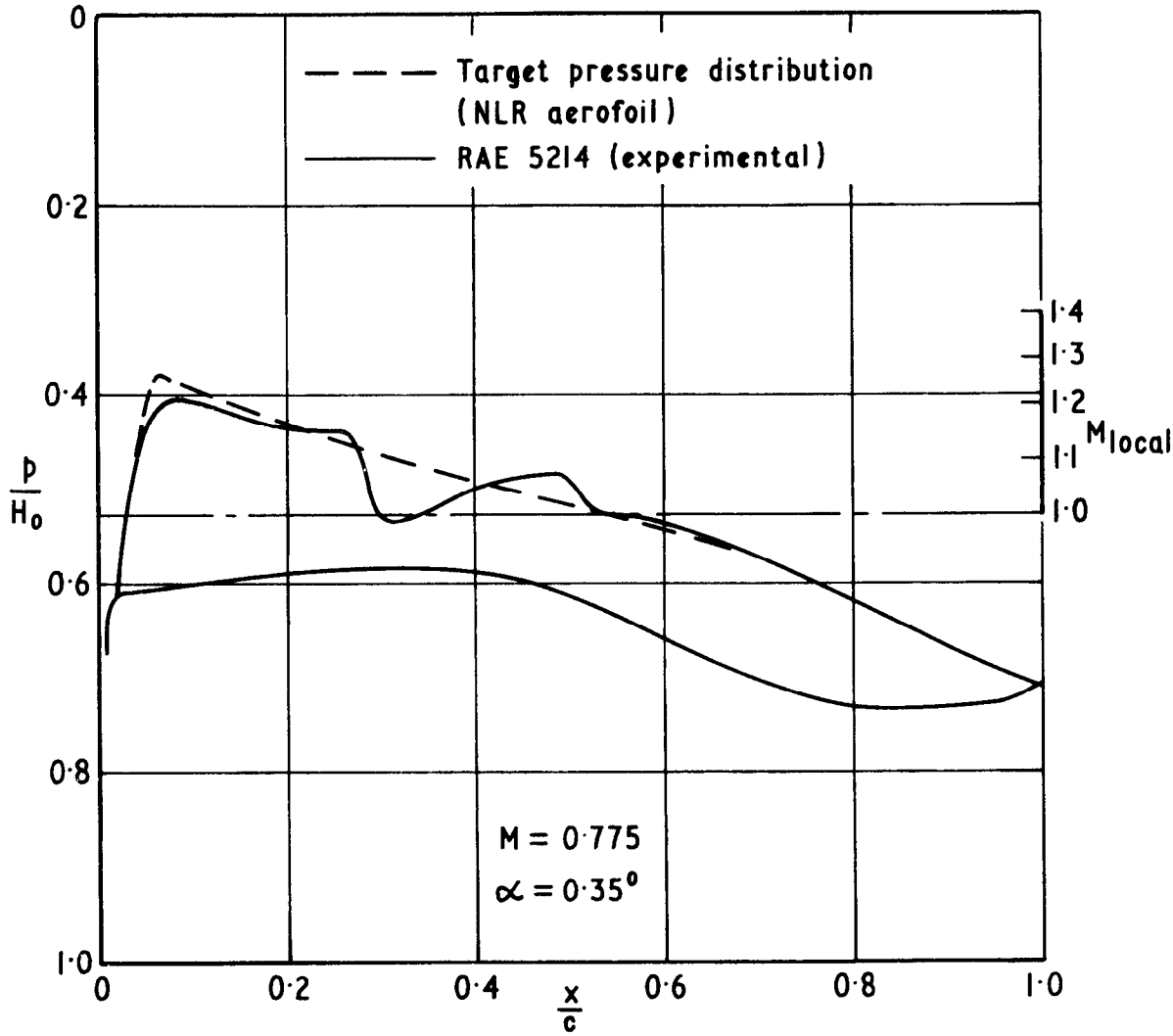

Fig. 15 Experimental pressure distribution for RAE 5214 at design condition

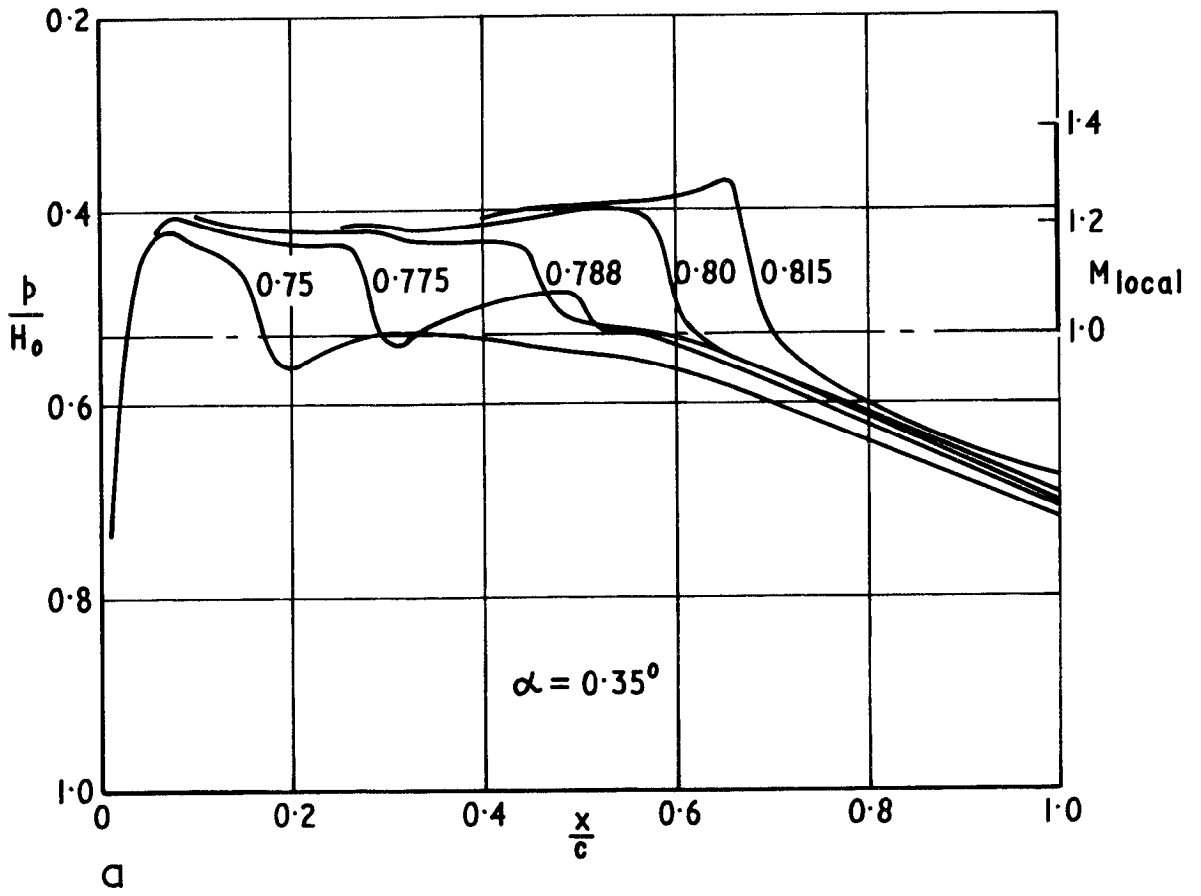

a

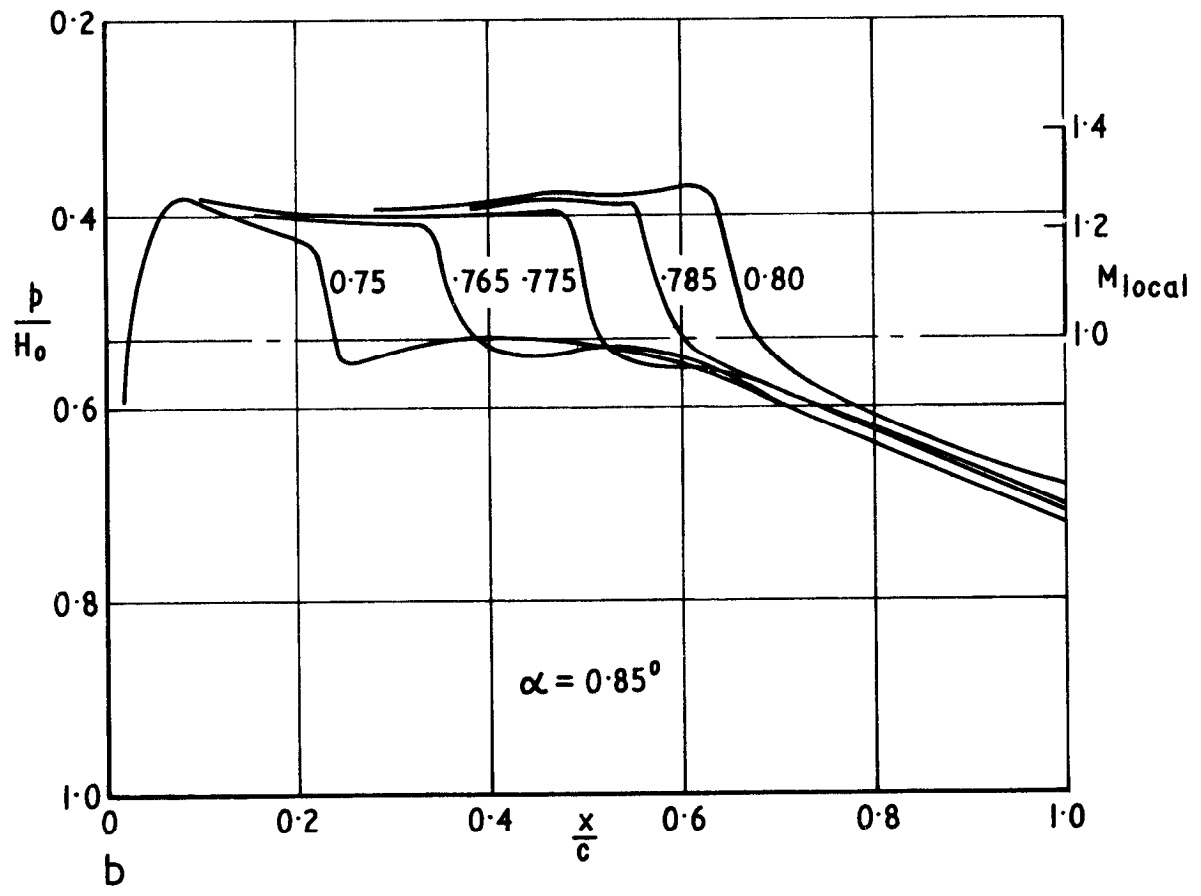

b

Fig. 16a & b Experimental pressure distributions for RAE 5214

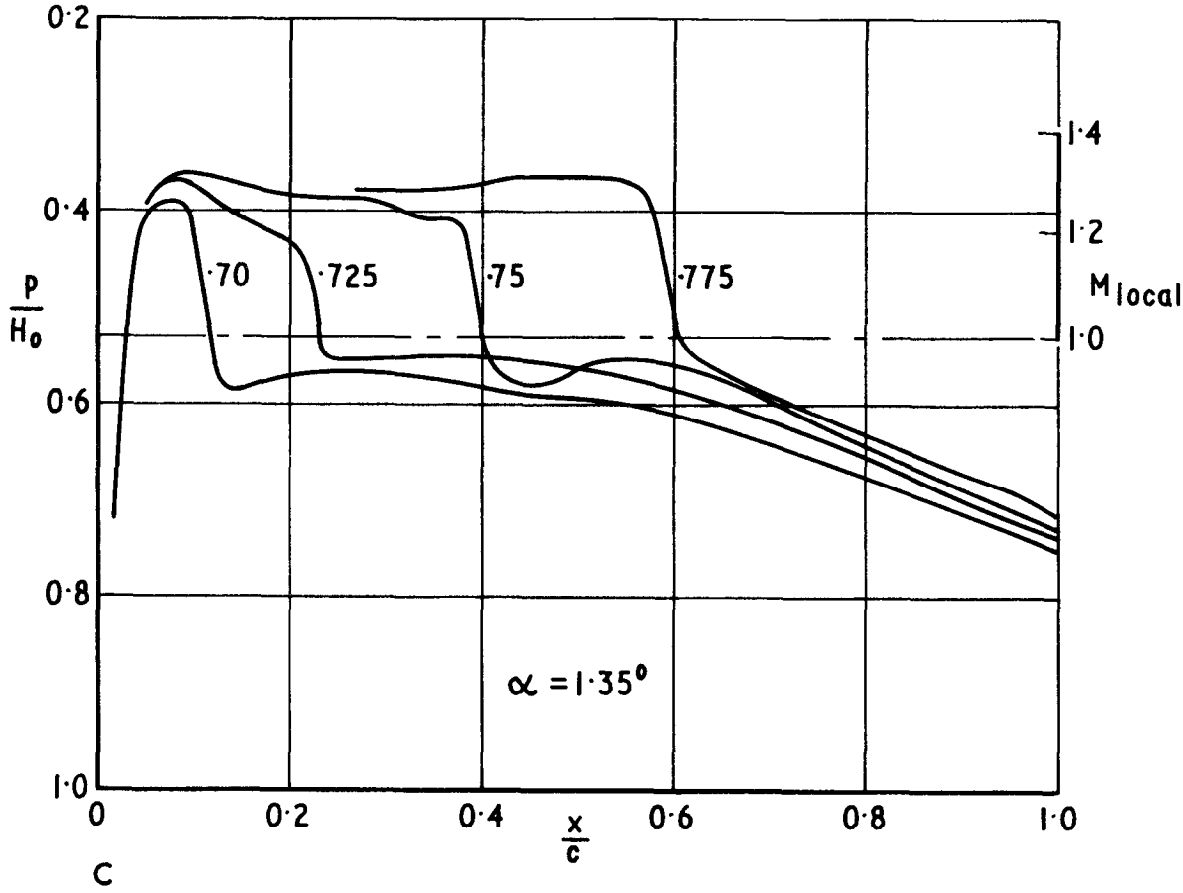

Fig. 16c Experimental pressure distributions for RAE 5214

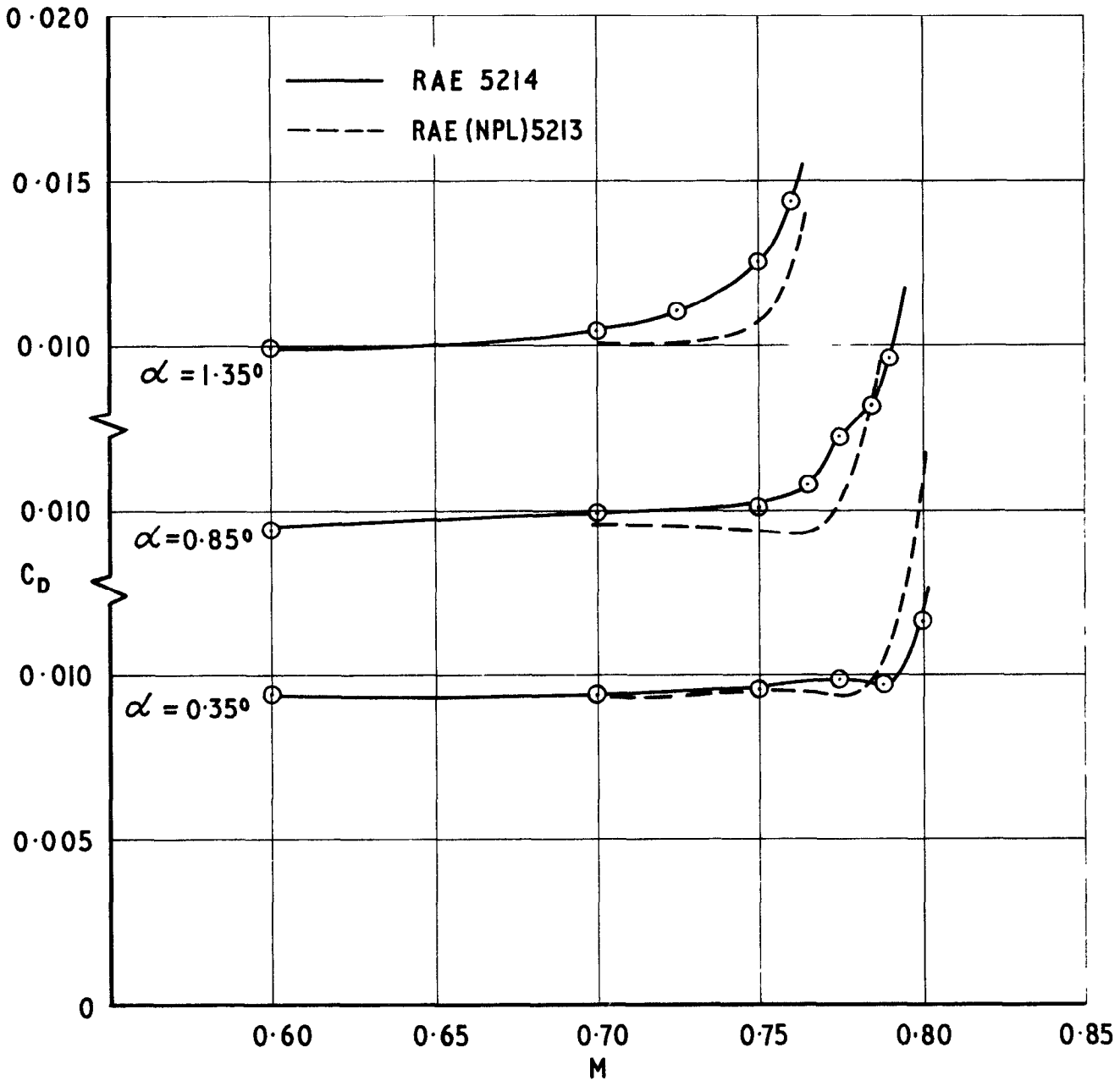

Fig.17 Measured values of drag coefficient

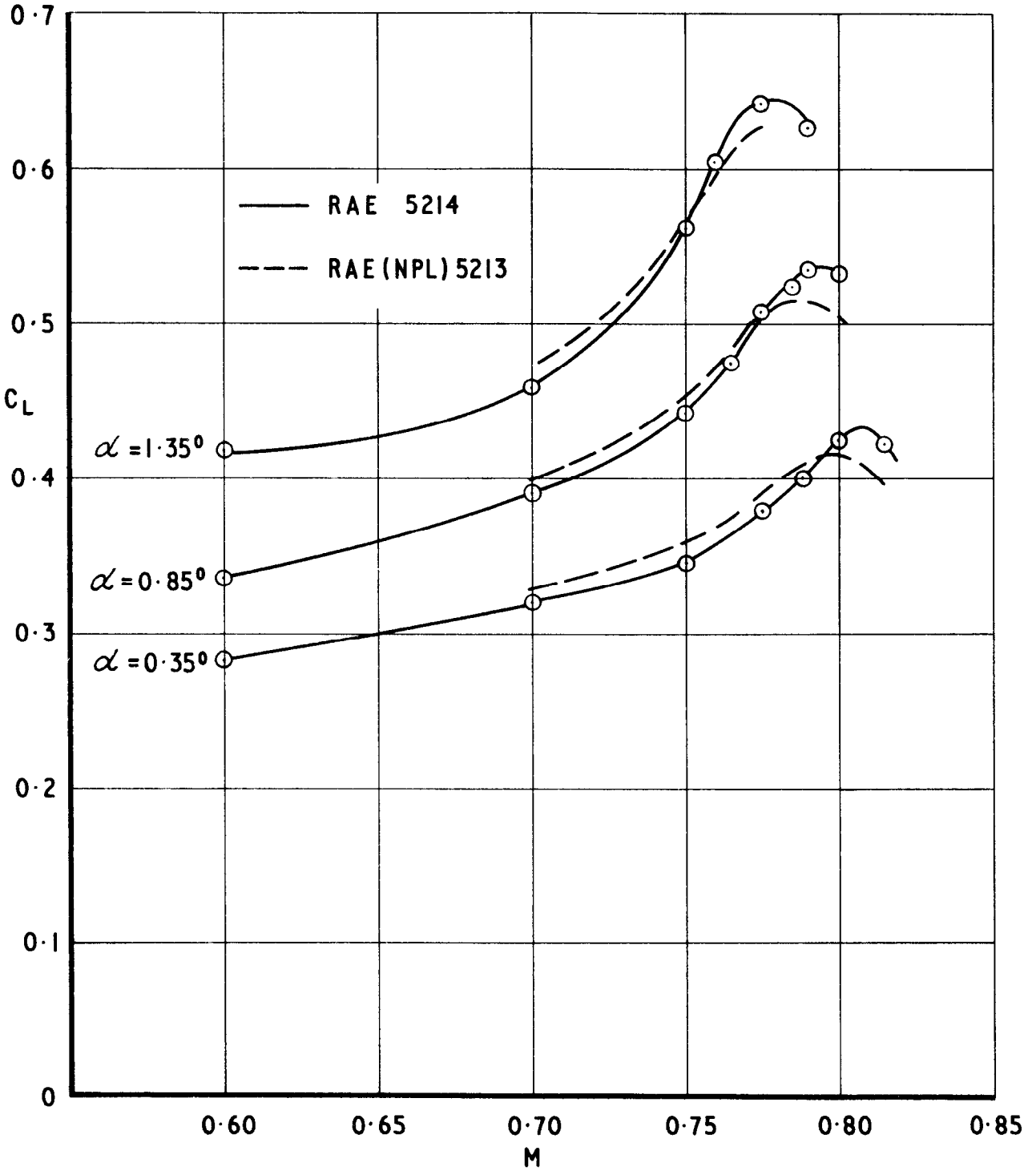

Fig. 18 Measured values of lift coefficient

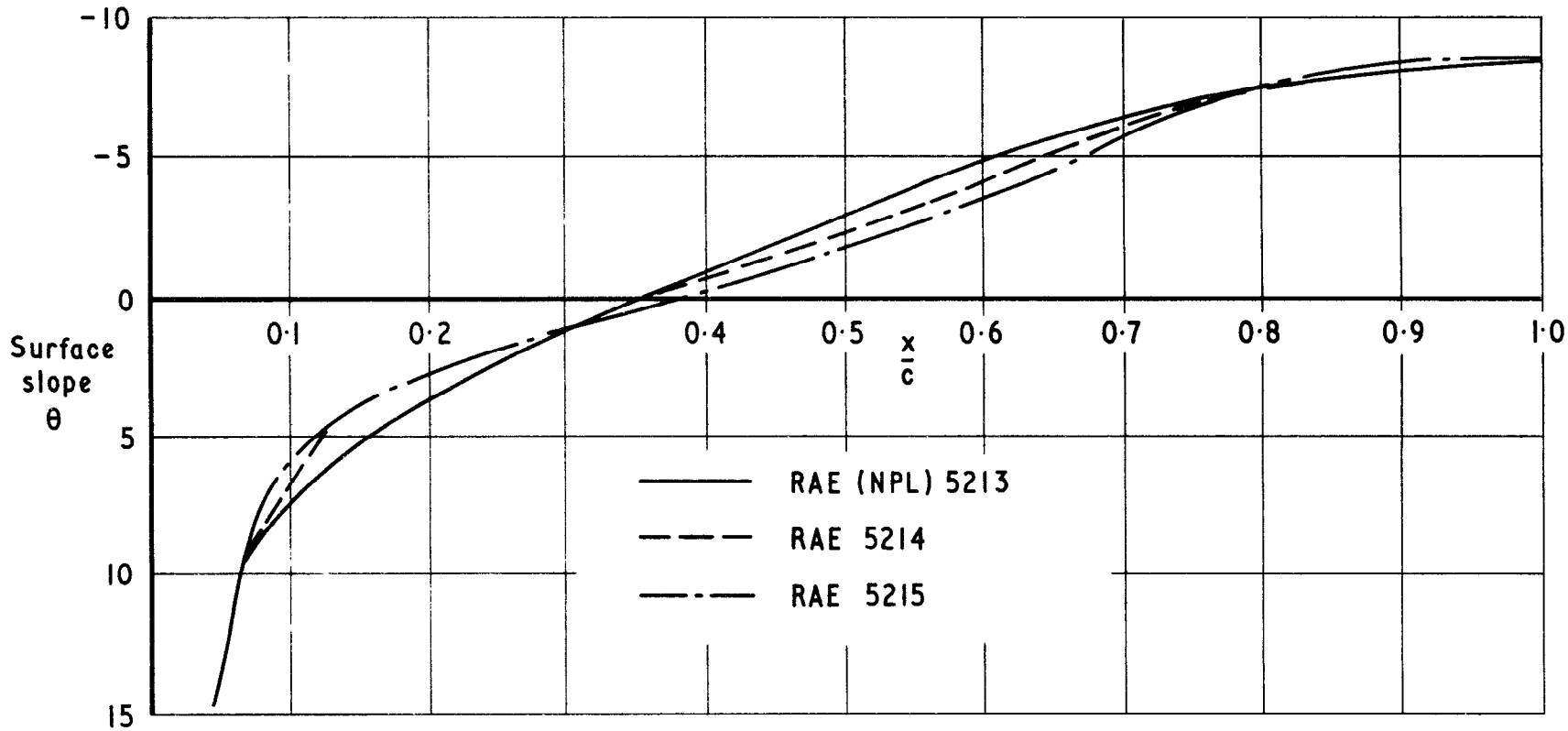

Fig 19 Upper surface slope distributions

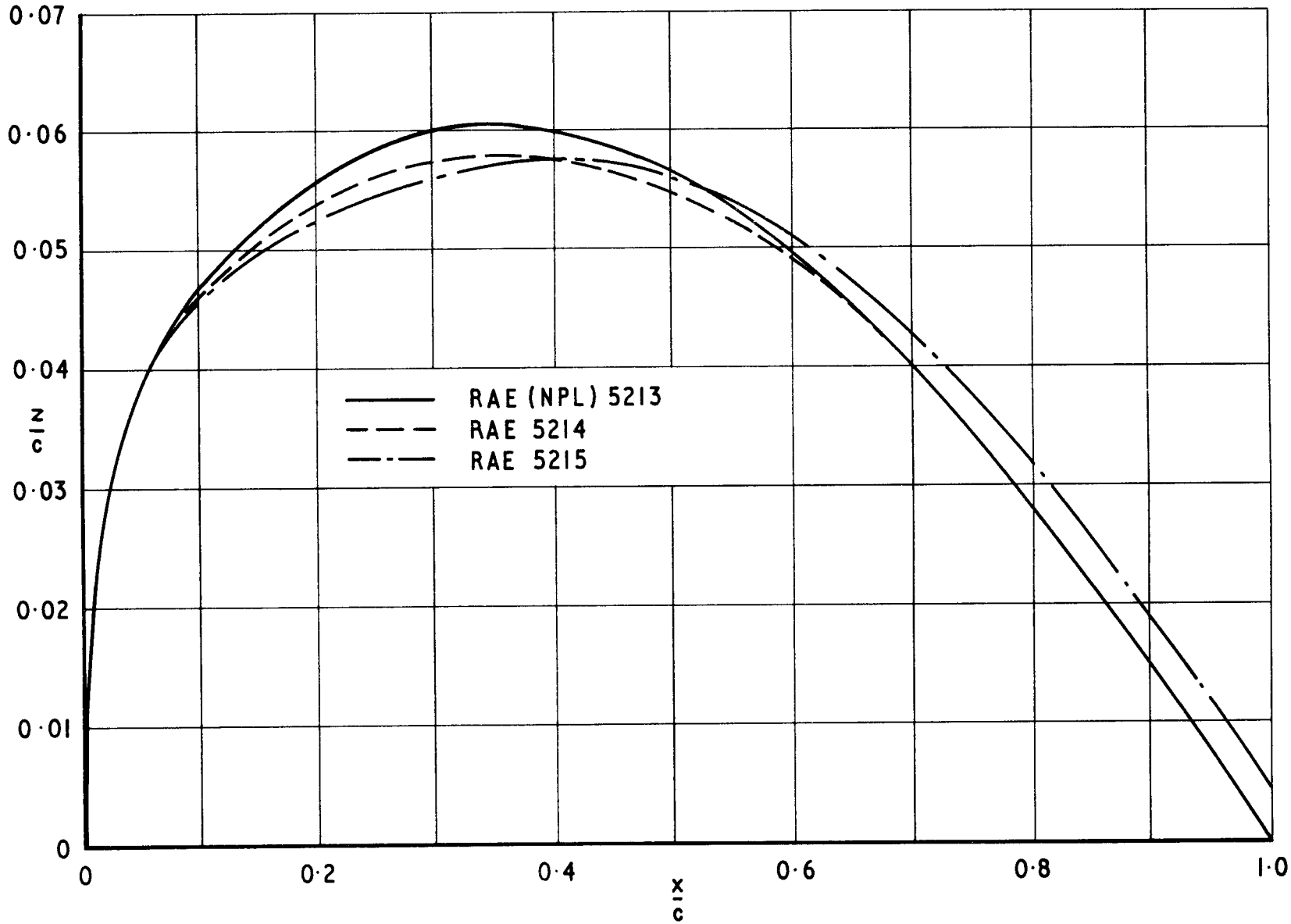

Fig.20 Upper surface ordinate distributions

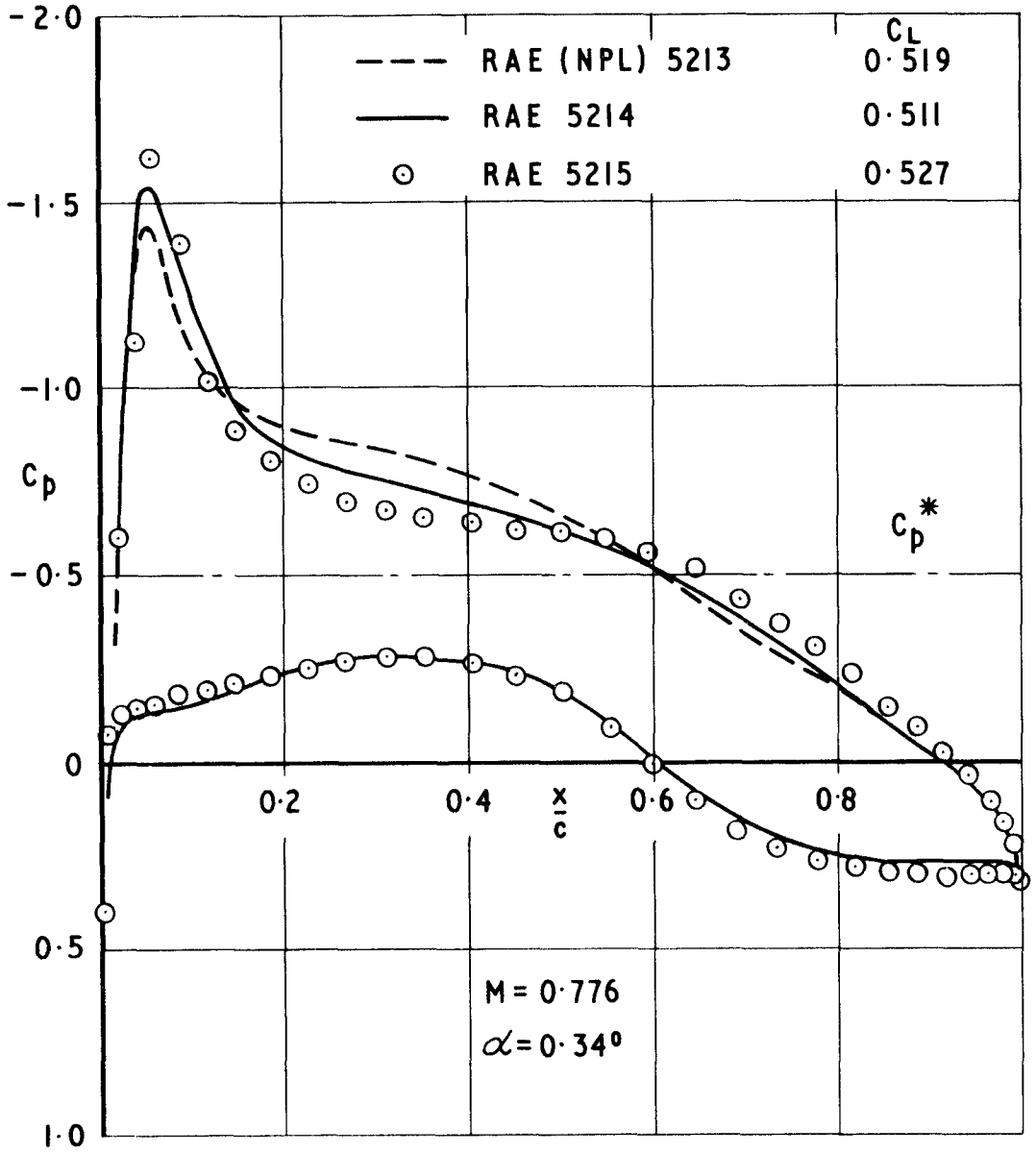

Fig.21 Comparison of upper surface pressure distributions given by approximate theory

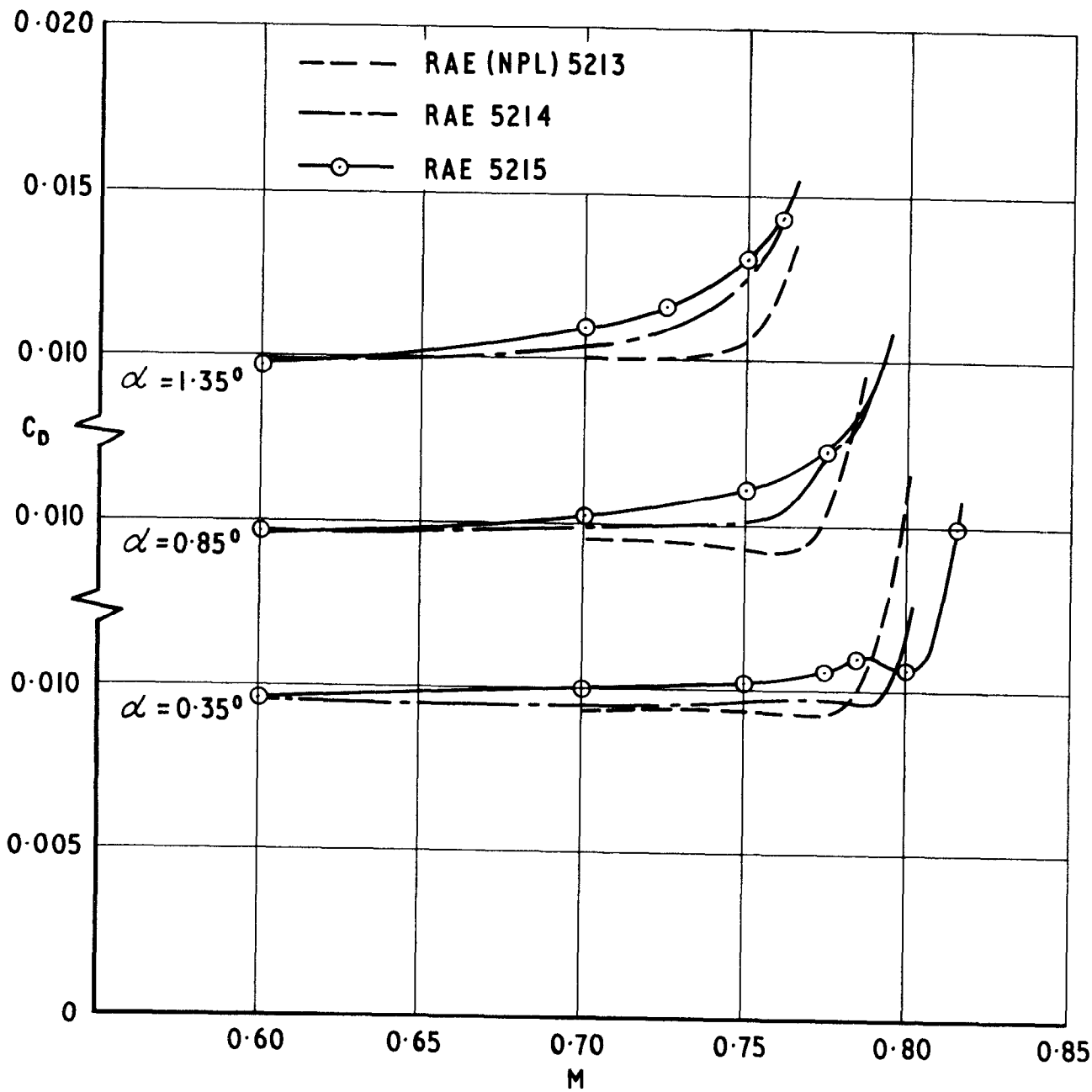

Fig.22 Comparison of measured drag coefficients

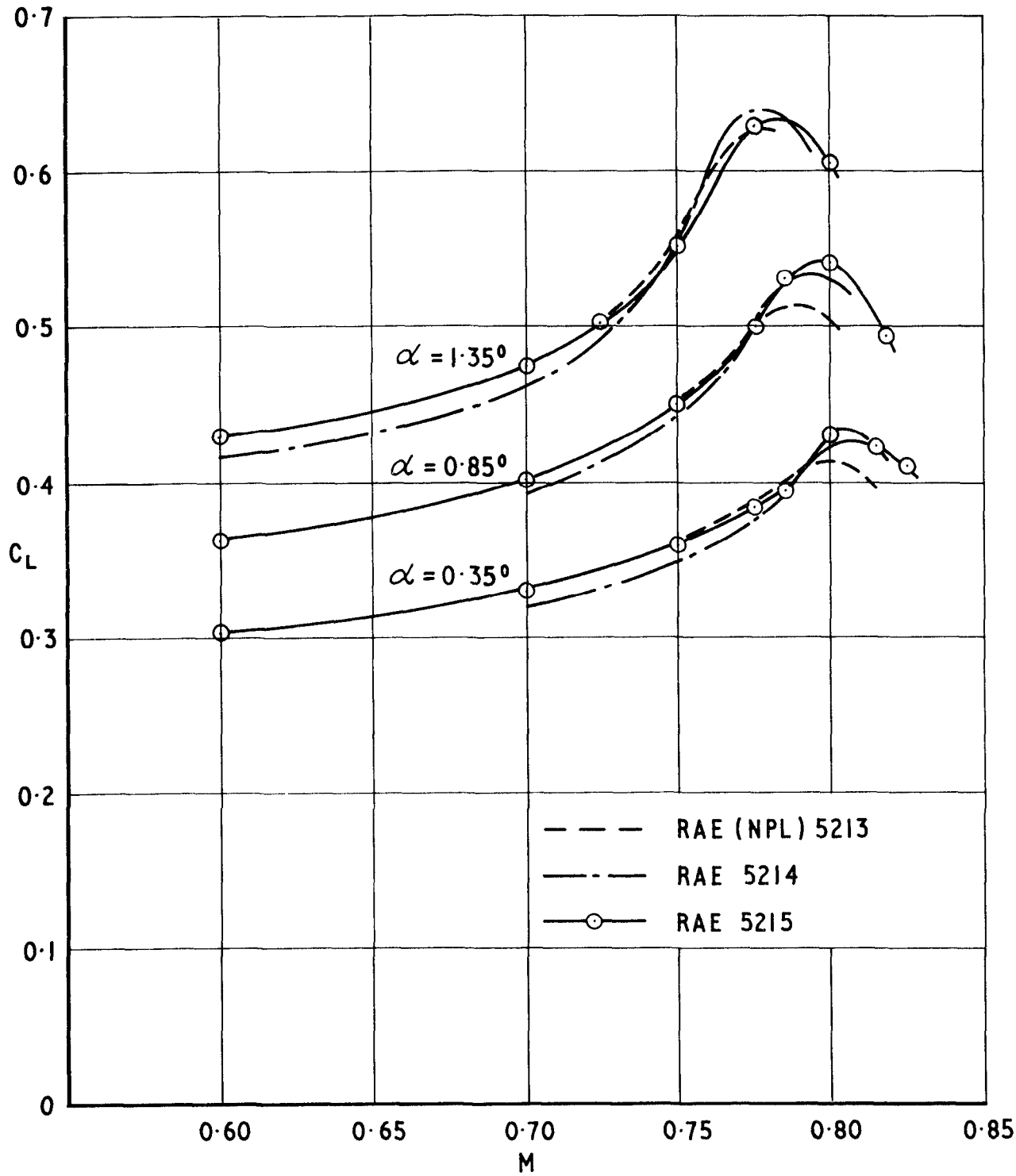

Fig.23 Comparison of measured lift coefficients

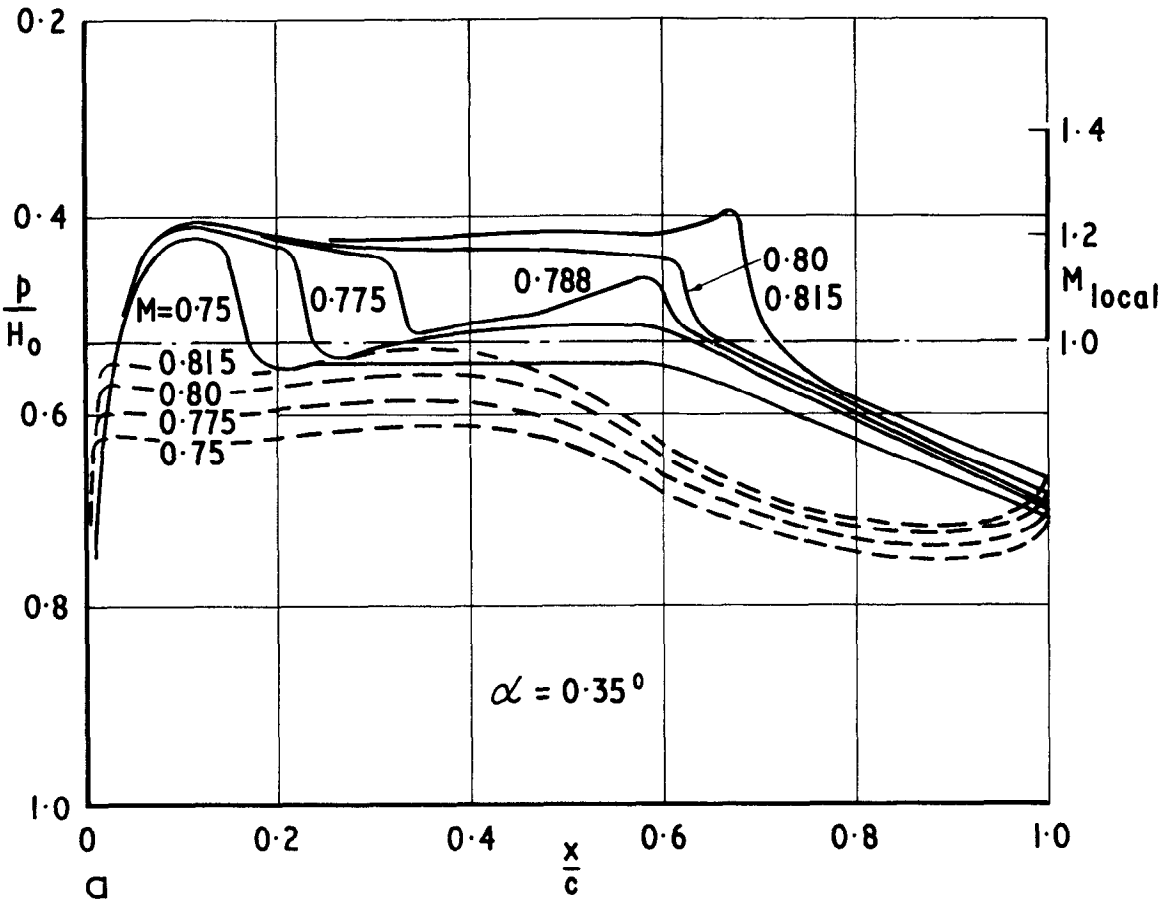

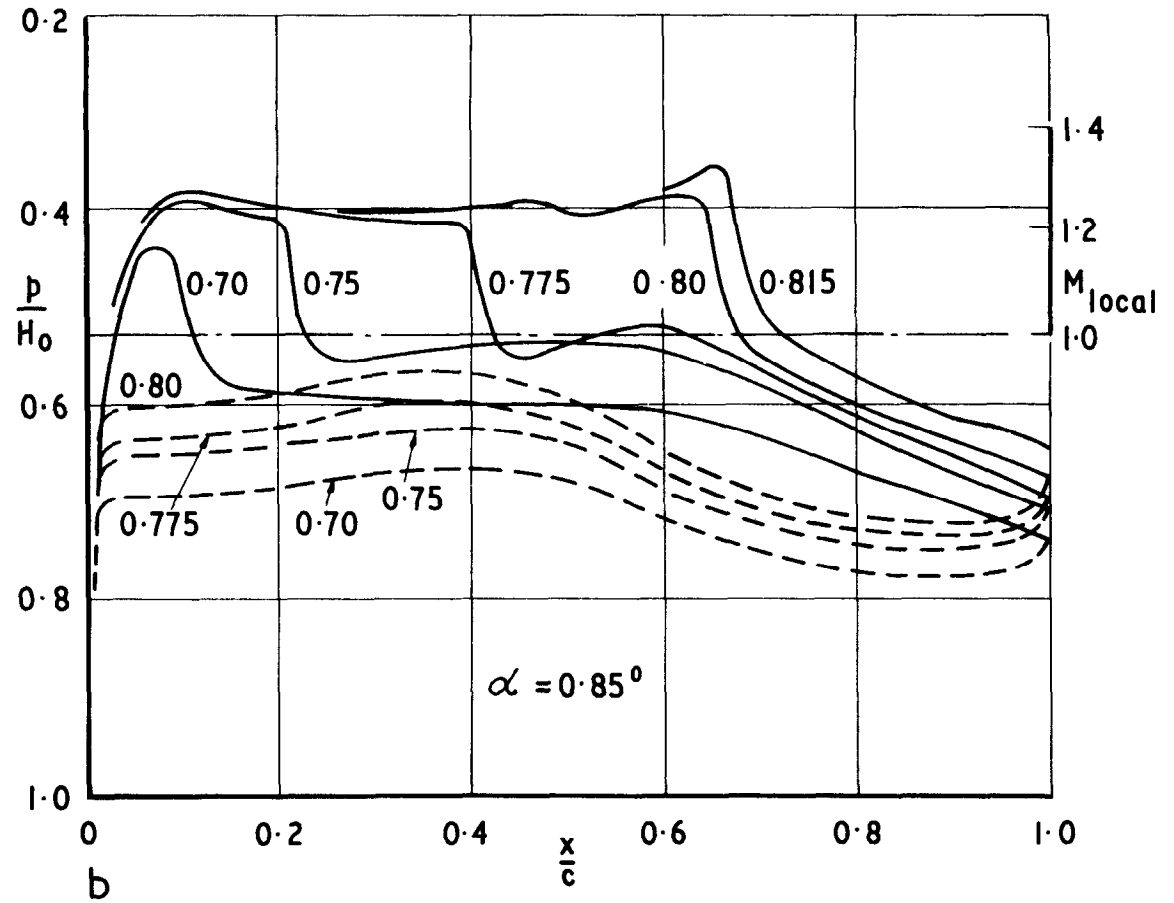

Fig.24a & b Experimental pressure distributions for RAE 5215

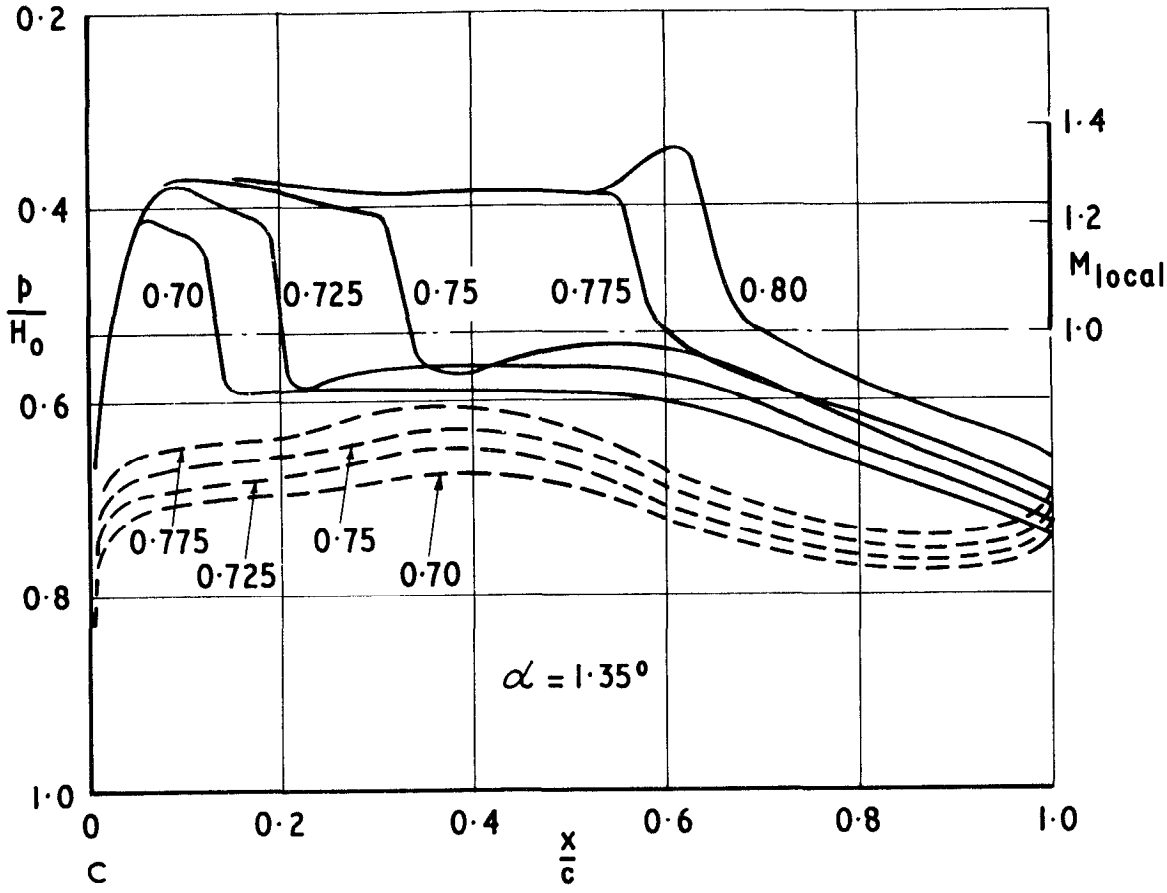

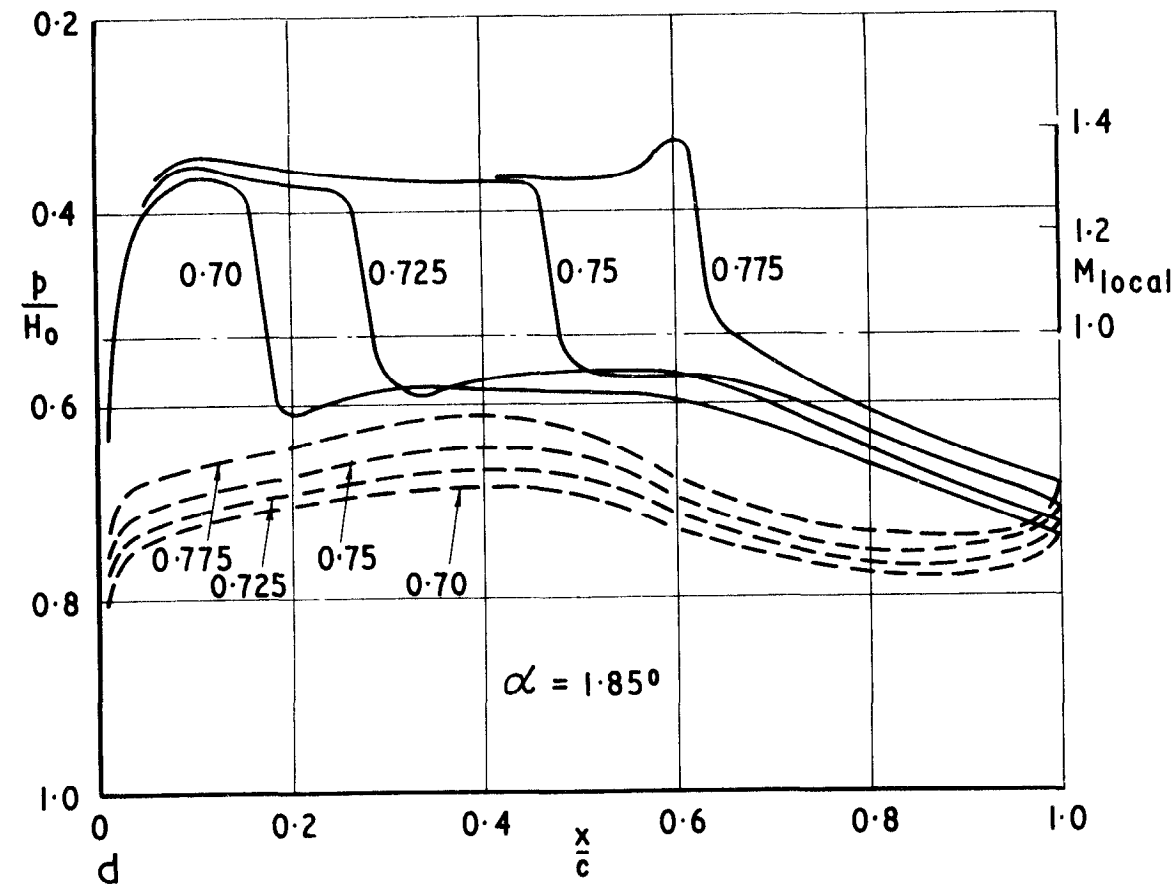

Fig. 24c & d Experimental pressure distributions for RAE 5215

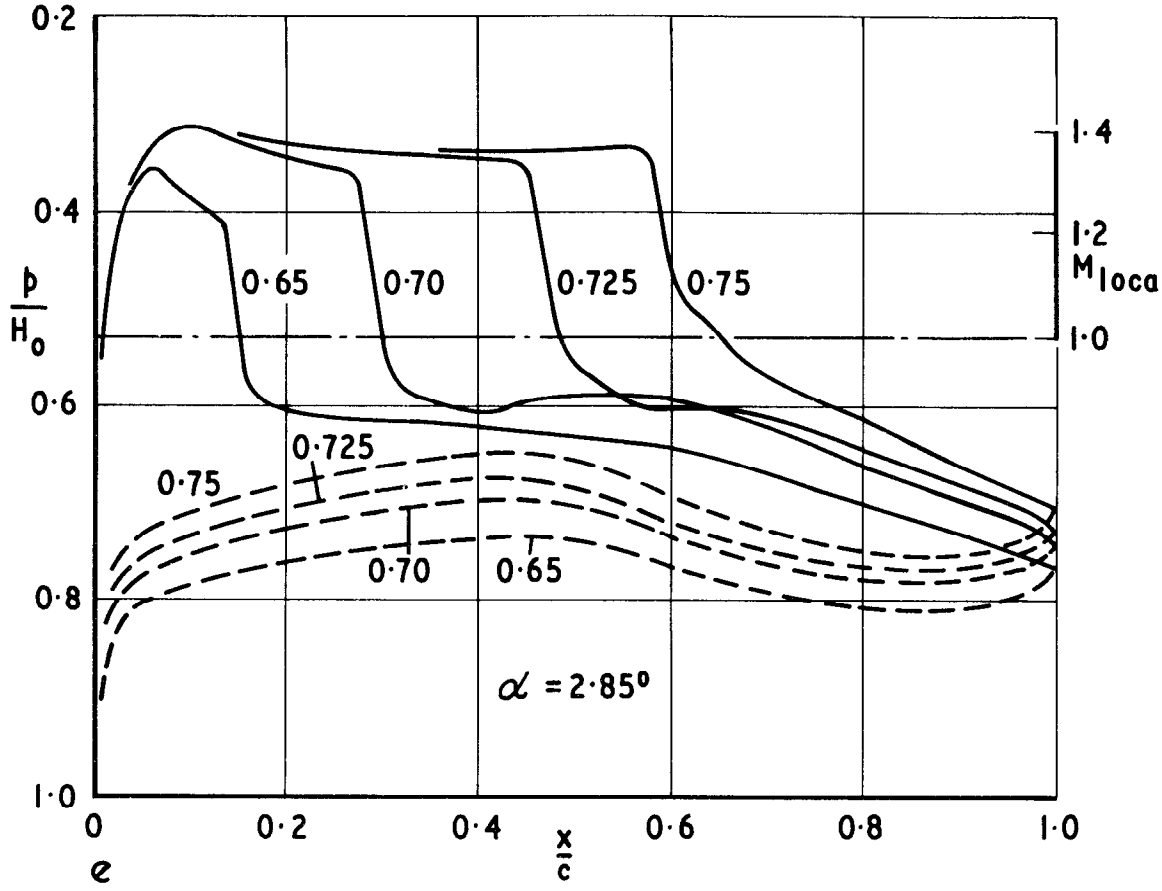

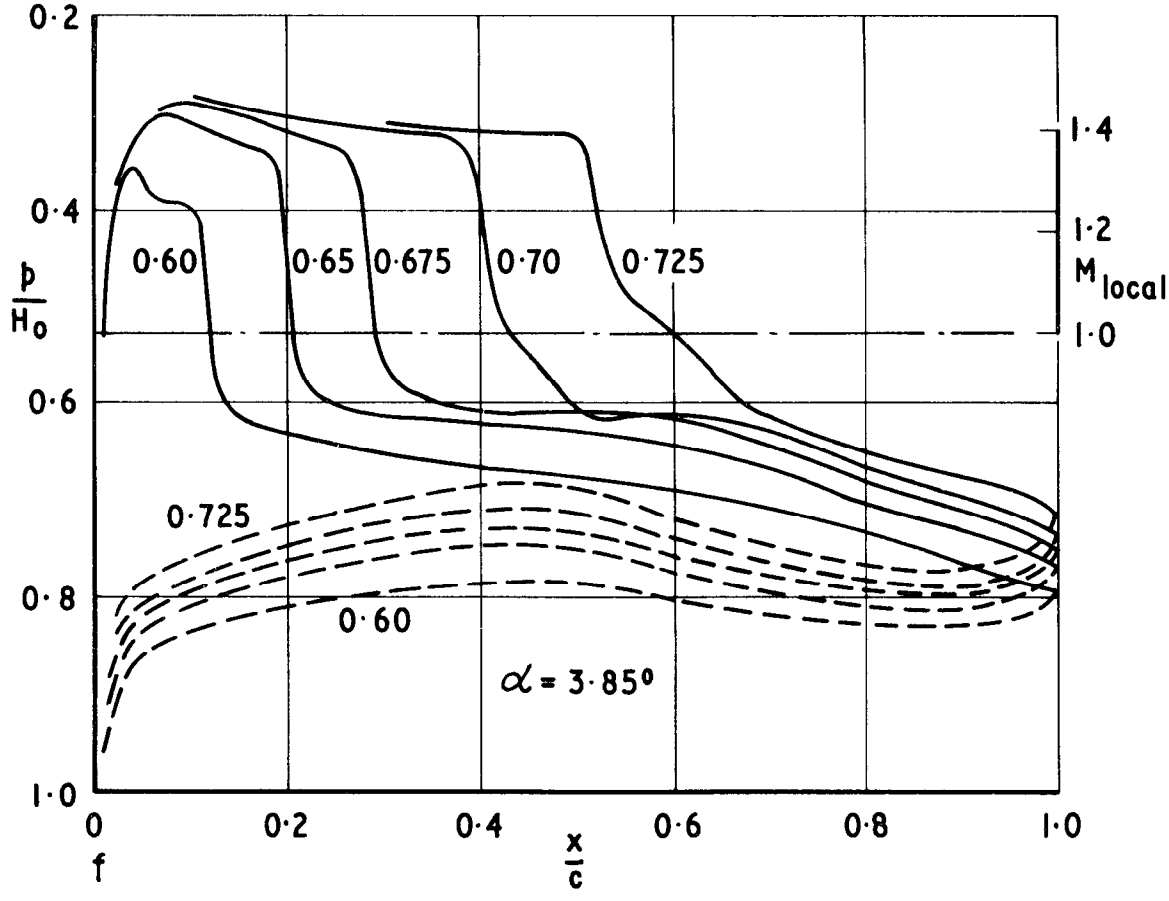

Fig. 24e & f Experimental pressure distributions for RAE 5215

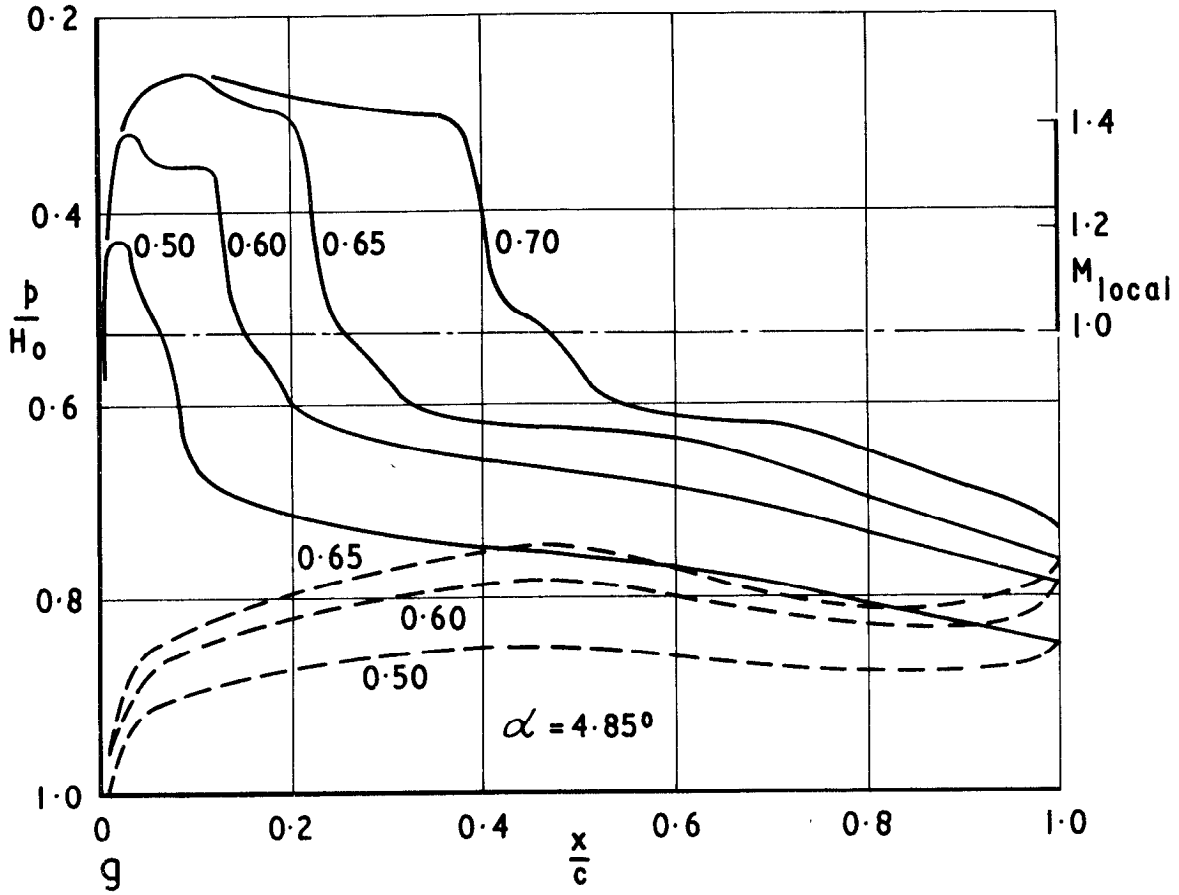

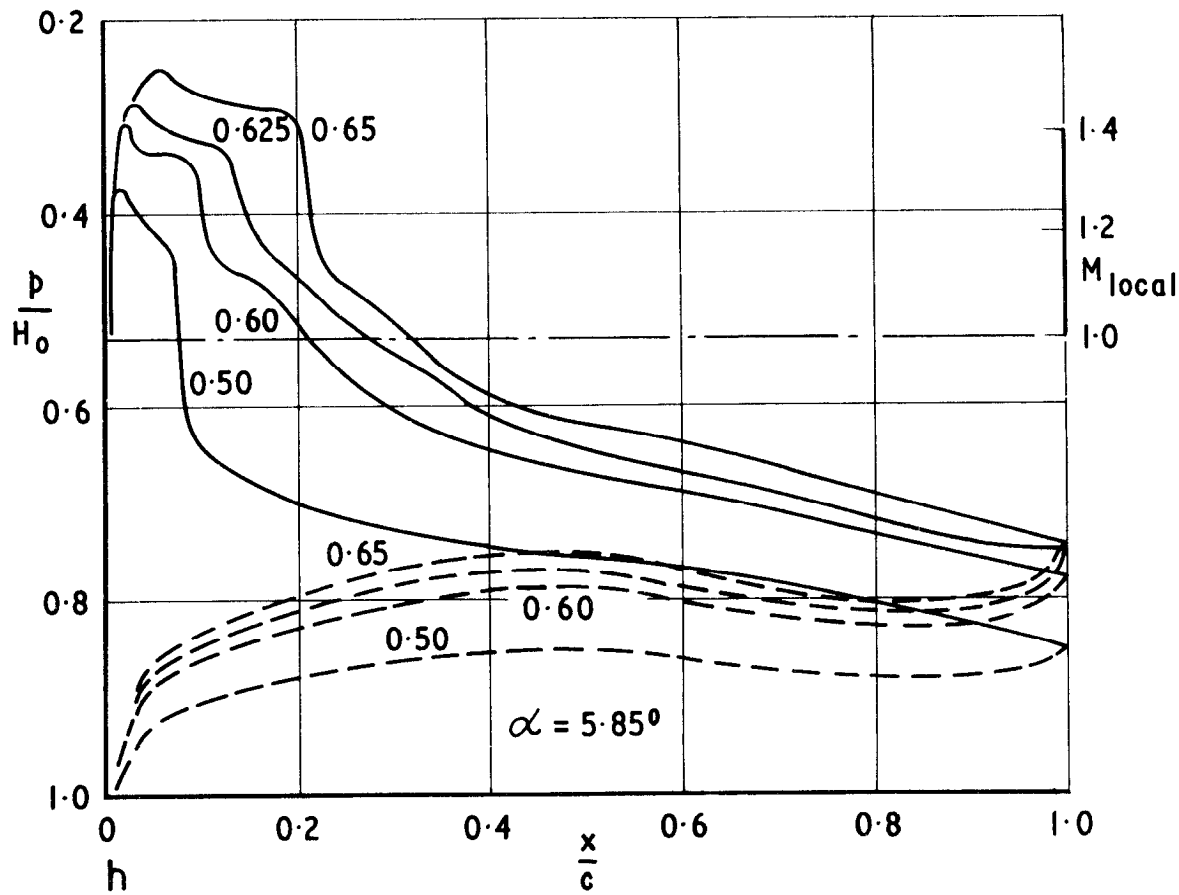

Fig. 24g & h Experimental pressure distributions for RAE 5215

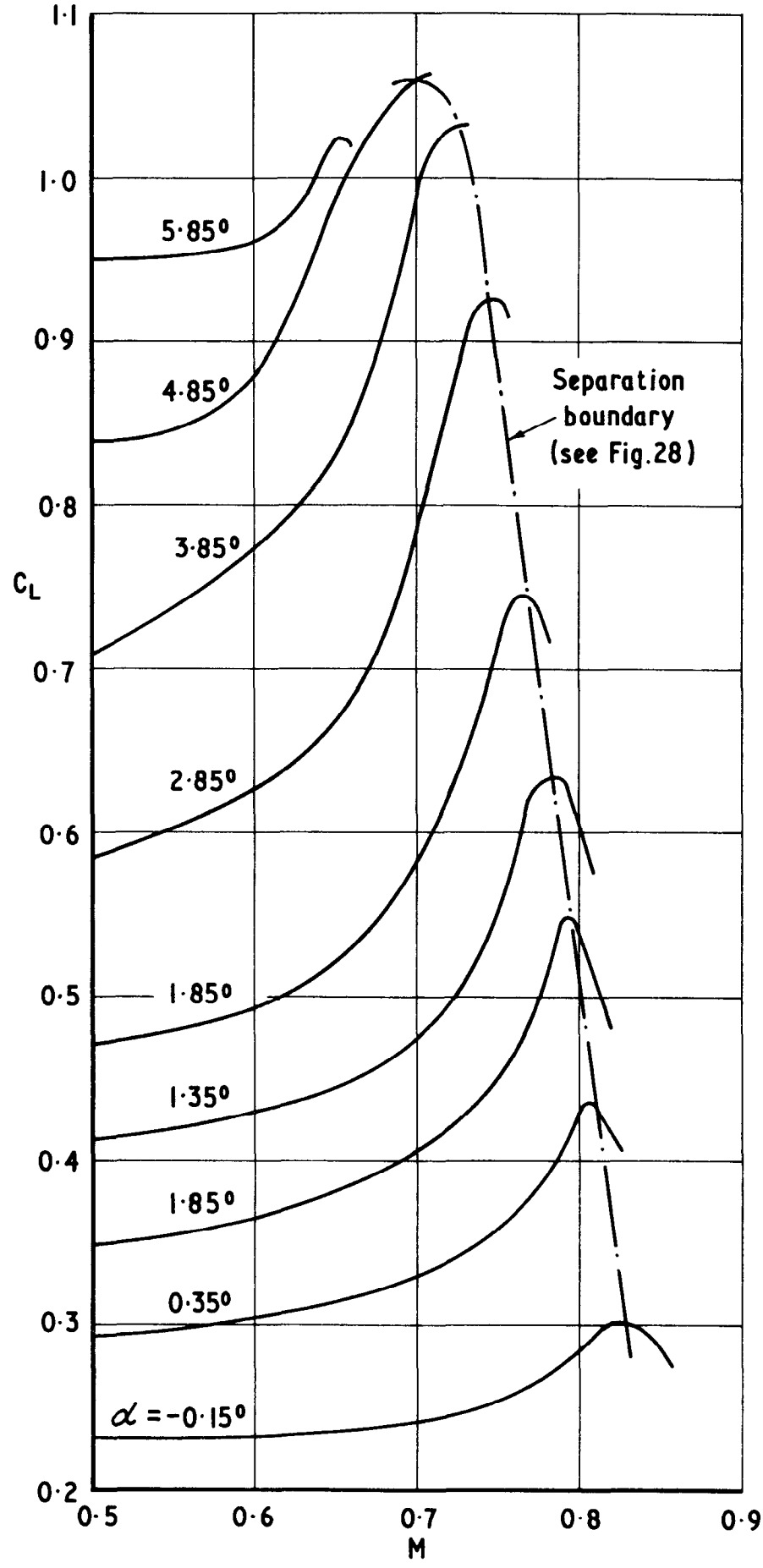

Fig.25 Measured values of lift coefficient for RAE 5215

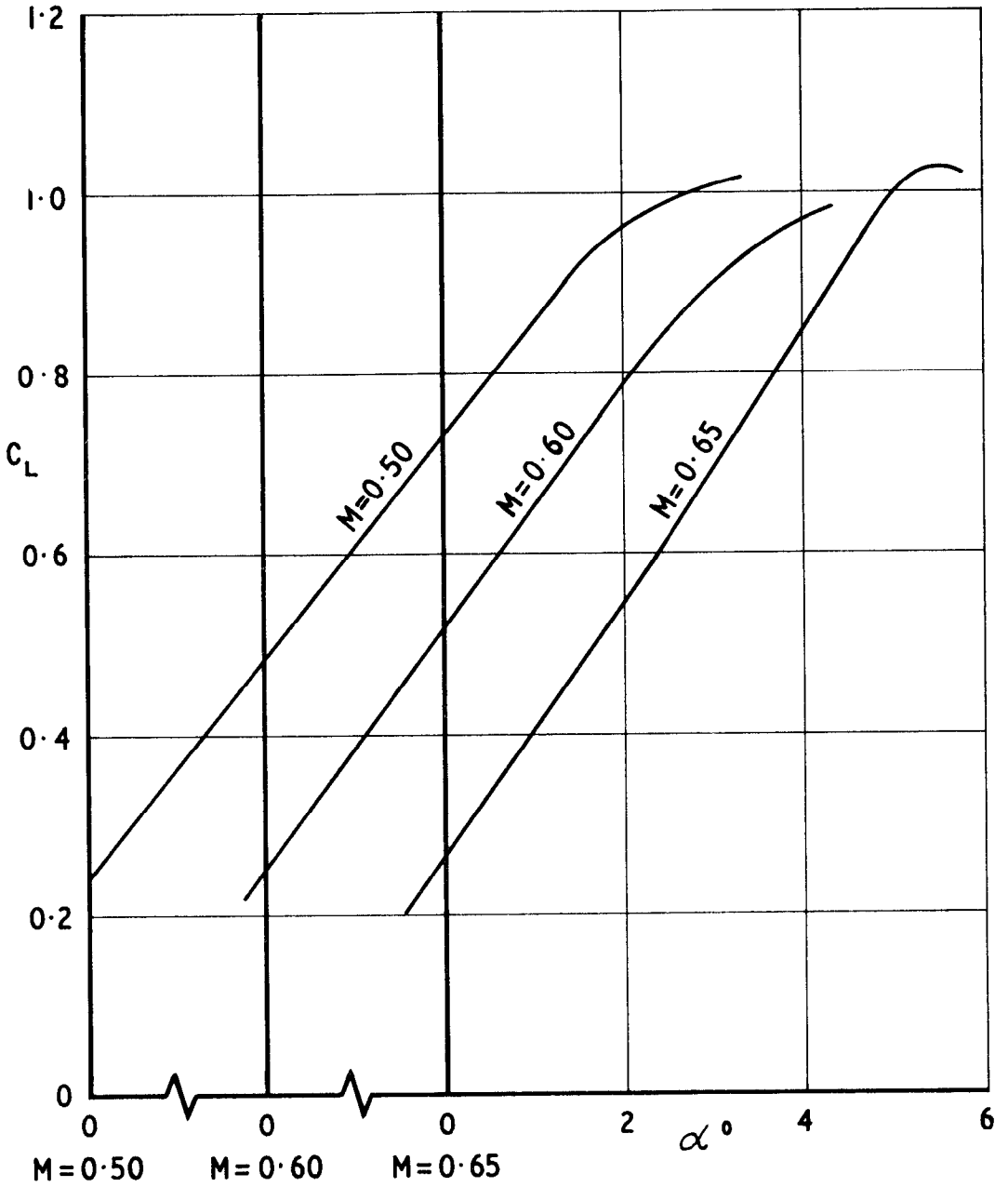

Fig.26 Measured values of lift coefficient for RAE 5215

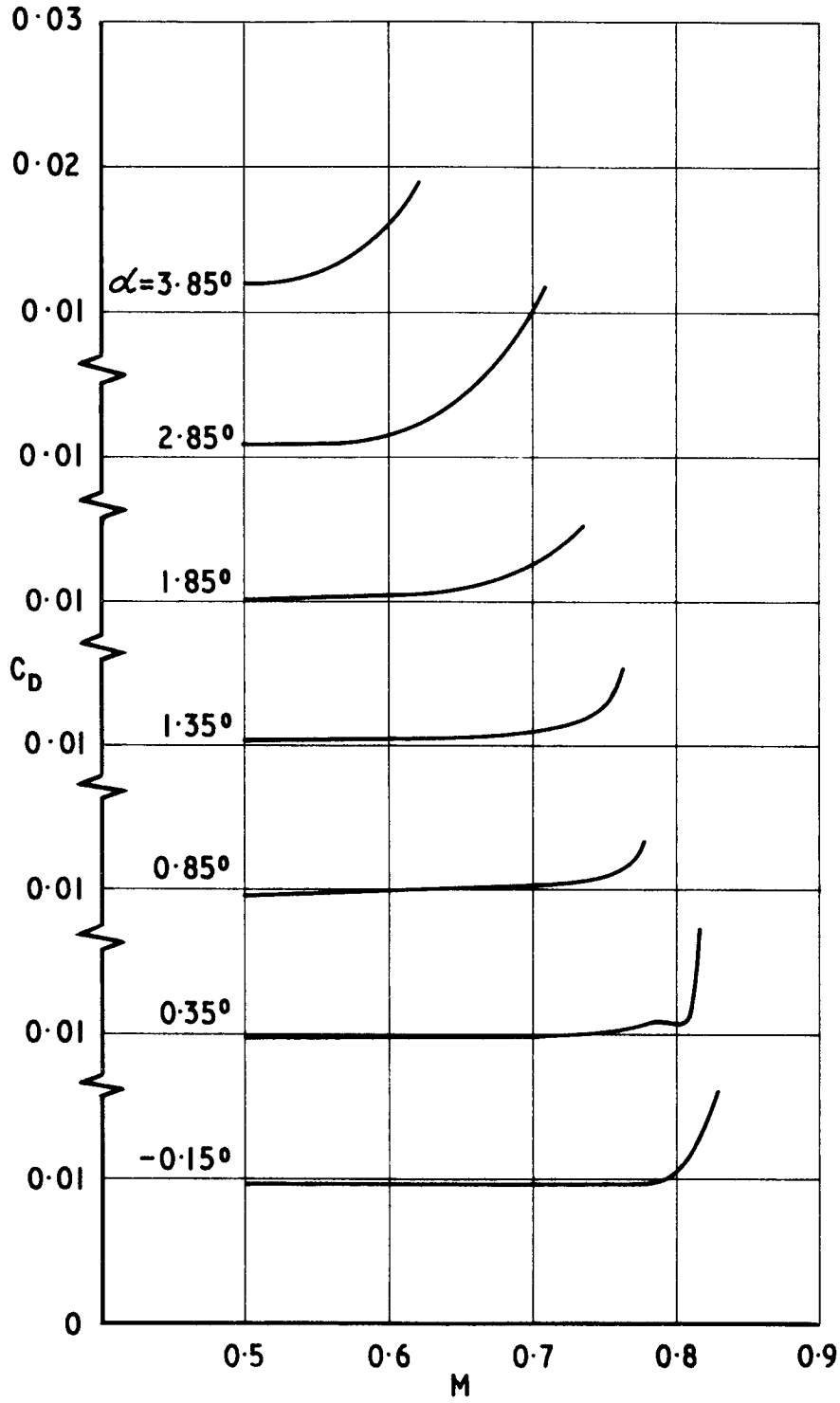

Fig. 27 Measured values of drag coefficient for RAE 5215

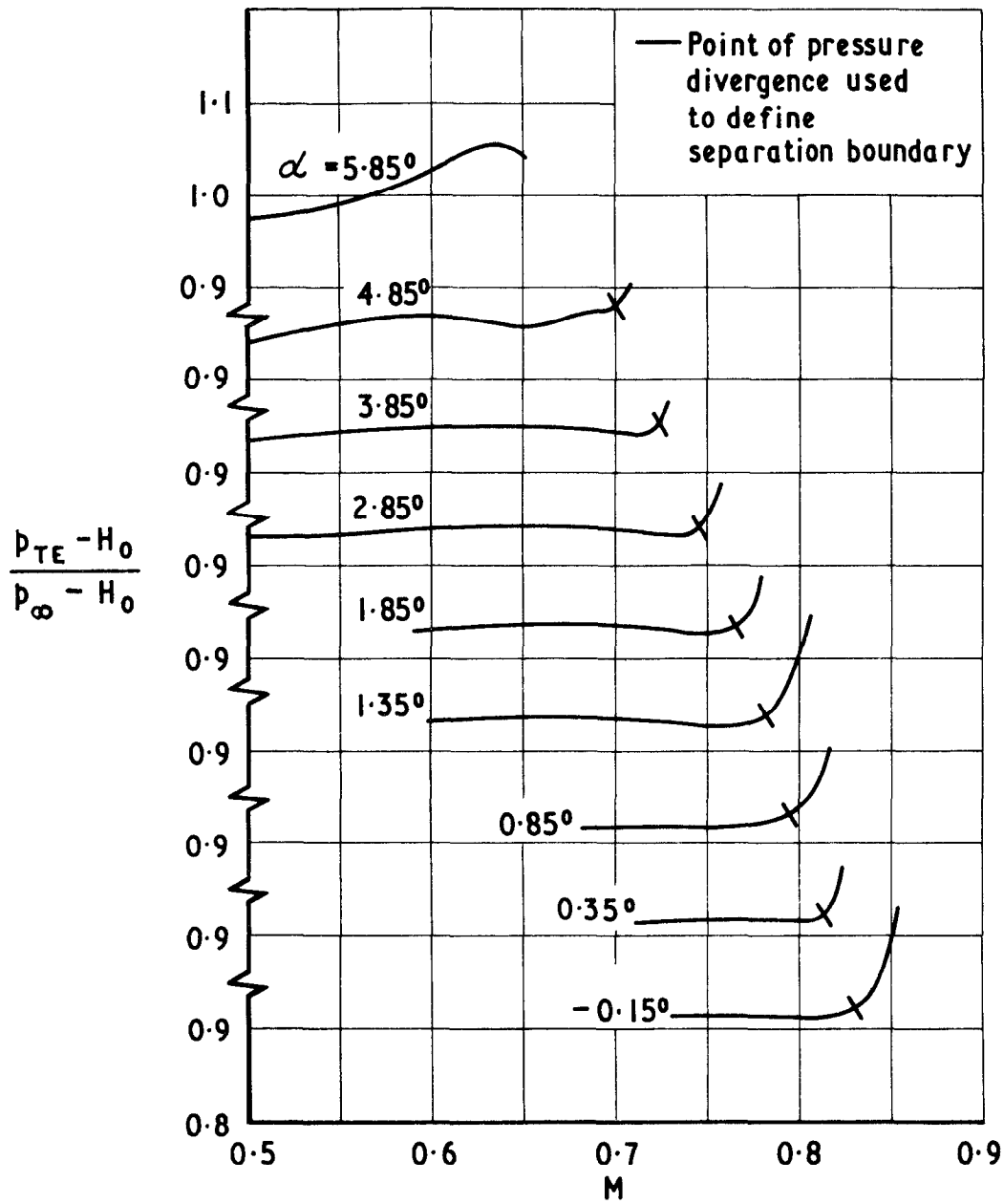

Fig. 28 Measured values of trailing-edge pressure ratio for RAE 5215

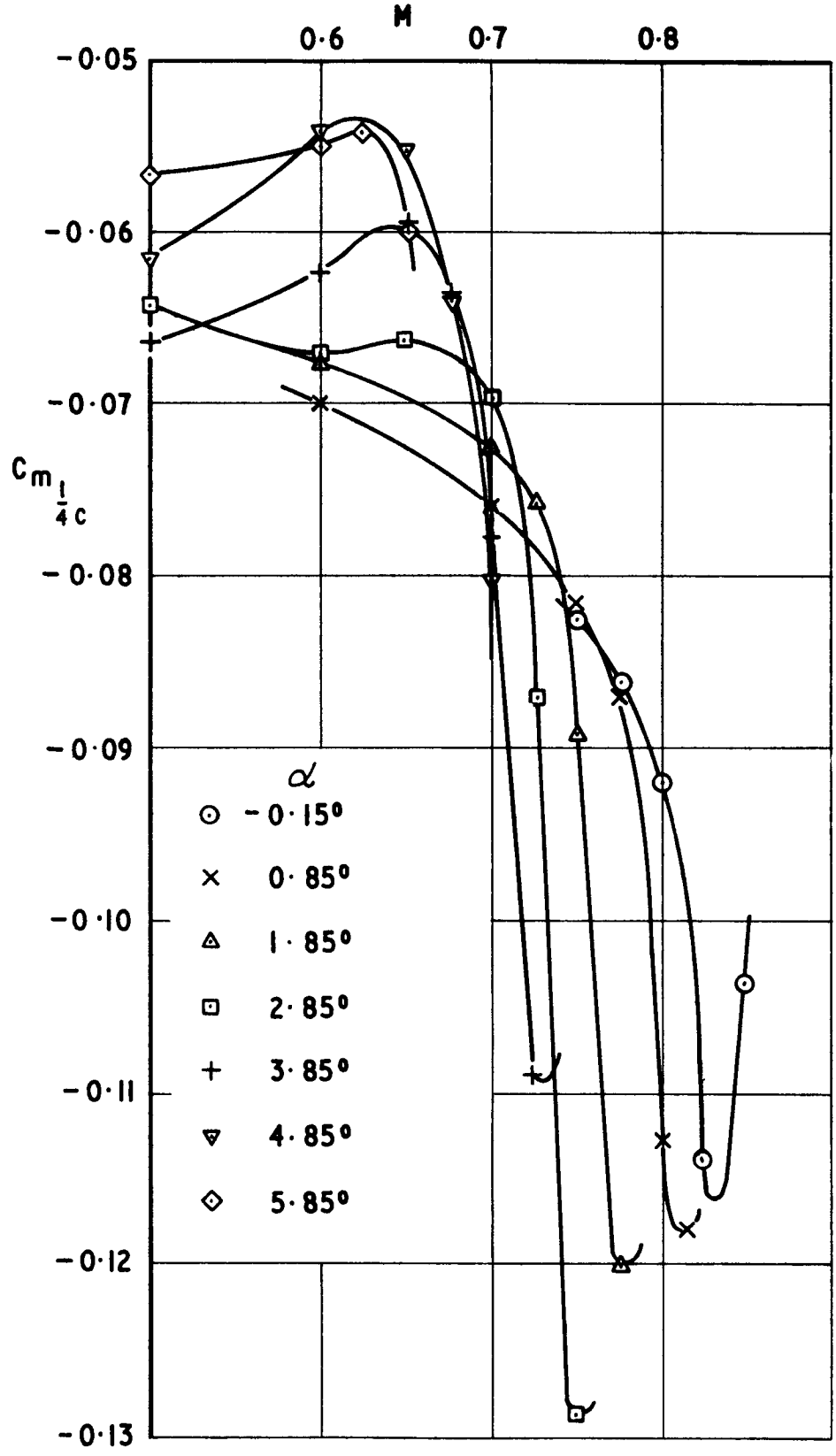

Fig. 29 Measured values of pitching moment coefficient for RAE 5215

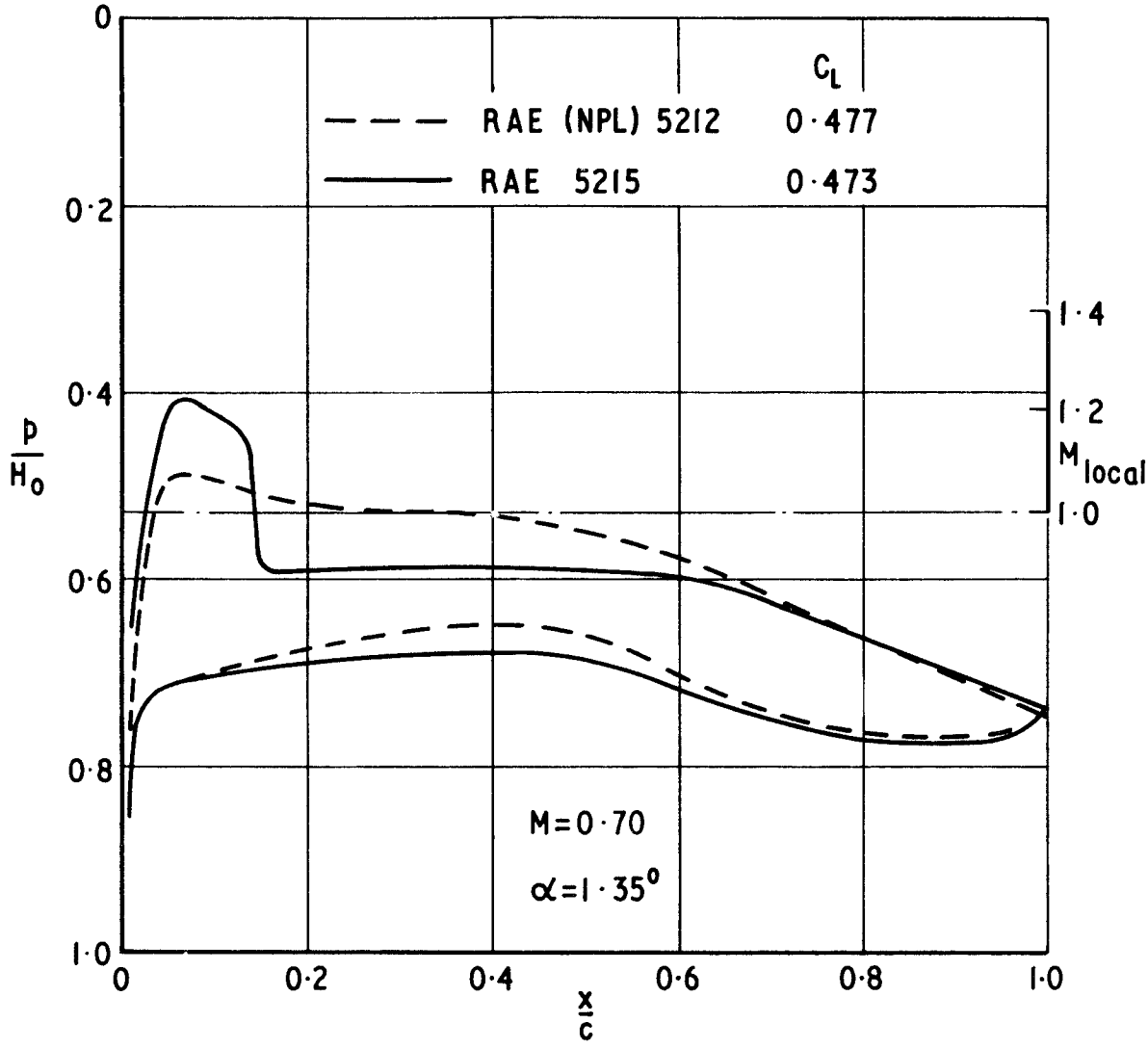

Fig.30 Comparision of experimental pressure distributions for RAE 5215 and RAE (NPL) 5212

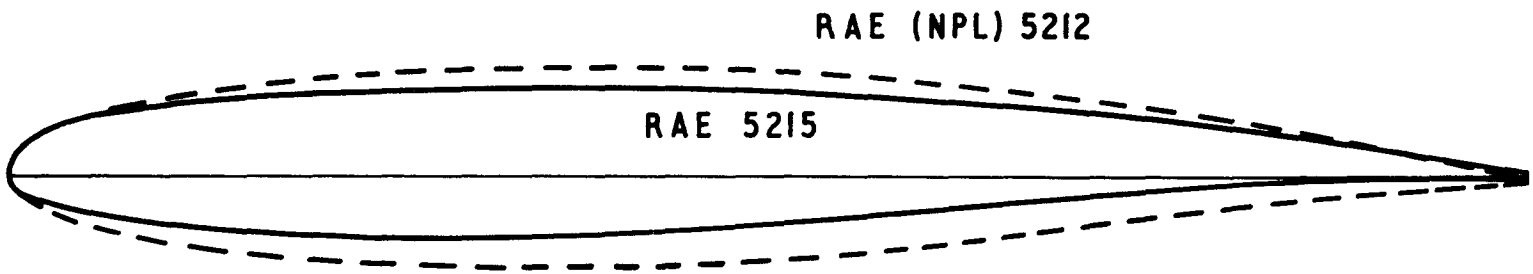

Fig. 31 Comparison of profiles for RAE 5215 and RAE (NPL)5212

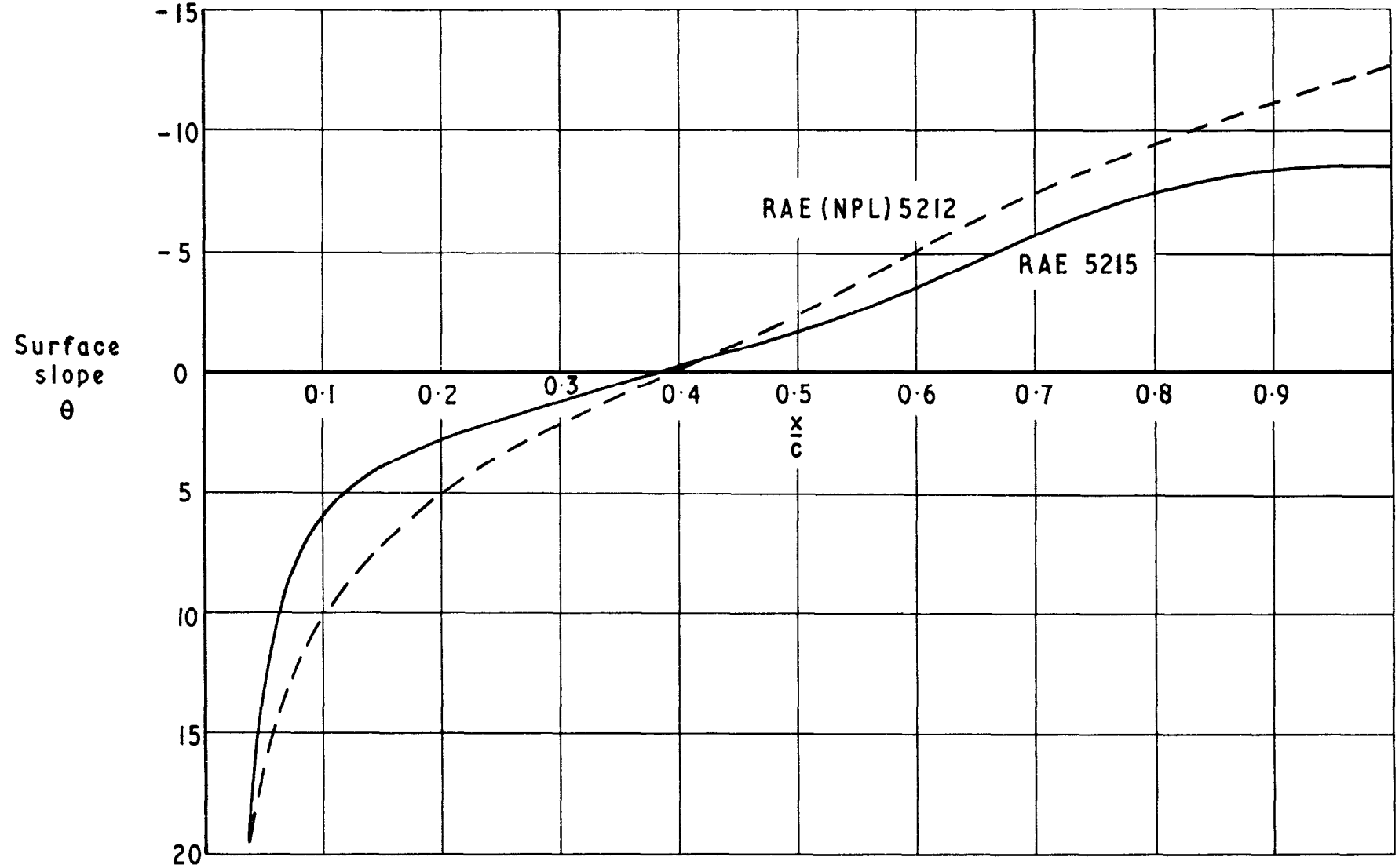

Fig.32 Comparison of upper surface slopes for RAE 5215 and RAE (NPL) 5212

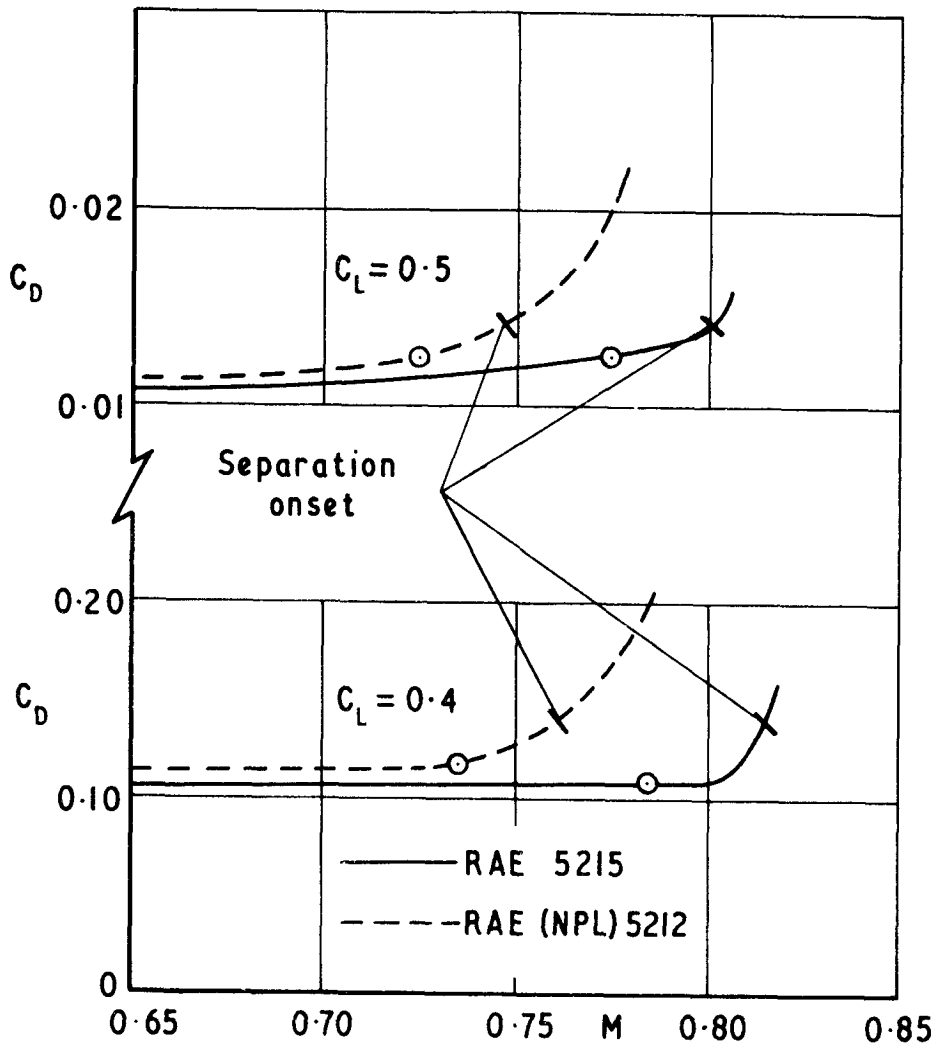

Fig.33 Conditions of comparable drag and Mach number margin for RAE 5215 and RAE (NPL) 5212 (Data taken from Fig.25, 27, 37 and 39)

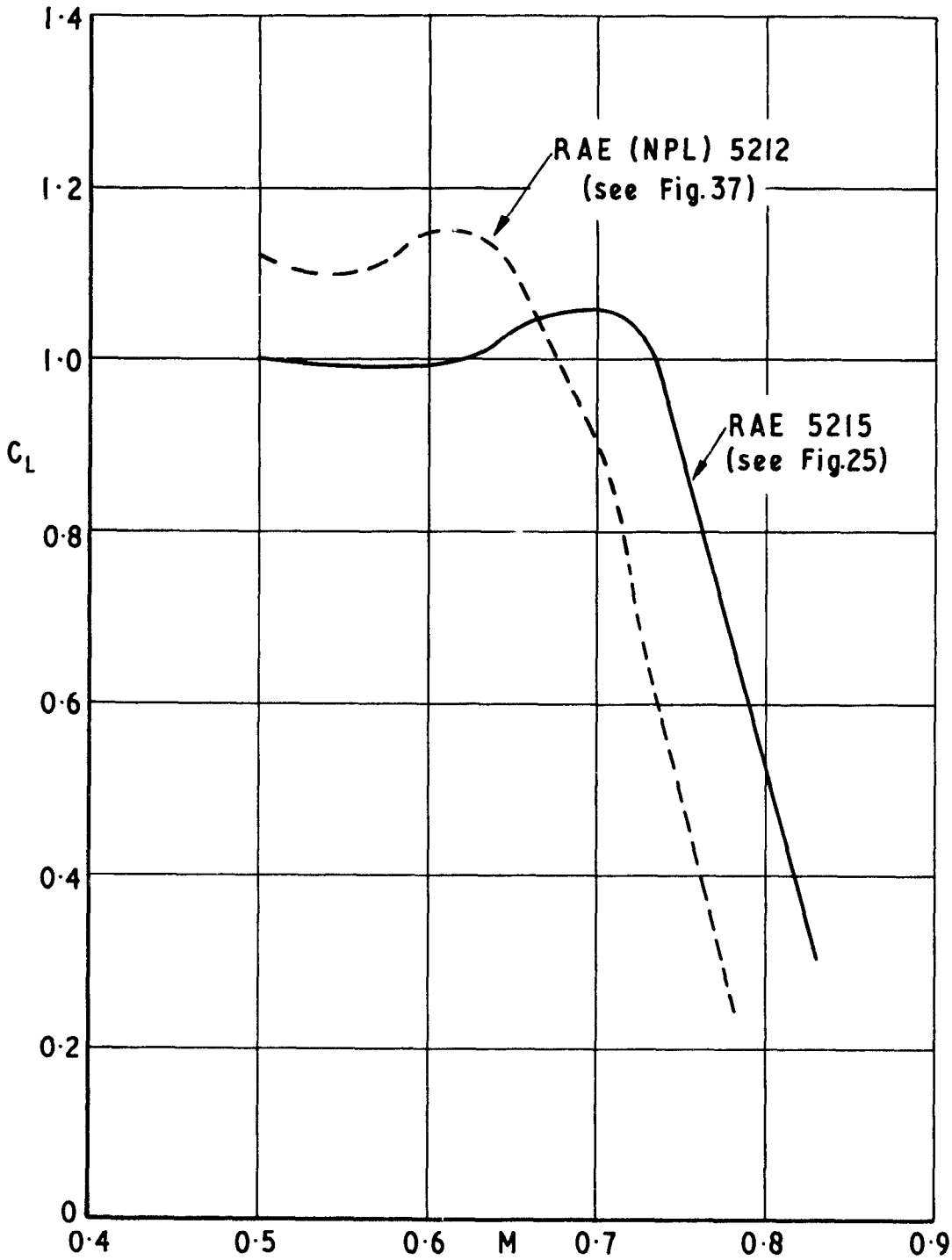

Fig.34 Separation boundaries for RAE 5215 and RAE (NPL) 5212

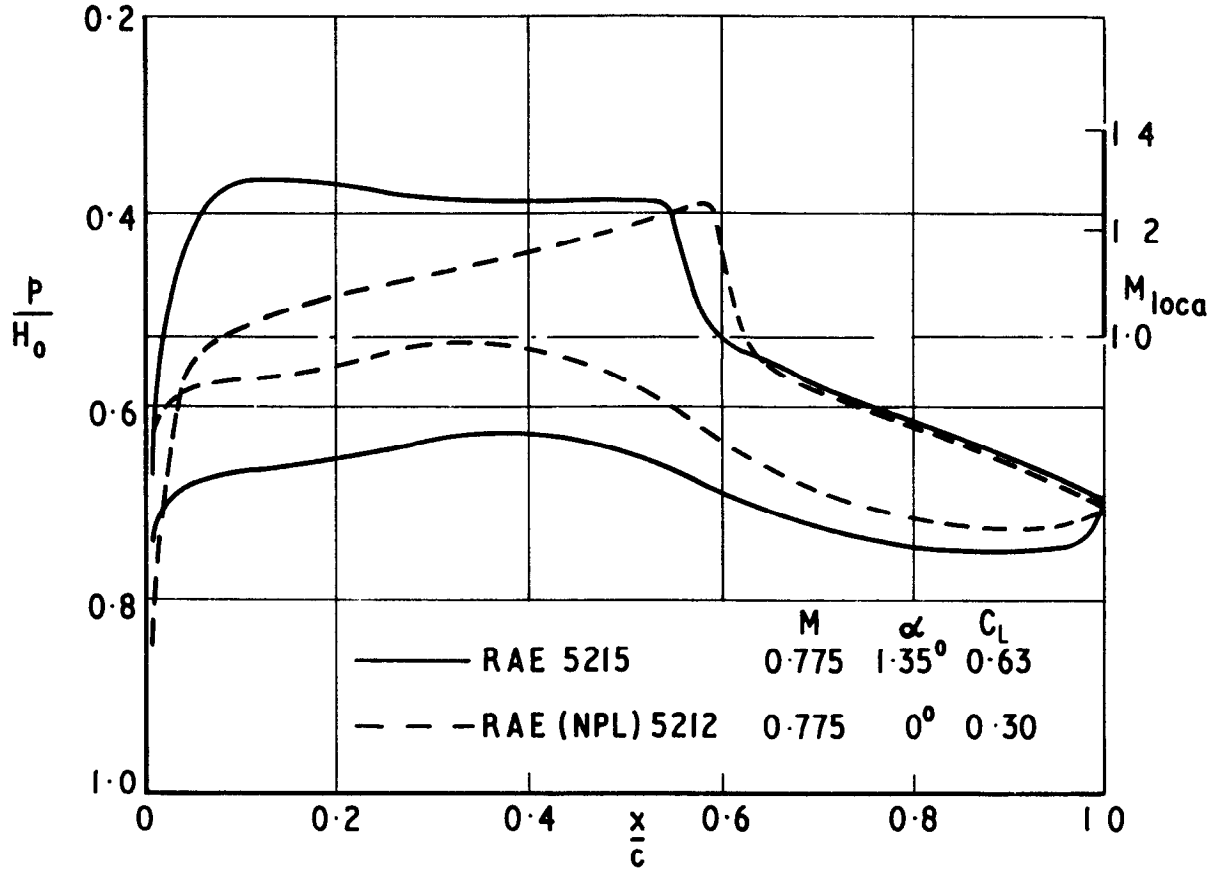

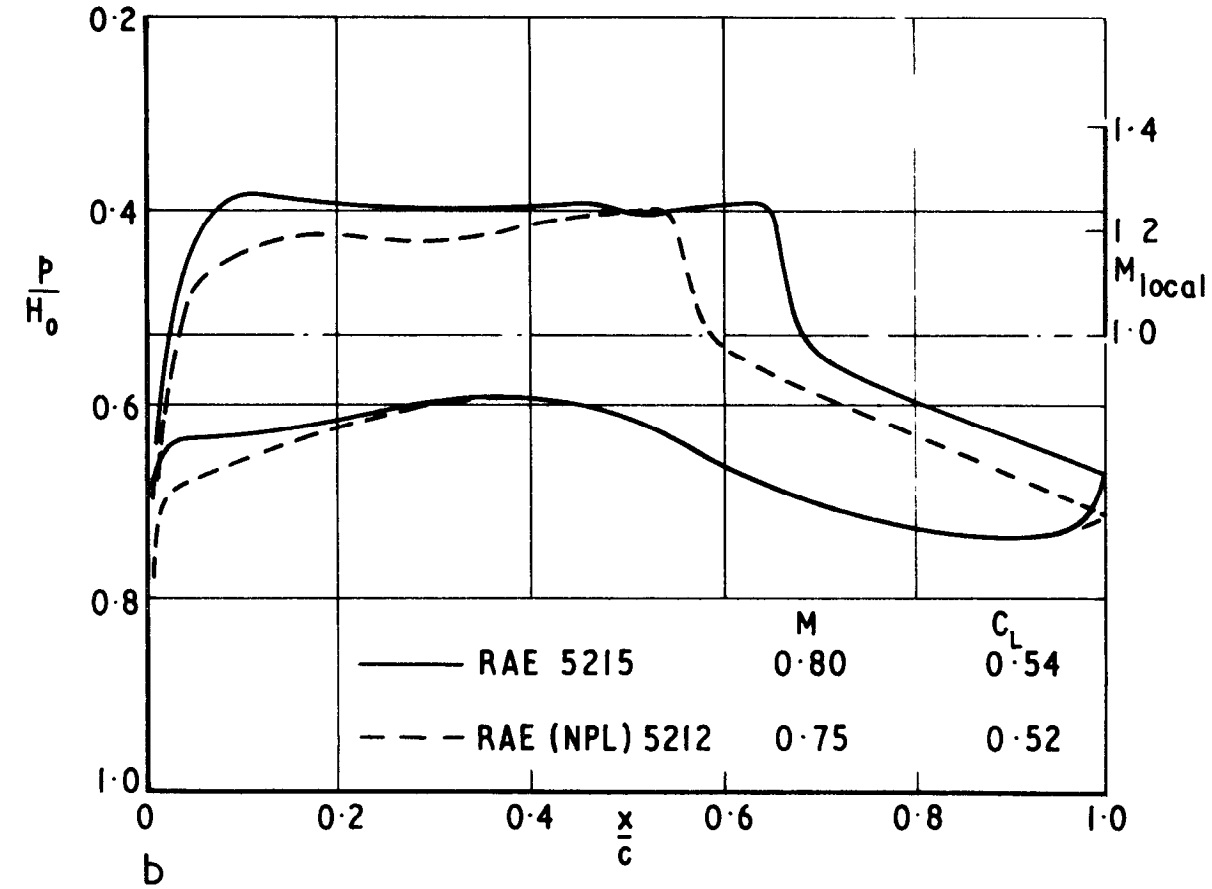

Fig. 35 a & b Comparison of experimental pressure distributions for RAE 5215 and RAE (NPL) 5212

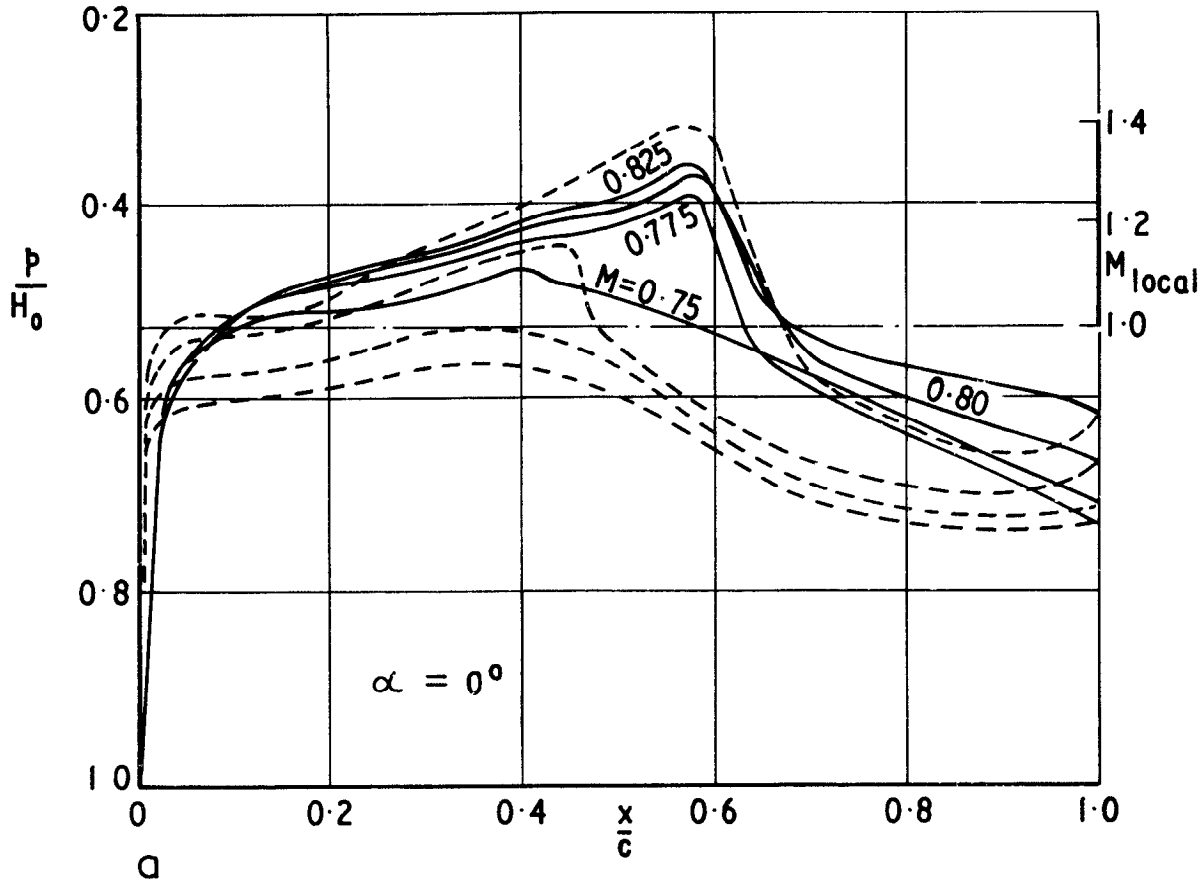

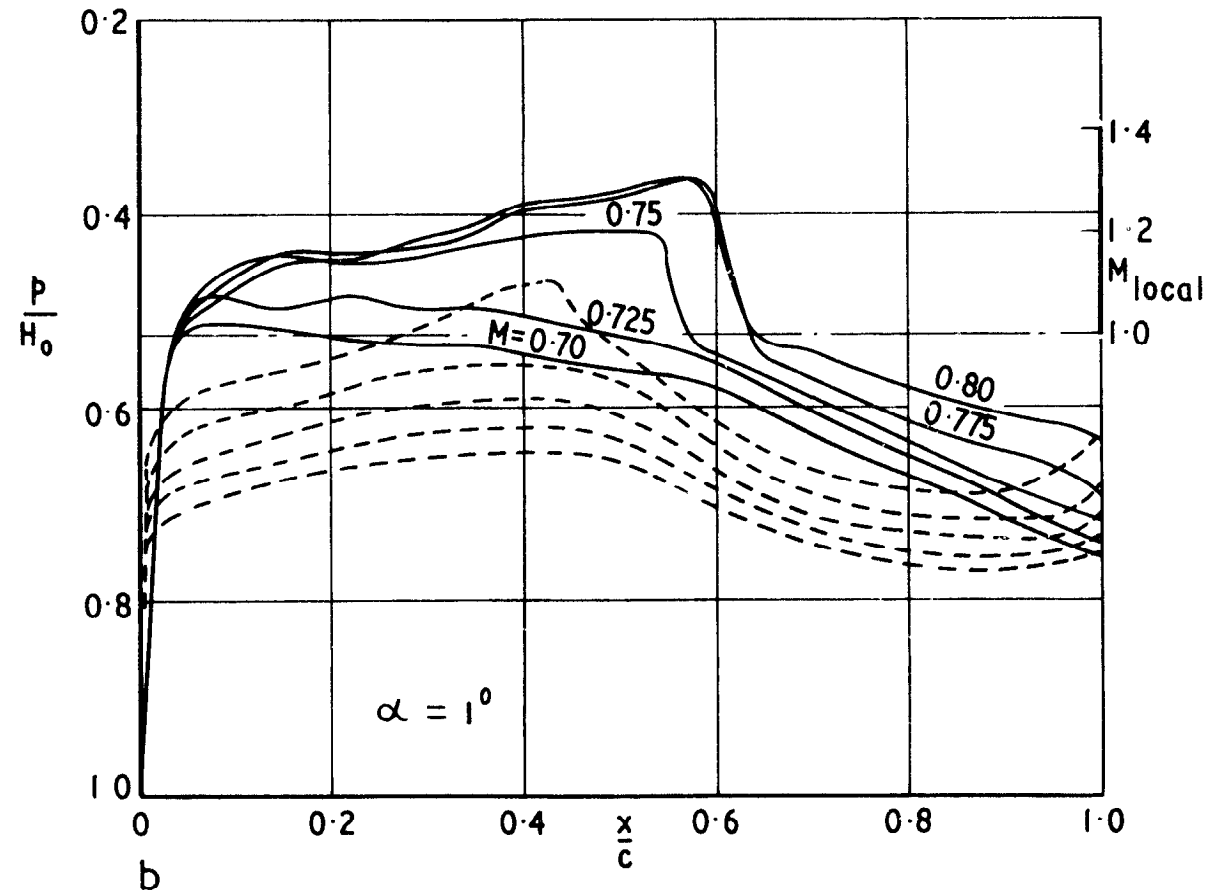

Fig 36 a & b Experimental pressure distributions for RAE (NPL) 5212

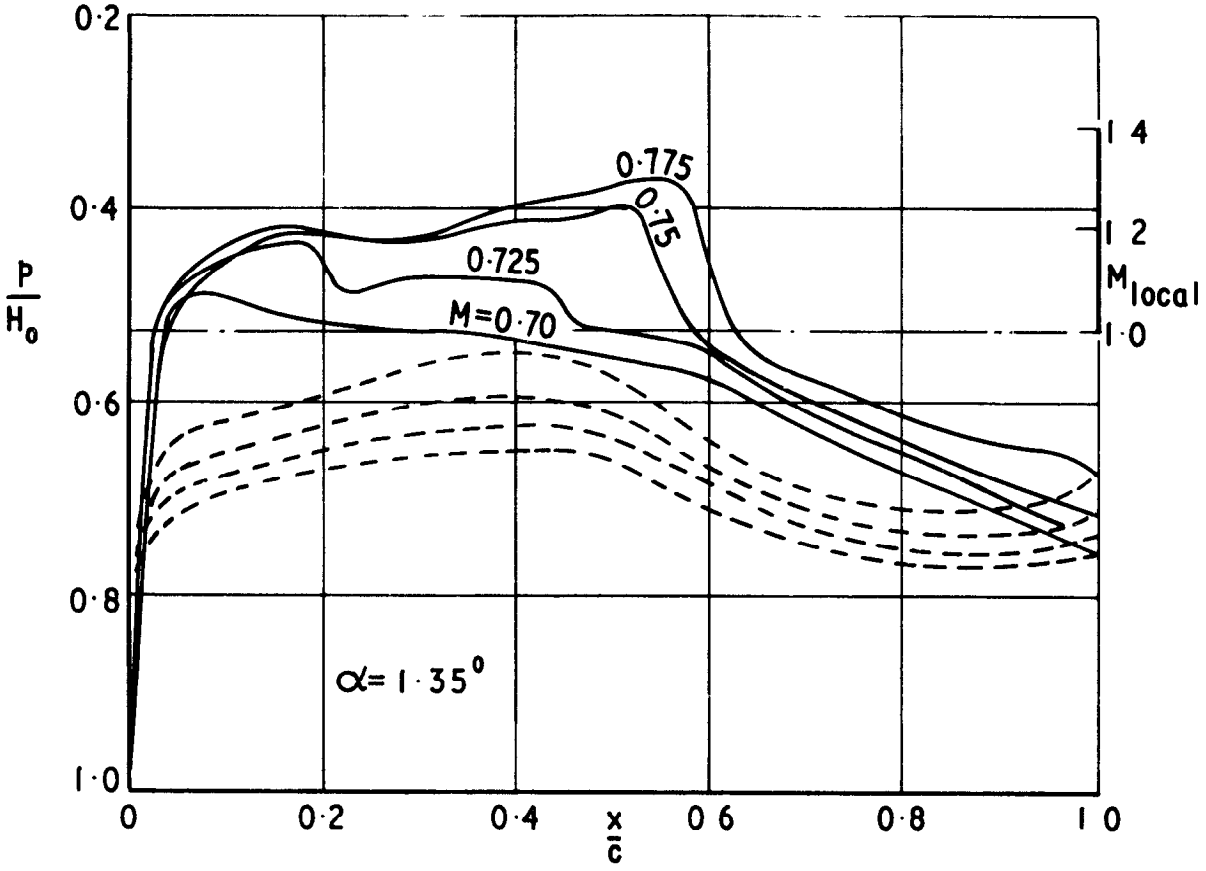

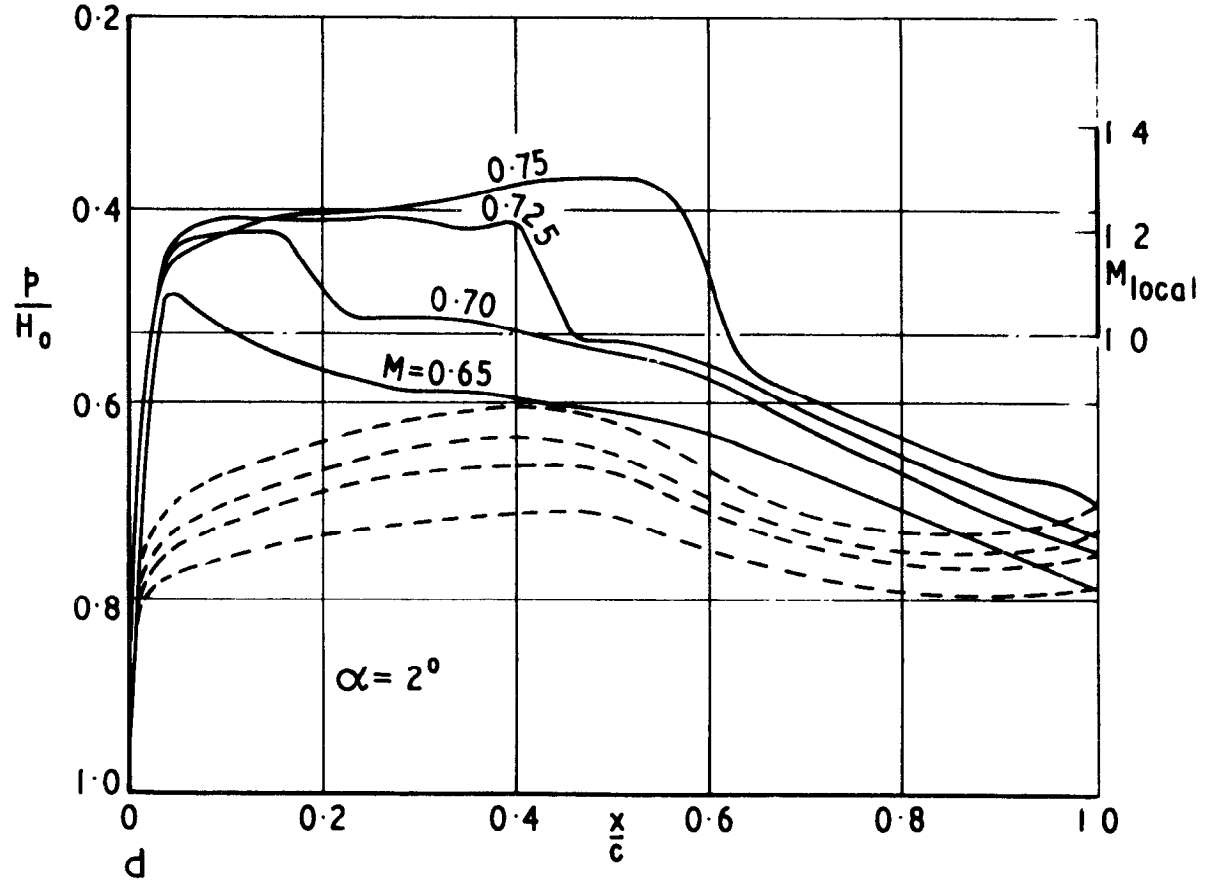

Fig.36 c & d Experimental pressure distributions for RAE (NPL) 5212

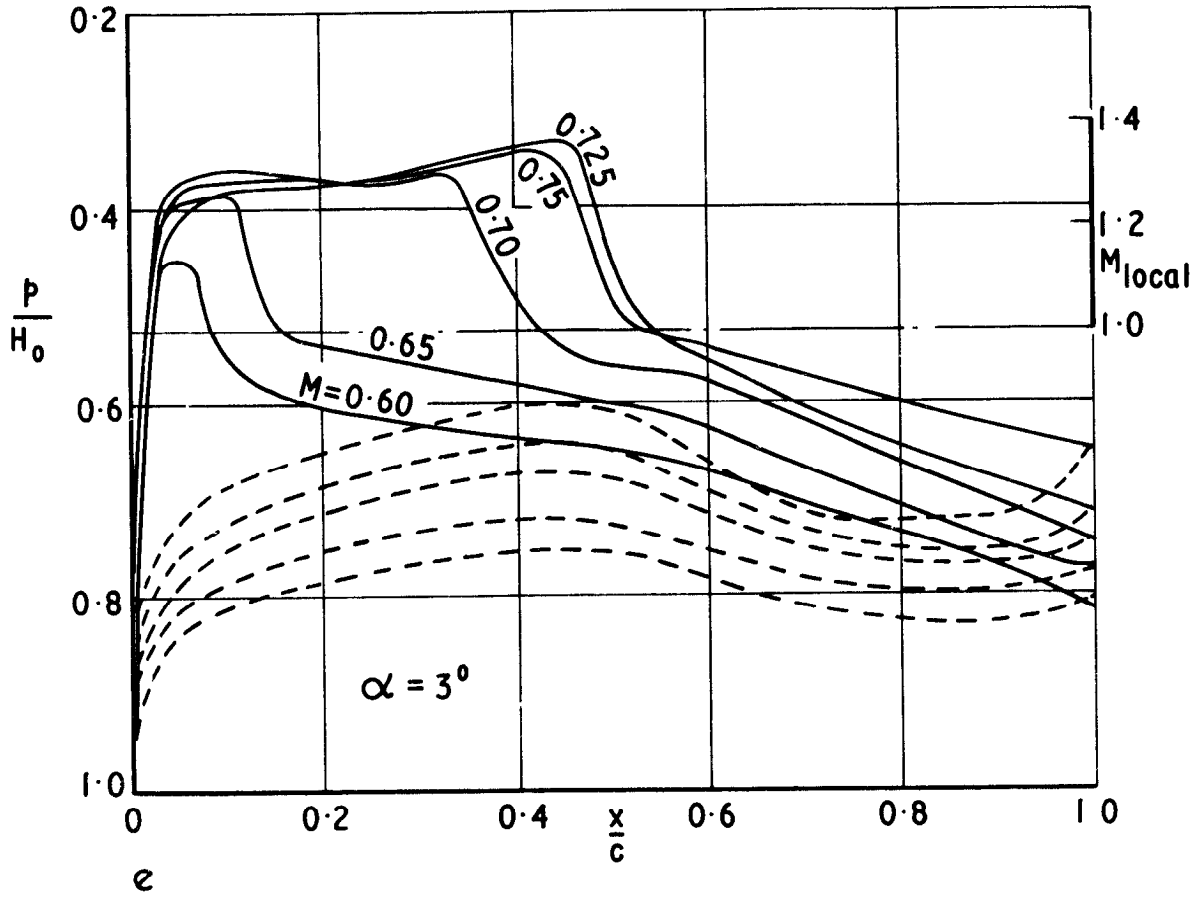

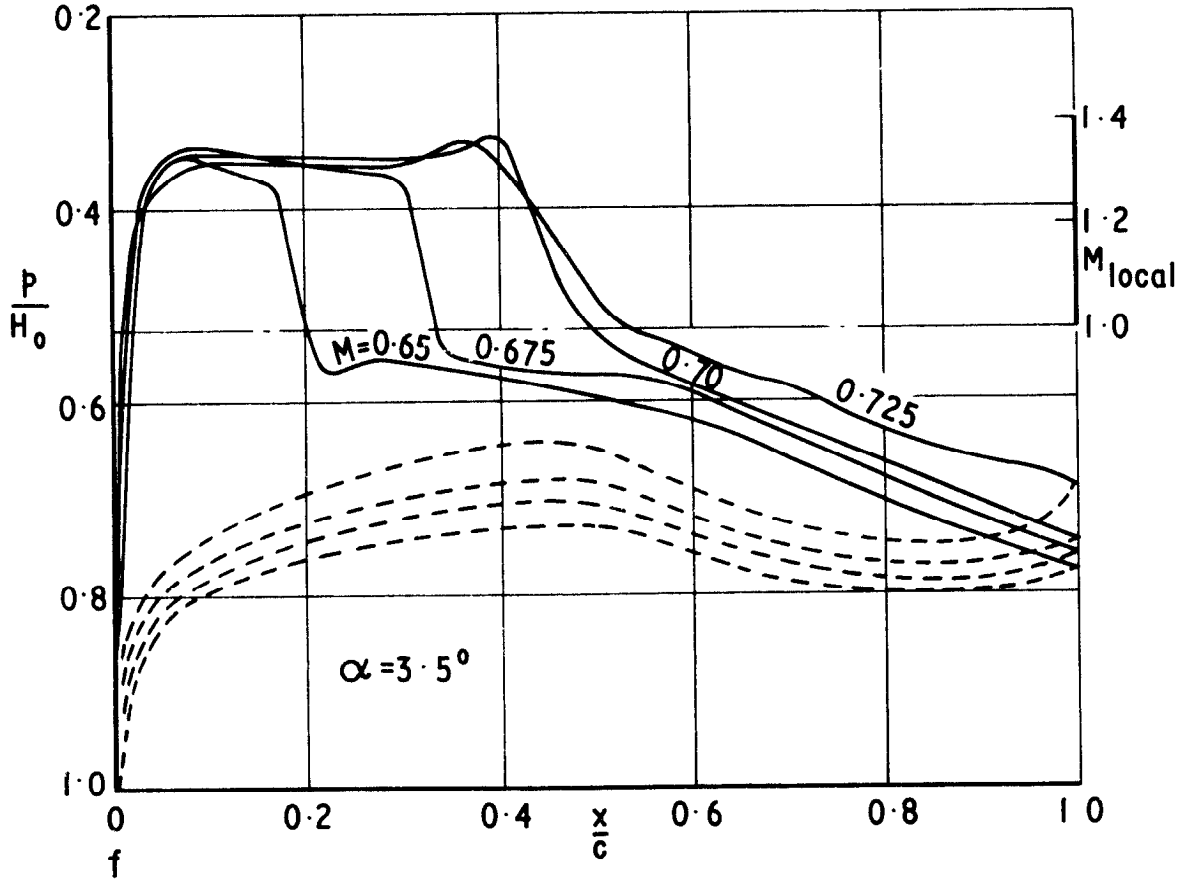

Fig.36 e & f Experimental pressure distributions for RAE (NPL) 5212

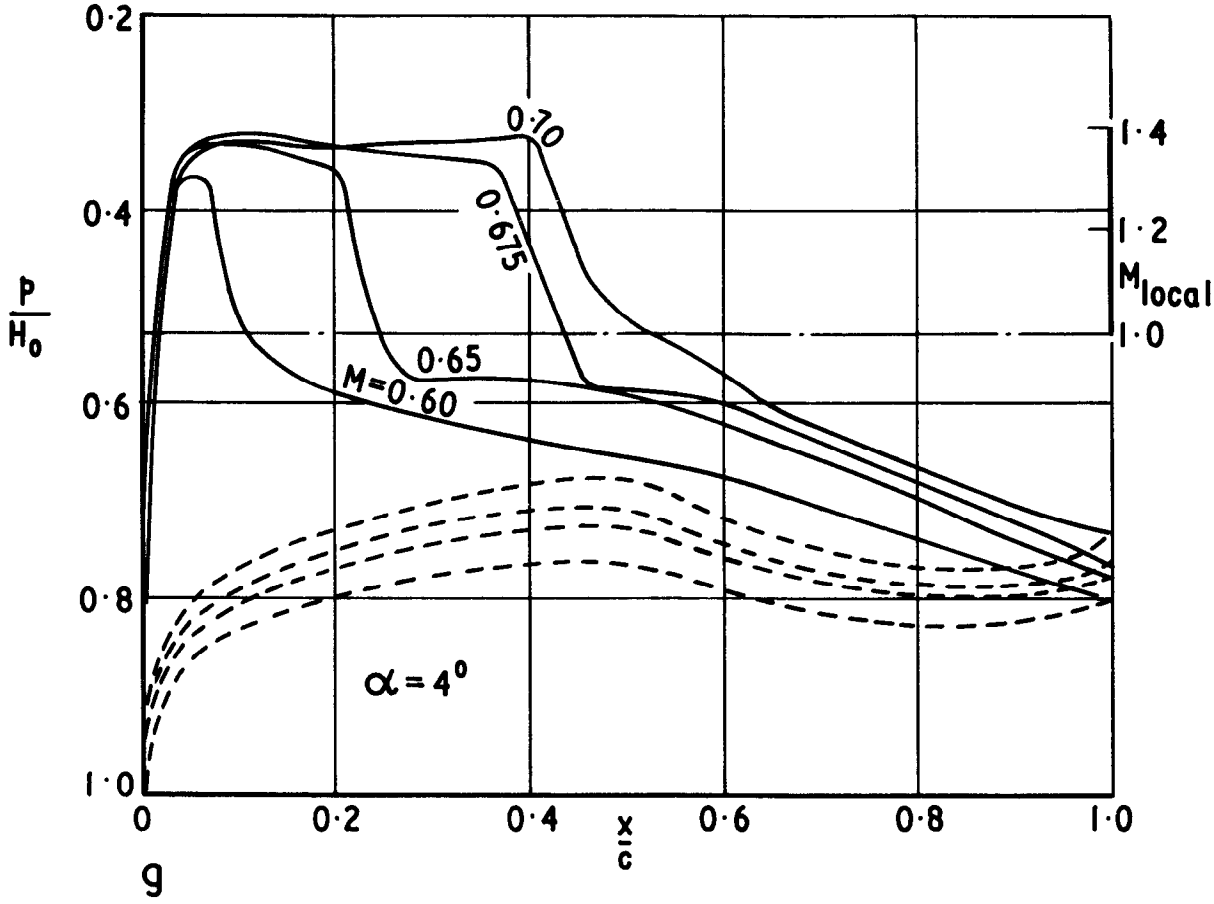

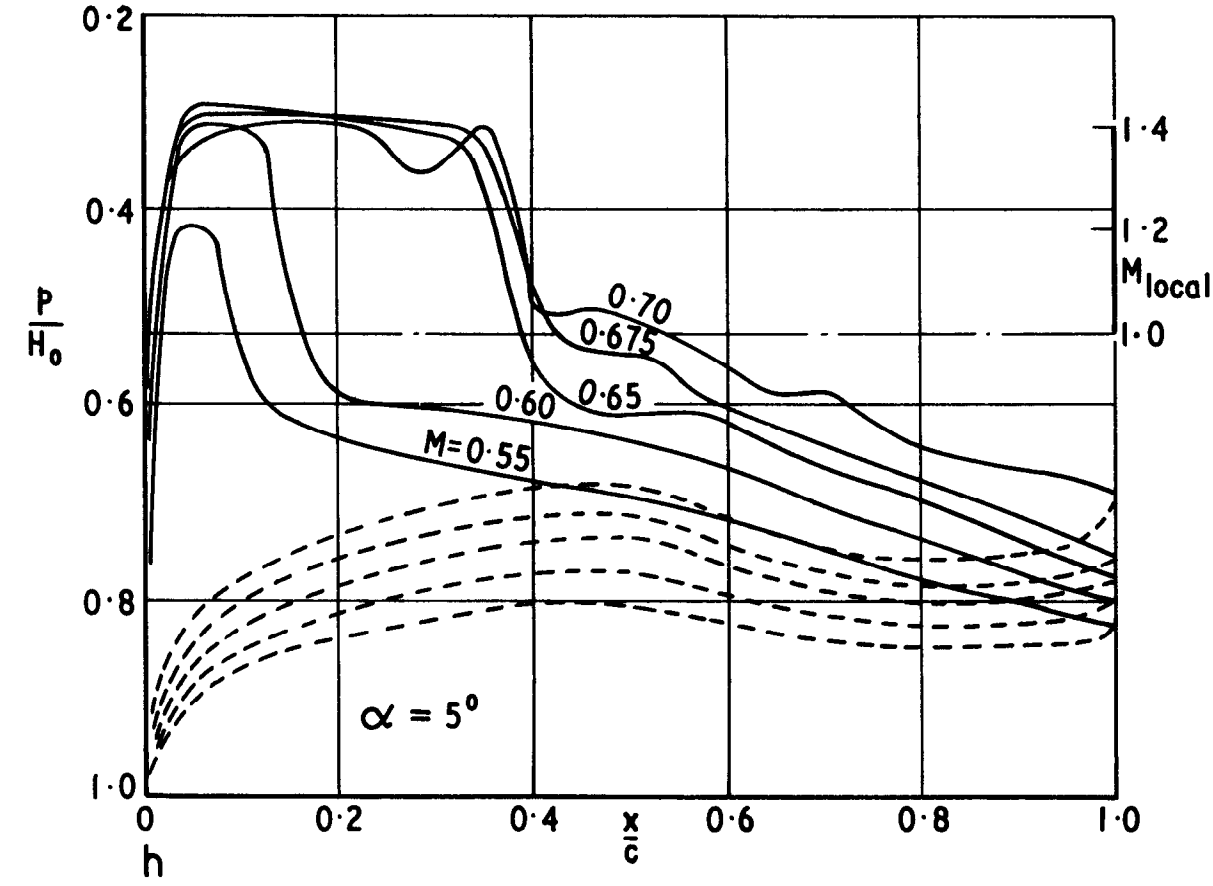

Fig.36 g & h Experimental pressure distributions for RAE (NPL) 5212

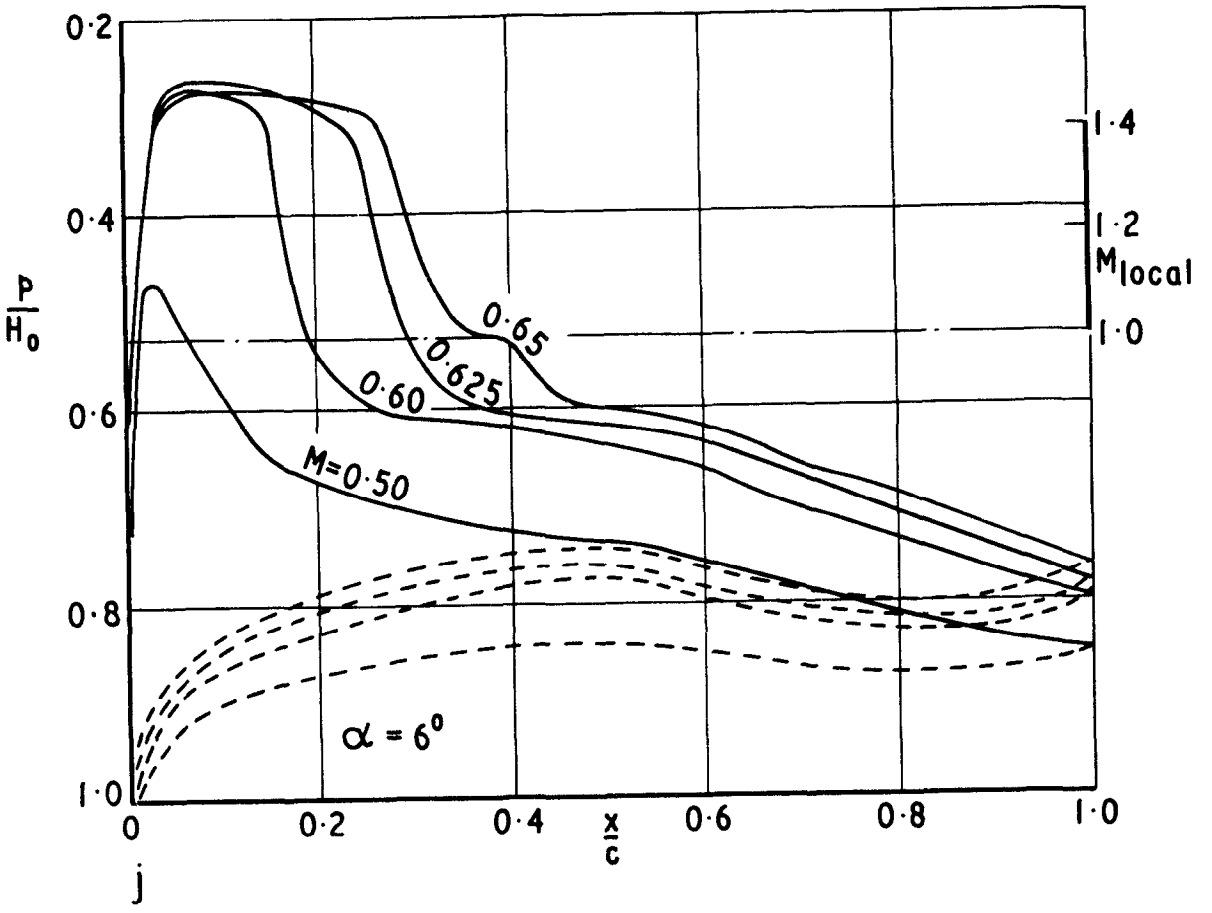

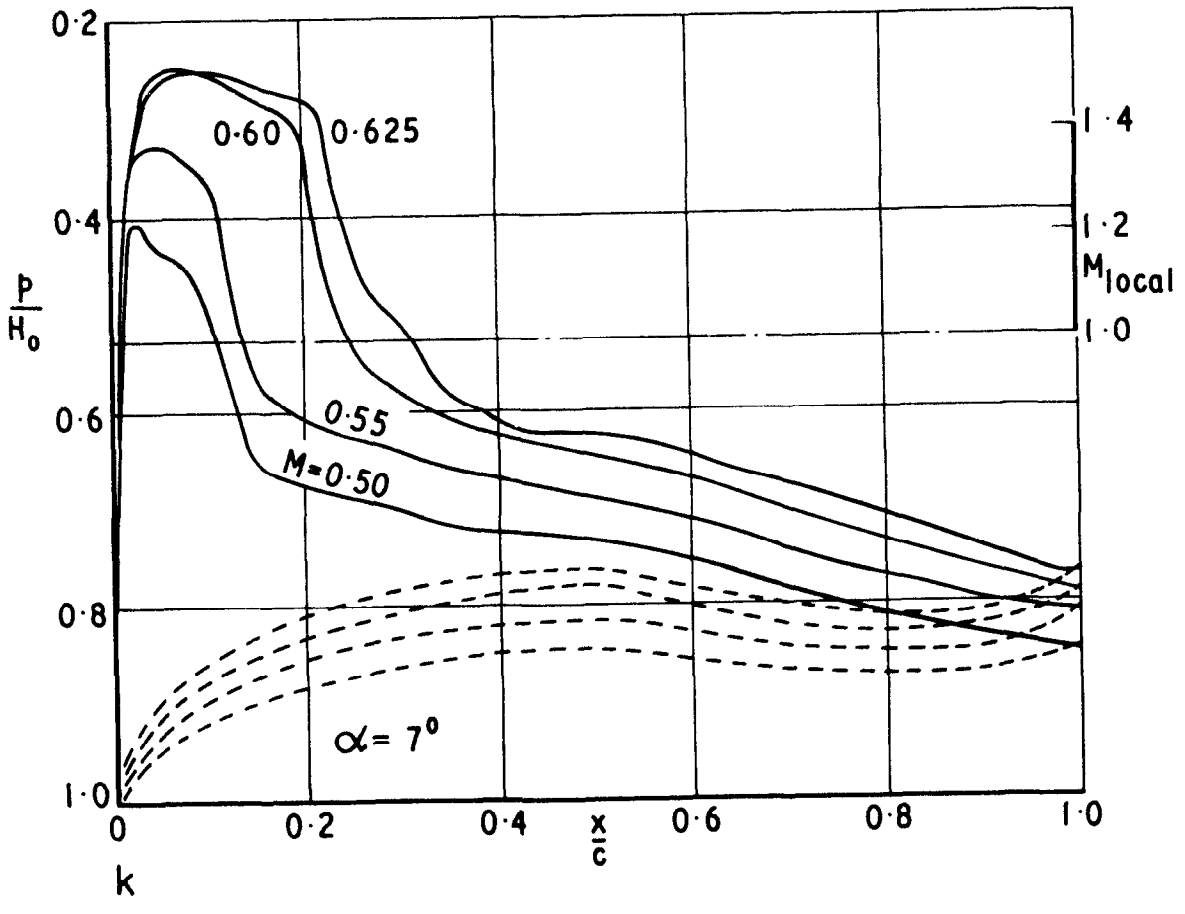

Fig. 36 j & k Experimental pressure distributions for RAE (NPL) 5212

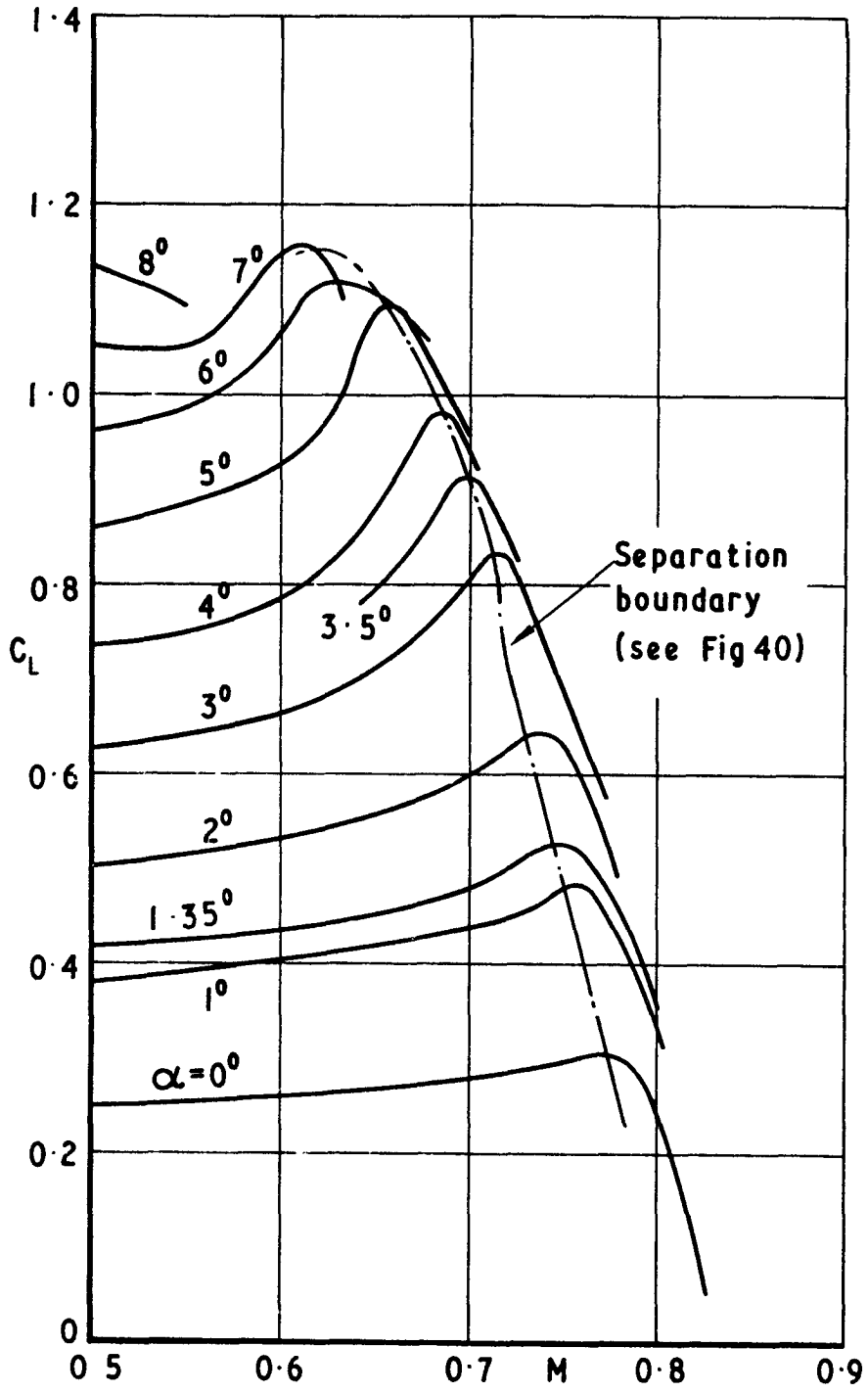

Fig.37 Measured values of lift coefficient for RAE (NPL) 5212

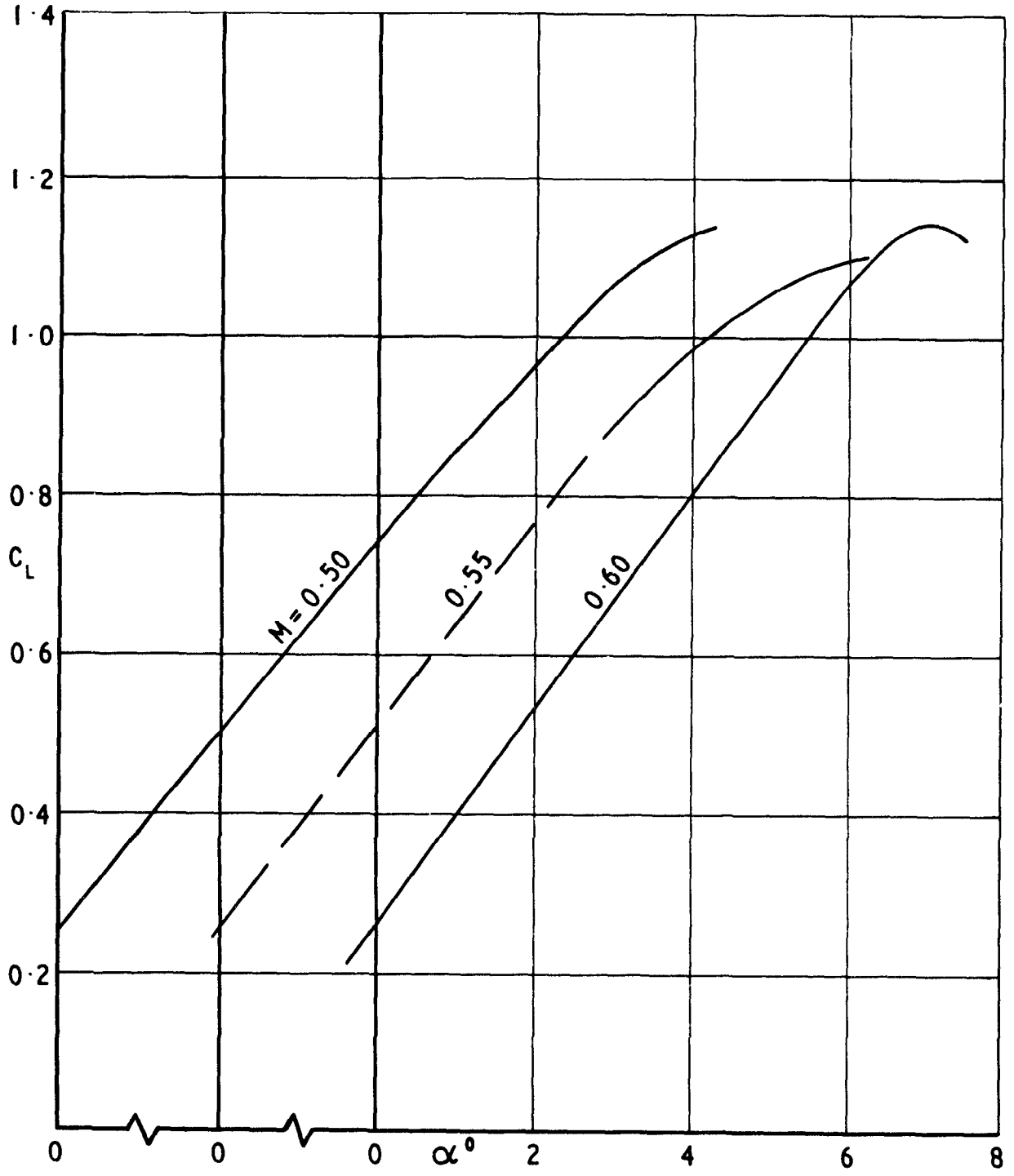

Fig.38 Measured values of lift coefficient for RAE (NPL) 5212

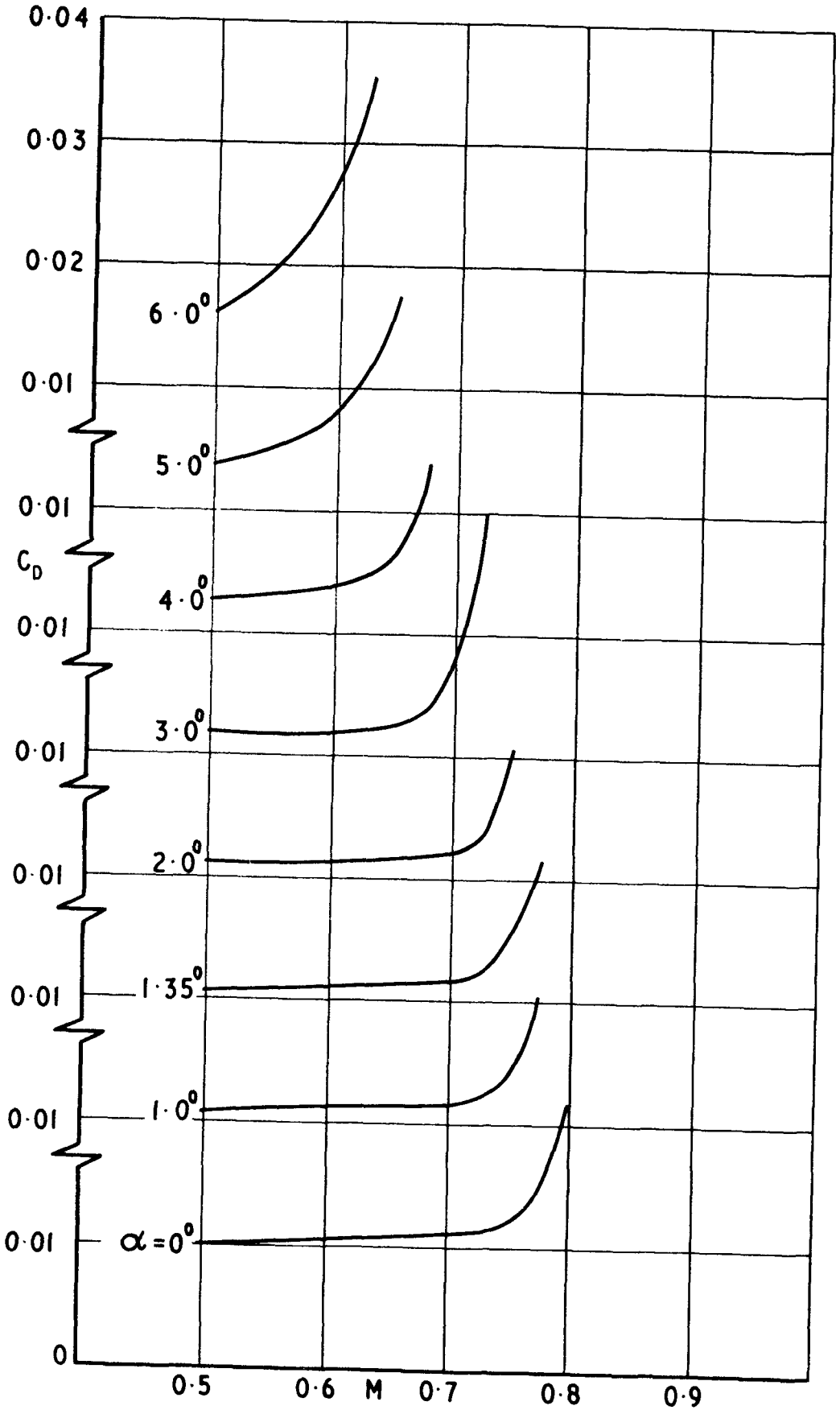

Fig. 39 Measured values of drag coefficient for RAE (NPL) 5212

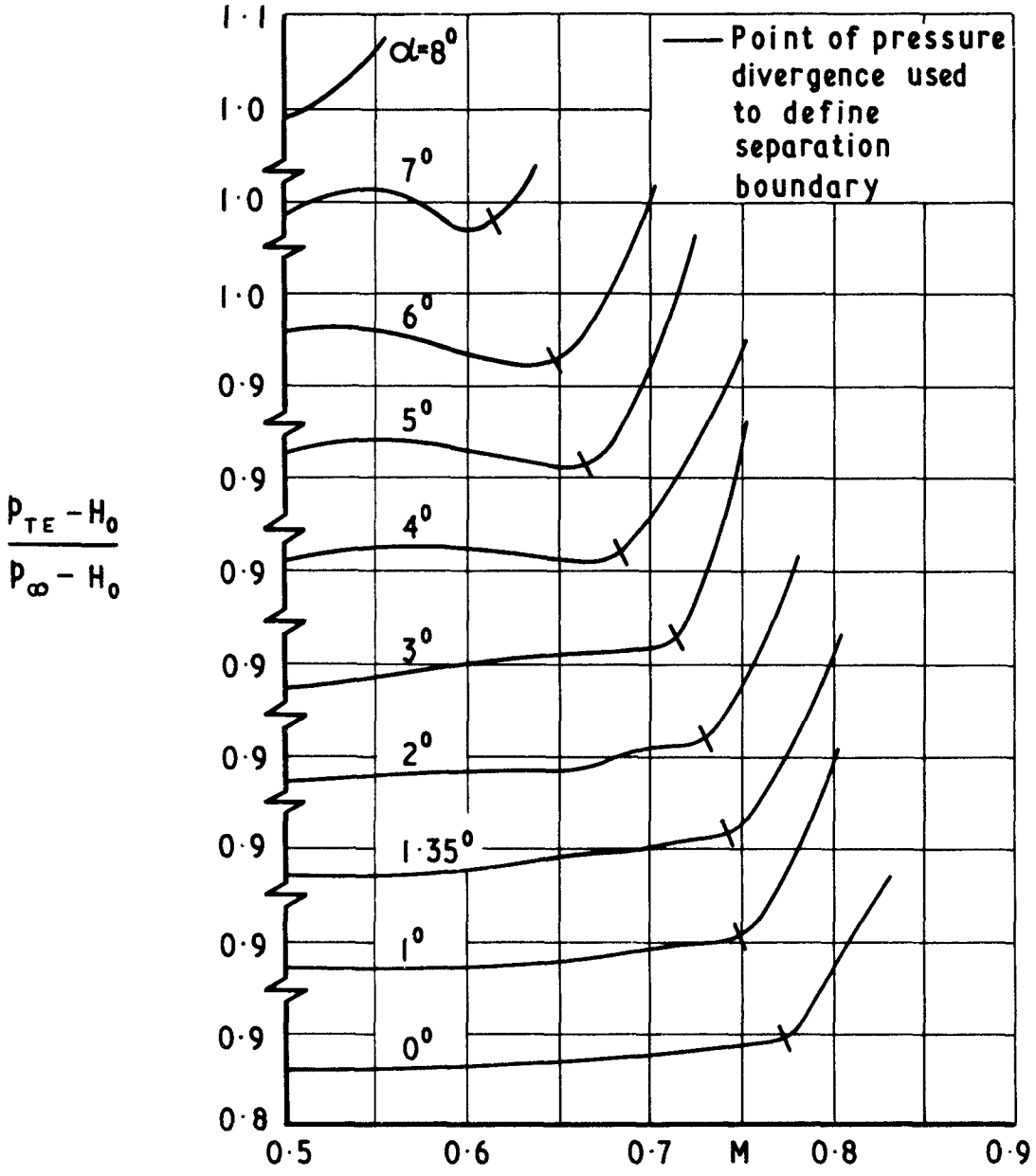

Fig.40 Measured values of trailing-edge pressure ratio for RAE (NPL) 5212

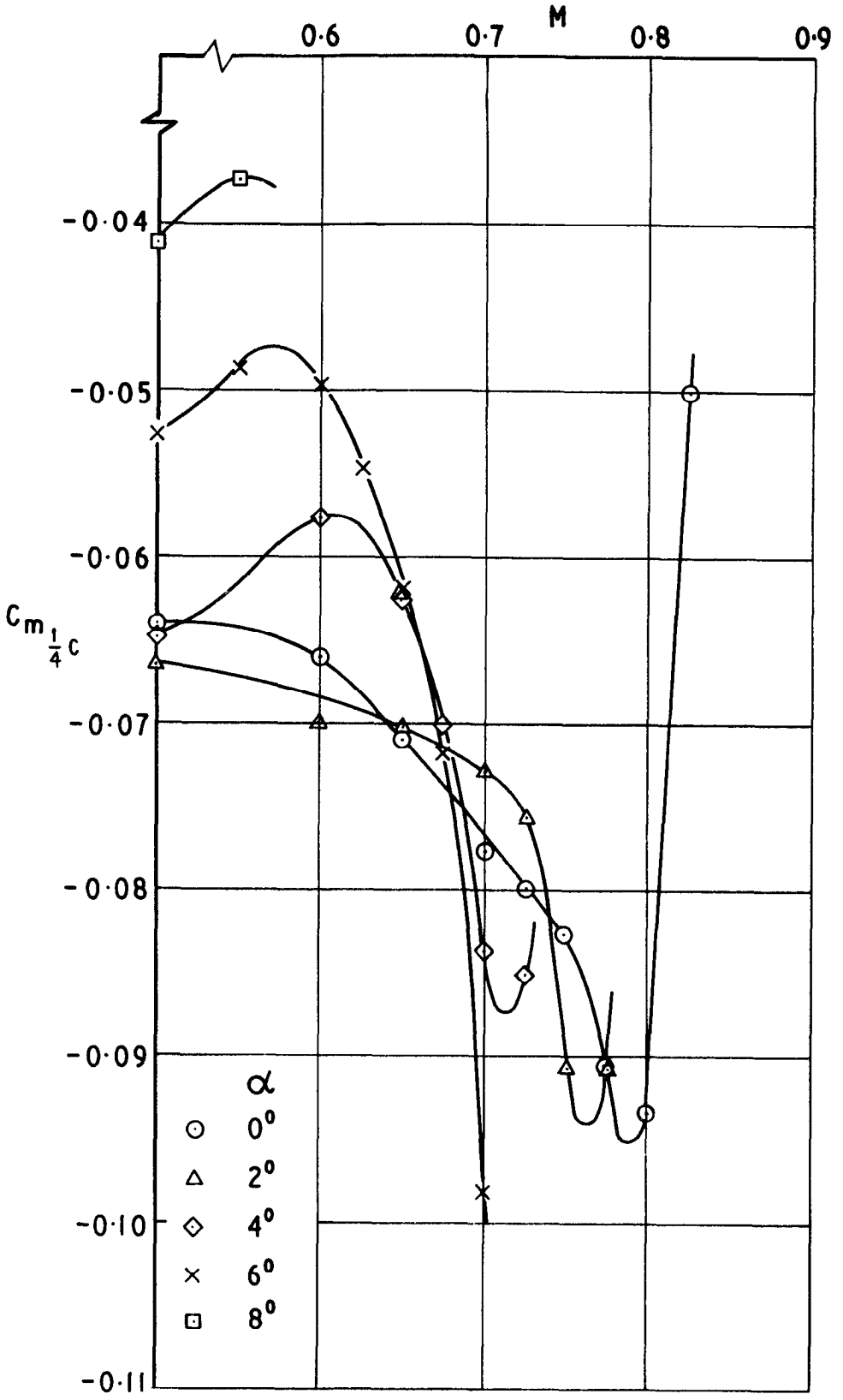

Fig. 41 Measured values of pitching-moment coefficient for RAE (NPL) 5212

Printed in England for Her Majesty's Stationery Office by the Royal Aircraft Establishment, Farnborough Dd 587483 K5 8/77

ARC CP No.1386
December 1974

533.692 :
533.6.013.12 :
533.6.011.35

Wilby, P.G.

THE DESIGN AND AERODYNAMIC CHARACTERISTICS OF THE RAE 5215 AEROFOIL

The design and aerodynamic characteristics of a series of aerofoils leading to the RAE 5215 aerofoil are described. This 9.7% thick section was developed to achieve a drag-rise Mach number of about 0.8 with a C_L of 0.4, without suffering from a rear separation at low (3×10^6) Reynolds numbers. Section characteristics are compared with those of a thicker section (RAE 5212) designed for operation at lower Mach numbers.

ARC CP No.1386
December 1974

533.692 :
533.6.013.12 :
533.6.011.35

Wilby, P.G.

THE DESIGN AND AERODYNAMIC CHARACTERISTICS OF THE RAE 5215 AEROFOIL

The design and aerodynamic characteristics of a series of aerofoils leading to the RAE 5215 aerofoil are described. This 9 7% thick section was developed to achieve a drag-rise Mach number of about 0.8 with a C_L of 0 4, without suffering from a rear separation at low (3×10^6) Reynolds numbers. Section characteristics are compared with those of a thicker section (RAE 5212) designed for operation at lower Mach numbers

Cut here

ARC CP No.1386
December 1974

533.692 :
533.6.013.12 :
533.6.011.35

Wilby, P.G.

THE DESIGN AND AERODYNAMIC CHARACTERISTICS OF THE RAE 5215 AEROFOIL

The design and aerodynamic characteristics of a series of aerofoils leading to the RAE 5215 aerofoil are described. This 9.7% thick section was developed to achieve a drag-rise Mach number of about 0.8 with a C_L of 0.4, without suffering from a rear separation at low (3×10^6) Reynolds numbers. Section characteristics are compared with those of a thicker section (RAE 5212) designed for operation at lower Mach numbers.

ARC CP No.1386
December 1974

533.692 ·
533.6.013.12 :
533.6.011.35

Wilby, P G.

THE DESIGN AND AERODYNAMIC CHARACTERISTICS OF THE RAE 5215 AEROFOIL

The design and aerodynamic characteristics of a series of aerofoils leading to the RAE 5215 aerofoil are described. This 9.7% thick section was developed to achieve a drag-rise Mach number of about 0.8 with a C_L of 0.4, without suffering from a rear separation at low (3×10^6) Reynolds numbers. Section characteristics are compared with those of a thicker section (RAE 5212) designed for operation at lower Mach numbers.

Cut here

DETACHABLE ABSTRACT CARDS

DETACHABLE ABSTRACT CARDS

Published by
HER MAJESTY'S STATIONERY OFFICE

Government Bookshops
49 High Holborn, London WC1V 6HB
13a Castle Street, Edinburgh EH2 3AR
41 The Hayes, Cardiff CF1 1JW
Brazennose Street, Manchester M60 8AS
Southey House, Wine Street, Bristol BS1 2BQ
258 Broad Street, Birmingham B1 2HE
80 Chichester Street, Belfast BT1 4JY
Government Publications are also available through booksellers

C.P. No. 1386

ISBN 011 471132 1